The Measurement (58.4–164.0 nm) and Analysis (40.0–600.0 nm)
of the
Atomic Scattering Factors of Diamond and Graphite

by

Matthew B. Squires

A thesis submitted to the faculty of

Brigham Young University

in partial fulfillment of the requirements for the degree of

Master of Science

Physics and Astronomy Department

Brigham Young University

August 2001

BRIGHAM YOUNG UNIVERSITY

GRADUATE COMMITTEE APPROVAL

of a thesis submitted by

Matthew B. Squires

This thesis has been read by each member of the following graduate committee and by majority vote has been found to be satisfactory.

Date	David D. Allred, Chair
Date	R. Steven Turley
Date	Robert C. Davis

BRIGHAM YOUNG UNIVERSITY

As chair of the candidate's graduate committee, I have read the thesis of Matthew B. Squires in its final form and have found that (1) its format, citations, and bibliographical style are consistent and acceptable and fulfill university and department style requirements; (2) its illustrative materials including figures, tables, and charts are in place; and (3) the final manuscript is satisfactory to the graduate committee and is ready for submission to the university library.

Date	David D. Allred, Chair

Accepted for the Department

Scott D. Sommerfeldt
Graduate Coordinator

Accepted for the College

G. Rex Bryce
Associate Dean,
College of Physical and Mathematical Sciences

ABSTRACT

THE MEASUREMENT (58.4–164.0 NM) AND ANALYSIS (40.0–600.0 NM) OF THE ATOMIC SCATTERING FACTORS OF DIAMOND AND GRAPHITE

Matthew B. Squires
Department of Physics and Astronomy
Master of Science

I have built a variable angle reflectometer capable of measuring absolute reflectance between 2.5° and 85° grazing incidence for use in the extreme ultraviolet, and it is possible to perform surface scans over a sample 5 cm square. The measurement system was constructed to be modular for future applications. The data collection and analysis is automated using LabVIEW and data acquisitions hardware. The data is corrected for time variations in the intensity of the plasma source.

The optical constants of fused industrial diamond and highly oriented pyrolytic graphite (HOPG) have been measured using the variable angle reflectometer. Qualitatively the measured values reasonably agree with previously published data for diamond and graphite. However, the measured data points are sparse and have only been measured at bright spectral lines of H, He, and N. The small size and unknown quality of the graphite and diamond made it difficult to quantitatively compare the measured optical properties to other published data.

I have analyzed the atomic scattering factors (ASF) of diamond and graphite, calculated from the n and k values reported in the *Handbook of Optical Constants I & II* (ed. E. Palik), by calculating the relative difference between the ASF of diamond and graphite. The relative error in f_1 at 8 eV is about 100% and between 15.5–25 eV it is about 25%. This large of a difference at 25 eV is greater than expected because the nearest resonance in the carbon spectrum is at 8 eV. At 30 eV this difference is about 10 times greater than the difference between the energies of the single and double bonds in carbon. The mechanisms that determine the optical properties of carbon are significantly affected by the crystal structure of the bulk carbon. There is a relative difference of 100% between the f_2 values about 8 eV. This is due to the near zero absorption of diamond below its band gap. At energies above 15.5 eV the average error is about 25%. This analysis shows that, at least for carbon, the energies of the valence electrons significantly affects the electronic structure at energies several times that of the binding energies.

ACKNOWLEDGMENTS

Dedicated to my wife Dionne

My wife (and still my friend) Dionne– Has put up with long nights, with several young boys, for a long time, with passed deadlines, and no breaks. With no compensation except a sore back and more dishes after dinner.

My Father in Heaven– Who has heard and answered my prayers when, because of my mistakes, equipment was damaged. But by a great miracle all the hydrocarbons were cleaned from the monochromator. Also for giving agency so I might choose what makes me most happy.

My Mom and Dad– For always loving me and teaching me the truth, while letting me follow my dreams and aspirations, and supporting me and my family emotionally and financially.

David Allred– For taking me on as a student, somewhat hesitantly, after failing (27%) my first E&M test. For letting me loiter in your office till I learned enough to do it on my own. For teaching me so I could become a valuable asset in your research. Even more valuable that all the equipment that was broken during my stay. For being a good friend and standing behind my ideas and discoveries when I needed the support. For giving me the chance to learn how to be independent by giving me reign over my lab.

Steven Turley– For being a wonderful co-advisor and example. For helping me with the statistical aspects of my thesis. For being understanding when I broke equipment in the line of service, and then finding the money to replace or fix the broken parts. For working very hard to get my thesis to the library.

David Balogh– For being a friend through Jackson, making that great garlic pizza, and teaching me most of what I know about computers. For taking on responsibilities during our last month of our Master's Degrees that you didn't want so I could finish my research before leaving. For being opinionated in the best way, and not making anyone feel like you would judge them when they did things different....but come high water I expect to find you in California!

Cynthia Mills– For being patient with a mentor who was learning the ropes, and building key parts of the reflectometer. During which you expecting your baby daughter and had very little energy. I admire you determination.

Robert Davis– For being a great teacher and talking to me about different aspects of my thesis. For taking the time to do some AFM scans when you were very busy. For giving good advice on my future plans.

For (in no sorted order)– Wes Lifferth (Design and machining), Greg Harris (Chamber lift and LabVIEW), Jason Rowland (Pre O-Chamber work, and lateral pushers), Jason Flint (Electrical feedthrough and general help), Mike Hales (Electrical Wiring), Joe Young (Vacuum help), Guillermo Acosta (Designing and welding new gas manifold), James Reno (Gas Lines), John Ellsworth (Help with stepper motors), Cort Johnson (Stepper motor controller and general help), Doug Markos (Help with measurements and deposition), Dan Allan (AFM work), Yenny Martinez (Cleaning and taking over), Fabian Walter (cleaning and alignment), Eric Hirshmann (Theory help and good advice), Spencer Olson (LabVIEW software and a bed in Michigan), Nan Ellen AhYou (Financial Patience, friendship, help finishing thesis), Dianne Sorensen (A happy person to talk to while waiting for Dr. Turley), Joe Fox (Diamonds from NovaTech), Jeff Taylor (Diamonds from DiamondCom), Scott Daniel

This work supported by: The Department of Physics and Astronomy at BYU, The Office of Graduate Studies at BYU, and The International Society of Photo Optical Engineers (SPIE)

Contents

List of Figures

List of Tables

Chapter 1

Background and Introduction

Between 1997 and 2001 the EUV research group at BYU has worked on coating surfaces for two space flight applications [1, 2]. This included optimizing high and low reflectance at specific wavelengths and angles. There were several issues that hampered efforts in both projects.

Difficulty making measurements in the EUV slowed both projects. EUV light is strongly absorbed by air so any measurements must be made in a vacuum. This is difficult because the materials and instruments used to make the measurement must be made from vacuum compatible materials. *In situ* alignment and pump down time are other difficulties when working in the EUV. From lessons learned during the completion of the first contract, a variable angle reflectometer (VAR) was designed, built, and successfully used to complete the second contract. The design and construction of the VAR are discussed in this thesis. Measurements of industrial diamond and graphite (HOPG) made using the VAR will be compared to previous measurements of diamond and graphite.

The other main difficulty in completing the contracts was uncertainty in the optical constants of the materials that were used to make the surfaces at extreme ultraviolet (EUV) and vacuum ultraviolet (VUV) wavelengths. In all cases there was disagreement between the published optical constants and the measured optical constants of the materials. In some cases the uncertainty may have been due to an unknown amount of water absorbed in the films after they were removed from the deposition chamber. Other films grew oxides when they were exposed to air. In some cases the oxides made little difference to the final design and performance of the mirror. In other cases the oxide was the only reason why the films met design specifications [3]. In all cases it was difficult to determine which optical constants were valid for an application, and then if the material absorbed water or oxygen, how to modify the published optical constants to match the observed optical properties.

At lower energies (visible light) and at higher energies (x ray) there are well defined theories to predict the optical properties of a material. This thesis will not entirely ignore low energy theories (i.e. Drude theory) but will concentrate on the theory of atomic scattering factors (ASF). ASF are successful at predicting the optical properties of materials in the x-ray portion of the electromagnetic spectrum, because ASF are independent of the density of the material. This allows the optical constants of a material of different densities and compositions to be predicted at x-ray wavelengths.

ASF theory does break down around absorption edges and in the EUV and visible. This is expected because the theory makes the assumption that the electrons are independent inside the atom. In the EUV and visible this assumption no longer holds because the energy of EUV and visible light is on the order of the energy of the bonds between atoms. Literature puts the lowest energy where ASF are successful at predicting optical constants at about 50 eV [4].

But atomic scattering theory is very useful at predicting the optical constants of compounds in the x-ray portion of the spectrum. If atomic scattering theory were used to predict the unknown optical constants of a material in the EUV what errors would be associated with the predicted optical constants? The error can be determined by calculating the relative error between the atomic scattering factors of diamond and graphite. Because diamond and graphite are only different phases of carbon, differing only in bonding, sp^3 versus sp^2, they should have the same atomic scattering factors independent of the density when the crystal bonding is unimportant. Any difference in their atomic scattering factors will show where and to what extent using ASF will introduce errors in the calculated optical constants in the EUV.

This thesis will contain two main points: 1) the design, construction, and measurements of the variable angle reflectometer and 2) analysis of the atomic scattering factors for diamond and graphite. The optical constants of industrial diamond and graphite (HOPG) measured using the variable angle reflectometer will not be used in the analysis because previous data sets were more extensive and reliable given that there was not enough time to measure the optical properties of diamond and graphite at more than a few wavelengths. This data is included, in part, as a test of the VAR. The analysis of the usefulness of ASF in the EUV will be evaluated using values published in References [5, 6].

Chapter 2

Experimental Setup

The EUV measurements are made using a variable angle reflectometer (VAR) that was designed and built with the help of Cynthia Mills. The operation of the VAR is automated using programs written in LabVIEW. The VAR is connected to a monochromator that is used to isolate one wavelength of light for measurement and a hollow cathode plasma lamp that is used to create the EUV light for the measurements. Figure 2.1 shows the relative sizes and positions of the VAR, monochromator, hollow cathode, and electrical components.

2.1 Hollow Cathode

The light source for all the measurements was a McPherson model 692 vacuum ultraviolet hollow cathode light source. It is also called a plasma lamp. Light is created by flowing gas into the cathode that is held around -700 VDC. A plasma is formed in the hollow cathode and the hot gas radiates spectral lines that are specific to the gas. For operating instructions see Appendix E and Reference [7].

Some sputtering occurs inside the hollow cathode because of the plasma. For lighter gases (hydrogen and helium) this is not a serious issue, but heavier gases (argon and neon) will significantly erode the interior walls of the hollow cathode. This occurred to the point, at one time in the past, that the cooling water eroded through the walls of the hollow cathode and flooded the monochromator! The majority of the erosion occurred in the tube where the gas flows into the cathode. All *in situ* alignment and testing were performed using the H Lyman α line at 1216 Å, because it was a very bright line, and there is a low sputtering rate.

Because the plasma was temporally unstable it was necessary to record the time variations of the intensity of the source. The gas pressure in the cathode affected the stability of the plasma lamp, but the optimal pressure changed from day to day. The gas pressure also influenced the intensity of the line emission [7]. The voltage was increased to 1 kV for very weak spectral lines. When running at high voltages it was important to make sure the ballast resistors were adequately cooled.

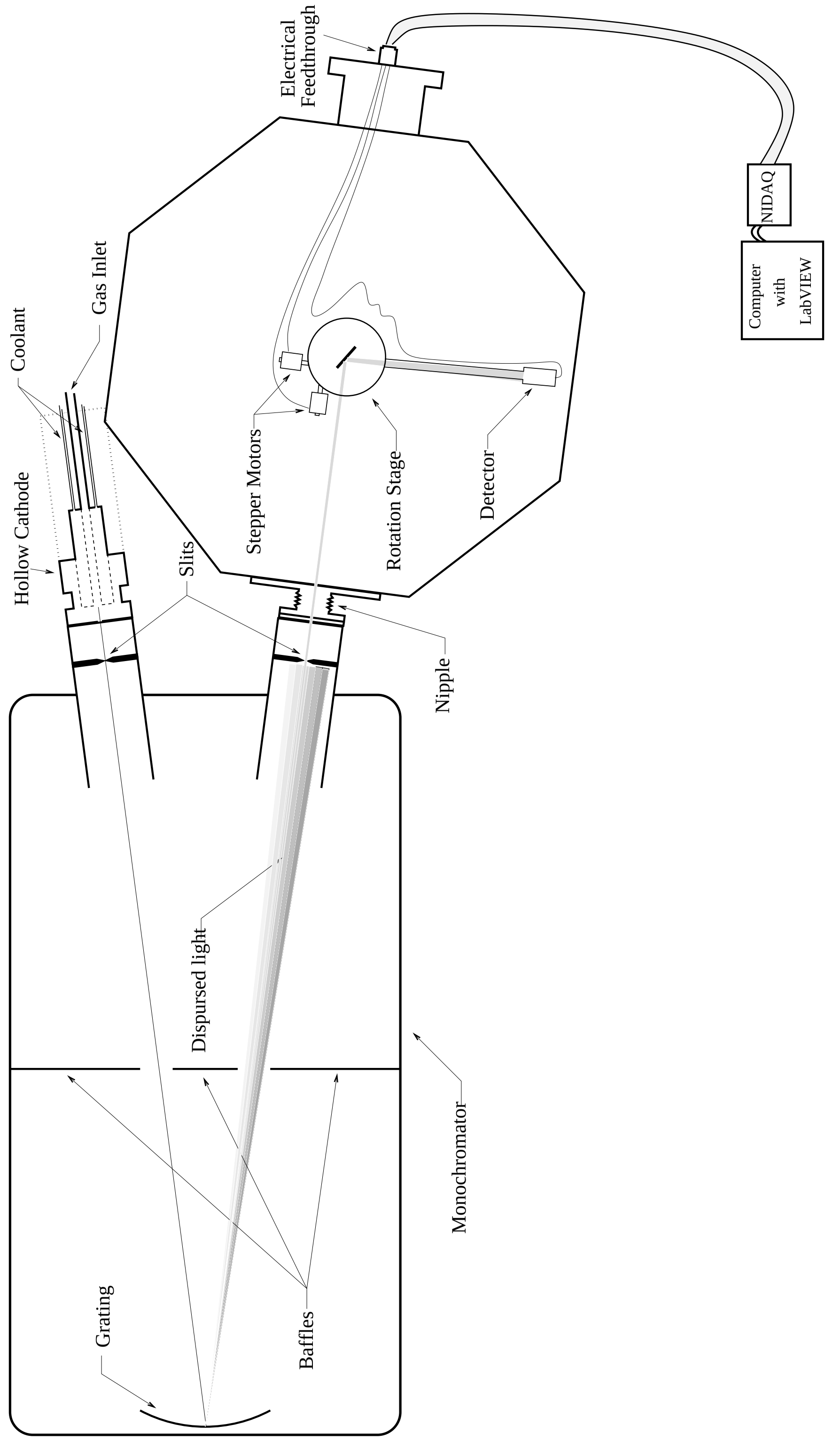

Figure 2.1: Schematic drawing of hollow cathode, monochromator, and VAR showing the relative sizes of the physical apparatus and electronic connections.

2.2 Monochromator

A McPherson model 225 vacuum ultraviolet (VUV) monochromator is used to separate and isolate one wavelength of light from other wavelengths that are created in the hollow cathode. The working principle behind function of the monochromator is similar to that of a glass prism. White light goes into the prism where the colors separate and come out at different positions. The process by which the light is separated is different but the light separating principle is the same. There are three essential parts for the operation of the monochromator. The entrance slit, the grating, and the exit slit.

The entrance slit is used to define the beam coming from the plasma lamp. The horizontal width is changed by turning a micrometer below the exit flange. The vertical width is changed by loosening the screws that hold the slits and moving the slits by hand. Only the horizontal width can be changed while the system is under vacuum. Changing the vertical width requires removing the hollow cathode (or VAR.) Practically it is used to adjust the amount of light entering the monochromator. Because a plasma is used for a light source opening the slits will also affect the distribution of light that enters the monochromator. Table 2.1 shows the horizontal widths of the entrance and exit slits used for measurements in this thesis.

λ (Å)	Entrance Slit (μm)	Exit Slit (μm)
584	250	250
1025	200	150
1084	175	175
1134	200	200
1164	200	200
1199	200	200
1216	200	150
1640	350	250

Table 2.1: Summary of horizontal slit widths used for different wavelengths of light.

The gratings used in the monochromator are concave reflection gratings coated with platinum or magnesium fluoride. The magnesium fluoride coated grating is used for wavelengths between 450 to 1600 Å, and the platinum coated grating is used for wavelengths from 250 to 1200 Å. The magnesium fluoride coated grating was exclusively used for all measurements because there was not enough time to clean the platinum grating which had been previously damaged by water spots.

The light that strikes the grating is comprised of several wavelengths of light that depend on the gas that is being used in the hollow cathode. The grating disperses, or reflects, each of these wavelengths at a different angle. By rotating the grating different wavelengths of light will focus on the exit slits. The basic equation for light reflecting off a grating is

$$\sin(\theta) + \sin(\phi) = \frac{n\lambda}{d} \tag{2.1}$$

where λ is the wavelength of interest, d is the distance between grooves on the grating, ϕ is the angle the light strikes the grating, and θ is the angle the light reflects off the surface of the grating. For a rigorous treatment of diffraction see Reference [8].

After the light has been diffracted it passes through the exit slits. The position of the slits only allows a narrow band of wavelengths of light to pass through because the exit slit is held at a fixed angle of 7.5° to the diffraction grating. The width of the exit slit determines the spectral purity of the monochromator. The wider the slits the more angles (wavelengths) will be able to pass through the slits. The width of the exit slit is typically not a problem because most of the light coming from the hollow cathode is spectral radiation at discrete wavelengths. If a continuous source was used it would be important to keep the exit slit small to limit the number of wavelengths that enter the chamber. Practically, as with the entrance slits, the exit slit is used to determine the intensity of the light entering the measurement chamber. In addition the larger the slits the more the intensity variations of the plasma will be blurred. Wider slits may also allow a larger amount of scattered light to exit into the measurement chamber.

2.3 Variable Angle Reflectometer

The variable angle reflectometer (VAR) was primarily built to measure specular reflectance at multiple wavelengths or $\theta/2\theta$ reflectance scans. It was also designed to be used for future needs, such as non-specular scattering, polarimetry, *in situ* deposition, and surface scans. The chamber is large enough to accommodate other equipment and there are enough free ports to add feedthroughs or other external equipment. The VAR was built with several short and long term goals in mind:

- Perform automated $\theta/2\theta$ scans between 5 and 85 degrees
- Rotate the detector and sample independently
- Move the sample out of the beam to make absolute reflectance measurements
- Scan the surface of the sample to verify uniformity
- Perform *in situ* deposition and measurements
- Interlock to transfer samples into the octagonal chamber (O-chamber)
- Polarimetry
- Transmission measurements
- Mount different types of detectors
- Be easily alignable

Not all of these goals have been realized by this writing but any of the goals can be implemented in the future with relative ease.

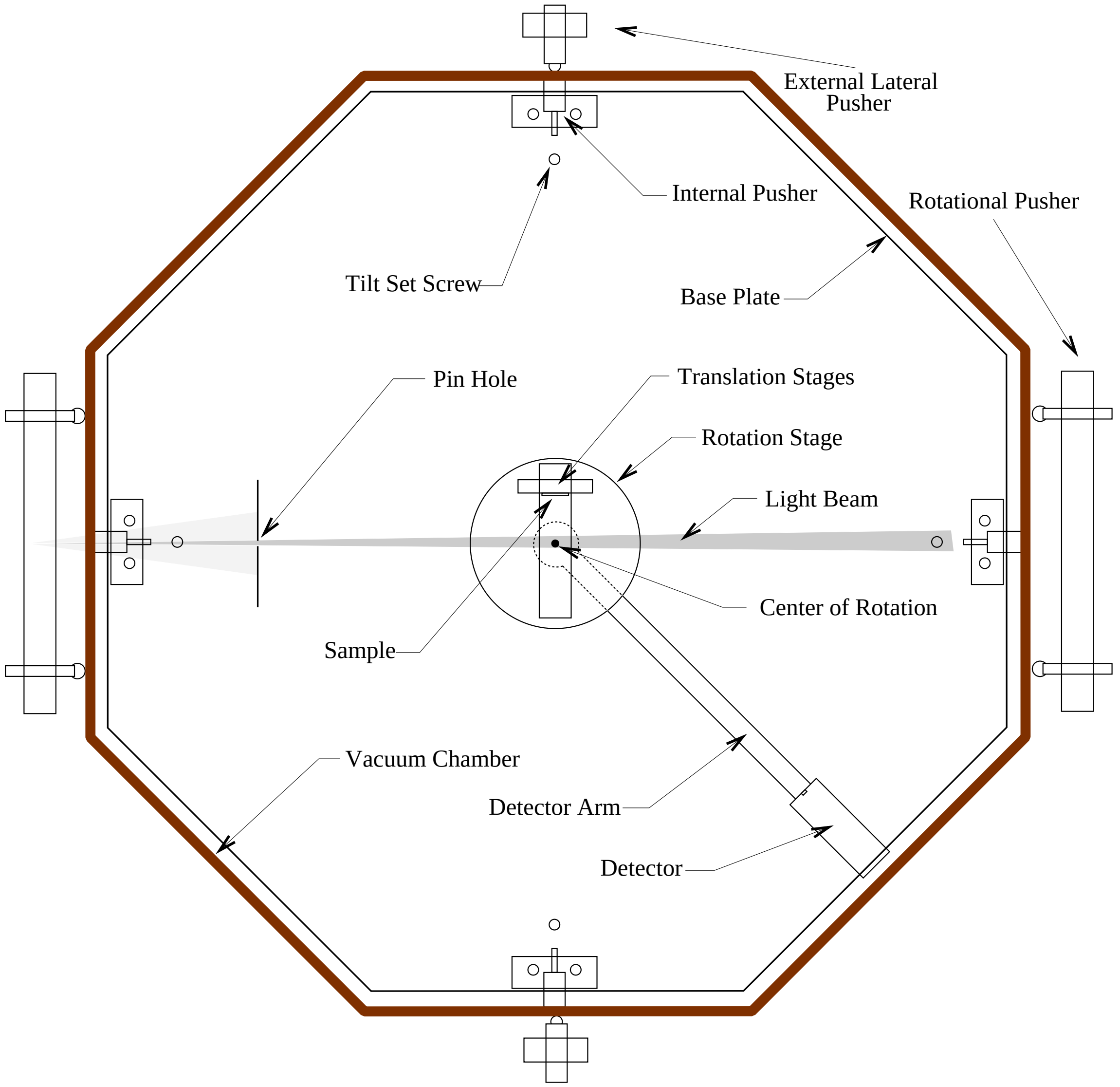

Figure 2.2: Schematic drawing of variable angle reflectometer, including internal and external hardware.

This section will focus on the design of the VAR and the principles and basics of how the VAR is aligned. As mentioned previously the VAR was designed to be flexible for future needs. To facilitate future research few parts are permanently fixed to the octagonal vacuum chamber, and as reasonable many elements of the VAR were designed so they could be adjusted to fit future needs.

Making accurate $\theta/2\theta$ measurements requires accurate alignment of the sample, detector, and light source [9]. An overview of the steps and alignment method is explained in the following sections. The full alignment procedure may be found in Appendix E.

2.3.1 Vacuum Chamber

The octagonal vacuum chamber (O-chamber) is connected to the monochromator by a stainless steel bellows that is welded to stainless steel flanges that correspond to the ports on the monochromator and octagonal chamber. The original nipple was a little too short so there was not sufficient room between the octagonal chamber and the hollow cathode. A 1/2 inch spacer plate was machined from aluminum that allowed the chamber to be properly aligned with adequate room around the hollow cathode. A mechanical lift was built by Greg Harris to lift the lid off the O-chamber. The chamber should be vented before opening the lid because the lift is strong enough to lift the entire O-chamber. At best, that would change the alignment and, at worst, break the bellows or the hollow cathode.

All parts inside the O-chamber at mounted on a 1/2 inch aluminum base plate that has holes drilled and tapped on a one inch square grid. This base plate is very convenient because it allows many different pieces of hardware to be mounted to fixed positions in the O-chamber. The rotation stages, rotational stepper motors, springs, and pinhole are all mounted to the base plate. The base may be positioned inside the chamber by adjusting four lateral pushers. The level or tilt of the base is adjusted by loosening or tightening four set screws mounted in the base plate. The position of the plate may be locked into place inside the chamber by equally tightening all the internal pushers against the walls of the O-chamber.

An electrical feedthrough is used to pass electrical signals to the motors, power the detector, and pass the detector signal out of the O-chamber. This feedthrough was constructed at BYU by Jason Flint, a student, and Joseph Young. It was made from a hermetically sealed military feedthrough that surprisingly held a vacuum down to 10^{-4} torr. However, this pressure was not acceptable for the operation of the detector. The pins on the vacuum side were extended and TorrSeal, a vacuum compatible epoxy, was applied to fill any remaining leaks. More details about the feedthrough construction may be found in Appendix C and Reference [10].

The vacuum pressure is measured by a Varian cold cathode gauge that is mounted on the chamber lid. The cold cathode gauge has set points that are used as a safety interlock for the channeltron detector so it is always operated at the correct pressure.

2.3.2 Exterior Alignment Hardware

The chamber is supported on a table that is used to adjust the height, angle, and lateral position of the O-chamber relative to the monochromator. The height and level of the chamber are adjusted by individually changing the height of the table legs. A carpenter's level is used to level the table by checking the level of the table along orthogonal directions. If the table is level the floor of the chamber should also be level. That was checked the first time the O-chamber was leveled before the base was installed in the chamber. The level of the O-chamber is important, but the level of the optical base in the VAR is much more important than the level of the table or O-chamber.

The lateral position of the VAR is adjusted by loosening and tightening screws in opposite lateral alignment blocks (see Figure 2.2). The angular alignment is changed by using the angular alignment blocks. The angle is changed by loosening and tightening the four screws in the angular alignment blocks. Changing the lateral alignment will change the angular alignment and visa versa. A good alignment may take several iterations of lateral and angular alignments.

2.3.3 Alignment of Monochromator and Measurement Chamber

Set up a laser on an isolated table with the table the VAR chamber sits on moved out of the way. The monochromator grating should be moved to zero angstroms so all zero order reflections may come out of the exit slit. Align the laser so it passes through the exit slits, reflects off the center of the grating, and comes out the entrance slits. If the laser does not come out vertically centered, the grating may need to be aligned. Consult the McPherson manuals for instructions on aligning the grating. The laser is now the reference for all alignments.

Center the VAR between the lateral and rotational alignment blocks by eye. Move the table and VAR into the beam of the laser so the laser passes through the cross hairs and the retroreflection from the cross hairs roughly returns to the laser. Bolt the bellows onto the monochromator. If the vertical alignment is off adjust the height of the table legs until the VAR is aligned in the vertical direction. Using the lateral and rotational alignment blocks align the VAR in the horizontal direction.

It is very important that the laser exactly retroreflects off the cross hairs because the cross hairs become the reference for major and minor alignments in the chamber. The laser can now be attached to the VAR table for easier use. A full alignment procedure is found in Appendix E.

2.3.4 Internal Alignment using Interior Alignment Hardware

As a general practice the interior hardware should be aligned or realigned after the O-chamber has been aligned with the monochromator. The interior hardware can be aligned with the O-chamber independent of the monochromator, but if the table is moved it may change the alignment of the interior hardware. There are two parts to aligning the interior hardware. Leveling the optical base and aligning the center of rotation with the laser.

The optical base is leveled by adjusting four set screws that are screwed in the optical base in front of the interior alignment blocks. If the base if has not be previously leveled use a carpenters level to roughly level the base. This angle of the base is changed by raising and lowering opposite set screws. The base can be leveled in any direction. The monochromator may not be perfectly level, so using a level is only the first step in aligning the VAR.

A laser is used to fine tune the level of the base. The laser is aligned perpendicular to the cross hairs on the back of the chamber. This defines what will be the path of light coming from the monochromator. Put a mirror in the sample stage. If the laser is able to reflect off the mirror and return along the same path, the optical base is aligned with the laser and the cross hairs. If the laser does not return along the same path, the optical base may be aligned by adjusting the set screws.

After the base has been leveled check to make sure the mirror is properly aligned with the detector. Swing the detector around until the laser is shining directly into the opening (This may require removing the rotational motors to get the needed range of motion.) Move the mirror into the beam and rotate the mirror and detector so the laser shines into the detector. The laser should hit the same spot on the detector both times. If it doesn't the mirror angle can be adjusted by loosening and tightening the screws on the base of the Z translation stage. Similar to other alignments this alignment may need to be refined using light from the monochromator.

Next align the center of rotation with a plumb bob. The laser is aligned with cross hairs and a plum bob is hung inside the chamber with the laser centered on the string. The optical base can be moved laterally using the interior alignment blocks until the center of rotation is directly beneath the plum bob. The mirror can also be used to align the center of rotation. Adjust the mirror so the laser is just grazing the surface of the mirror. Rotate the mirror 180° (The length of the cables that are connected to the XYZ stage may need to be increased). The laser should also just graze the surface of the mirror after it was rotated.

The position of the optical base is "locked" into place by tightening all of the interior alignment blocks into the walls of the O-chamber. Some care needs to be taken to preserve the alignment when locking the optical base into place. It is important to have the internal alignment blocks push directly into the walls without rotating. Any rotation in the blocks while pushing against the wall will change the level of the optical base. The original interior alignment blocks were screws with brass buttons on the ends to try to eliminate rotation due to friction. The brass buttons did not prevent the base from rotating and were redesigned. Even though the current blocks are slightly more complicated it is necessary for the interior alignment blocks to push on the wall without rotating.

2.3.5 Shaping the Beam with a pinhole

The beam coming from the monochromator is divergent with a cone angle of about 3^o. This causes several problems: 1) the beam will reflect off the mirror and into the detector even when the mirror is moved 15 mm out of the beam, 2) this also limits the smallest angle that may be used for analysis, and 3) there is more scattered light in the chamber. To solve these problems a pinhole is placed in the path of the light to narrow the beam. Using a pinhole also has the benefit of being a second

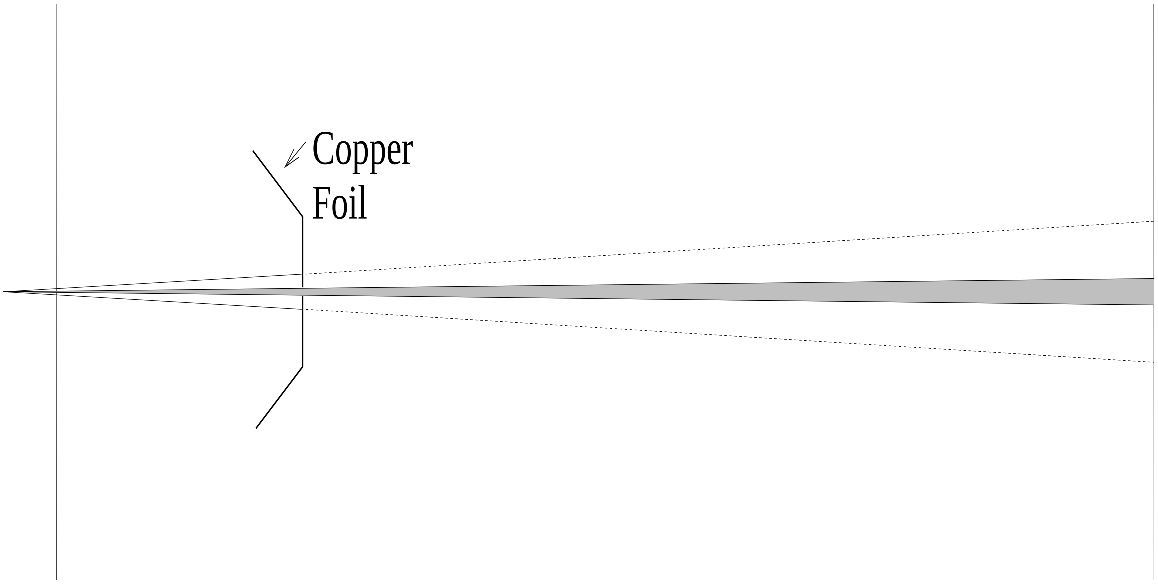

Figure 2.3: Schematic of pinhole redefining the beam from the monochromator.

reference point for the laser in the O-chamber. Because the size of the hole is much larger than EUV wavelengths it is assumed diffraction is a small effect and is ignored.

The pinhole is aligned using a small translation stage mounted to the baseplate. The laser is centered on the pinhole by monitoring the intensity of the laser coming through the pinhole. The vertical and lateral position can be adjusted until the intensity is maximized. The position of the pinhole will determine what part of the beam is sampled[1]. If the pinhole is not aligned there will be a shoulder on one side of the source beam profile. This can slightly be seen on the left side of the most intense beam in Figure 2.4.

It may be asked if the pinhole will change the width of the beam if the widths of the entrance and exit slits are changed. If the width of the beam profile changes at full width half max (FWHM) or at full width full max (FWFM) then the pinhole is changing the beam profile in a non-reproducible way. Figure 2.5 shows two sets of data that are normalized to unity by dividing by the intensity at the peak of each curve. Despite different slit sizes and source intensities (see Figure 2.4) the two curves are identical. The beam width at FWHM is about 1.5°. Figure 2.5 also shows the signal to off-peak noise ratio is about 1 part in 10^3. It can also be seen that the curve that corresponds to the lower intensity is slightly more noisy, as would be expected if the beam was ruled by Gaussian or Poisson statistics.

2.3.6 Rotation Stages

To get the $\theta/2\theta$ sample detector movement and independent sample detector movement there needed to two distinct rotation stages that could be moved independent of all other parts. Cynthia Mills

---

[1] The position of the pinhole may be used to aim the path of the light in the chamber. I know this should work but I have not explored what errors, if any, it introduces.

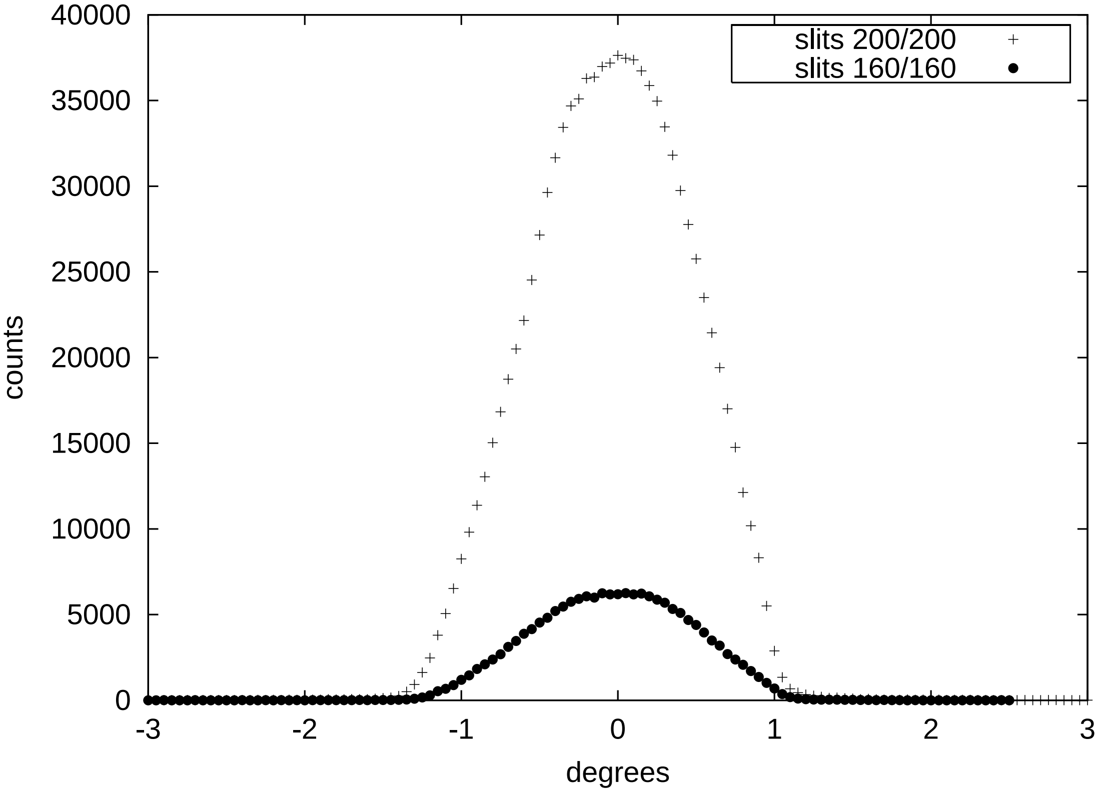

Figure 2.4: Measured angular width of beam after pinhole. The slits widths are reported as (entrance/exit) in μm. The size of the pinhole used for all measurements is about 0.5 mm in diameter

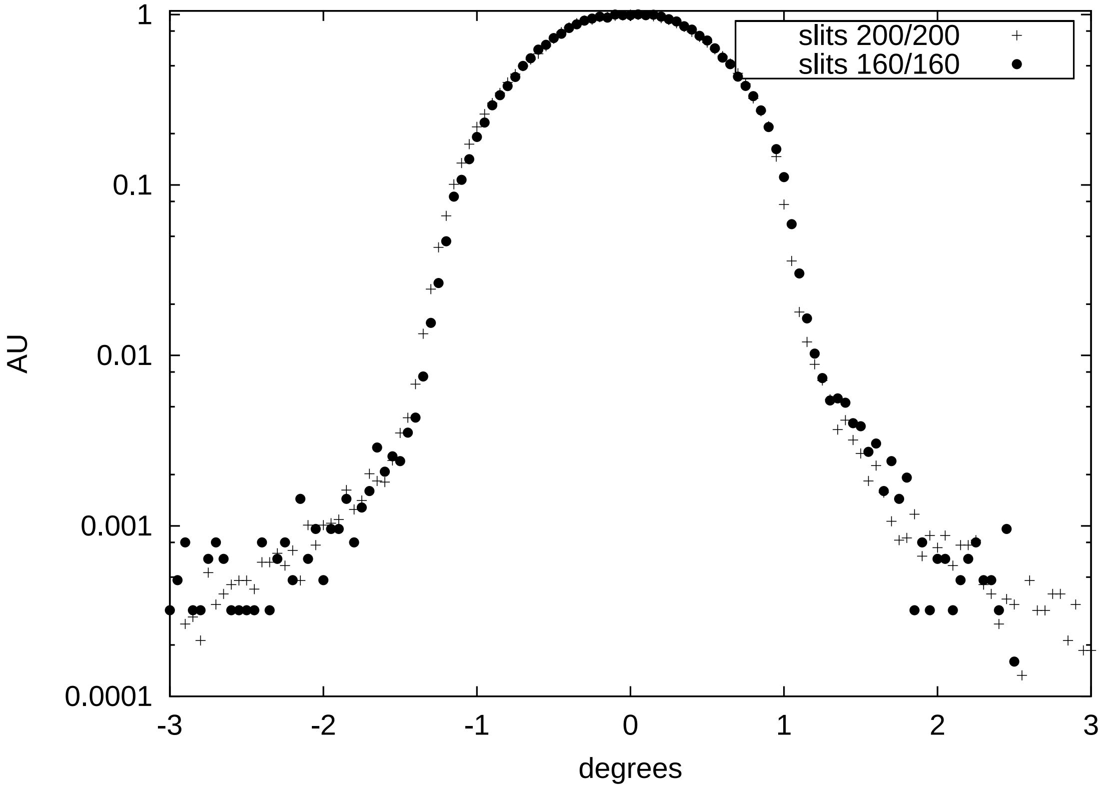

Figure 2.5: Measured angular width of beam after pinhole. The slits widths are reported as (entrance/exit) in μ m. The size of the pinhole used for all measurements is about 0.5 mm.

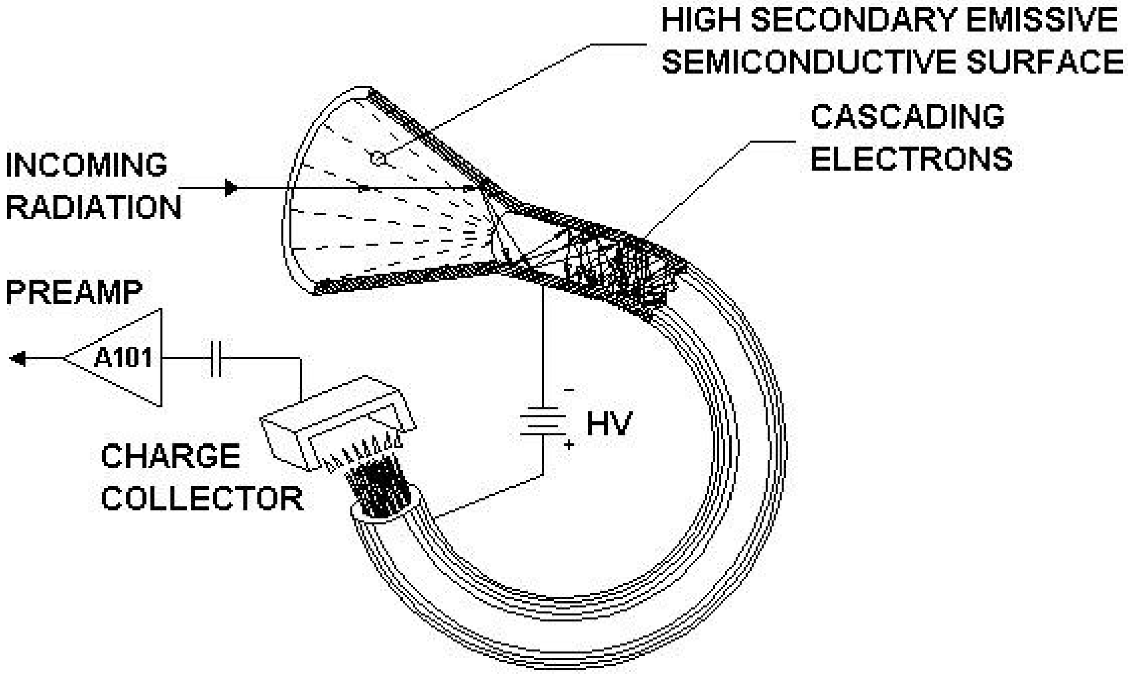

Figure 2.6: Schematic of CEM operation showing electron avalanche triggered by incoming photon [11].

looked for commercial rotation stages, but could not find rotation stages that would be able to rotate 180° with no coarse adjustments and would meet the space constraints of the chamber. Because there were no commercial parts available, Cynthia and Wes Lifferth designed the rotation stages. Then Wes machined the two rotational parts. The mechanical drawing for the rotation stages may be found in Appendix C.

2.3.7 Translation Stages

An XYZ translation stage was built to make it possible to move the sample out of the beam path, and scan the beam across the sample to check for uniformity. The stage was built by Cynthia Mills using a design that Dr. Peatross had previously used. He gave us a part that attaches the Z stage to the X and Y stages. The stages are moved by stepper motors purchased from Haydon Switch and Instrument. The carriages were made by Techno-Isel Linear Motion Components. The carriages use ball bearings to reduce the friction while keeping the carriage fairly stable. These ball bearings can pop out when the carriage is being placed on the rail. Work over a cloth or towel so if a bearing does escape it is not lost. The bearings can be pushed back into their original position very easily. There was also a little wobble in the translation stages. This wobble was removed by attaching a spring from the top of the Z stage to the bottom of the X stage.

2.3.8 Channeltron Detector

A model MD-501 Ampteсktron made by Amptek Inc. was used to measure the intensity of the light. The MD-501 uses a channel electron multiplier (CEM) to detect light. The CEM works by creating an electron avalanche of 10^7 electrons for every one photon. The avalanche is initiated when a photon strikes the opening of the CEM. If the photon has enough energy it will eject one or more electrons from the surface of the CEM. That electron is accelerated by a high voltage to the other side of the CEM where it ejects more electrons that cascade inside the CEM until they exit and are detected (see Figure 2.6).

The CEM is integrated in a package that contains all the necessary electronics to supply the high voltage that drives the CEM, then amplifies, and shapes the output signal. The MD-501 has a dark count of less than one count/sec. This dark count was ignored in all measurements because it is so small.

It is important to be very careful when operating the MD-501 because the CEM requires 2.4kV to operate[2]. The MD-501 *must* be operated at a pressure lower than 1×10^{-4} torr or the high voltage will create a plasma in the CEM that will act like a short circuit and destroy the electronics in the MD-501. The plasma is also bad for the CEM because it can erode the walls of the CEM.

2.4 LabVIEW Programs

Making measurements by hand is a difficult and error-prone process. By automating the process it is faster to make measurements and easier to account for source fluctuations in the calculation of the reflectance. This was done using the LabVIEW software and a National Instrument Data Acquisition board (NIDAQ). Several programs were used to make the measurements. This section will only outline how the key components of the programs work. There are three main programs: FindMax, T2T (Theta 2 Theta), and VAR (Variable Angle Reflectance). In the future these file names may change but the concept of making measurements should be the same.

The LabVIEW VAR virtual instrument (VI) that was used to make all the measurements is heavily dependent on the FindMax.VI to find the peak of the reflected beam. Because of round off in the subVI (StageControlSpring.VI) that controls the motors it was necessary to make sure the detector was centered on the beam each time it made a measurement. Most of the time spent in making the measurements is finding the maximum position of the beam. If the round off can be eliminated from the StageControlSpring.VI, it will be possible to use fewer steps to find the peak or be able to center on the peak with no addition searching for the peak intensity. Figure 2.7 outlines the process for finding the maximum intensity of the beam.

The FindMax.VI is used in T2T.VI a $\theta\backslash 2\theta$ program that will perform a simple theta two theta reflectance scan. This subVI is not a workhorse like FindMax.VI, but simplifies programming a more complex reflectance scan that checks the source intensity at various times during a multiple

---

[2] It is always a good idea to be careful around high voltages, but from my experience the MD-501 is not lethal under normal circumstances. It does hurt if you happen to touch it.

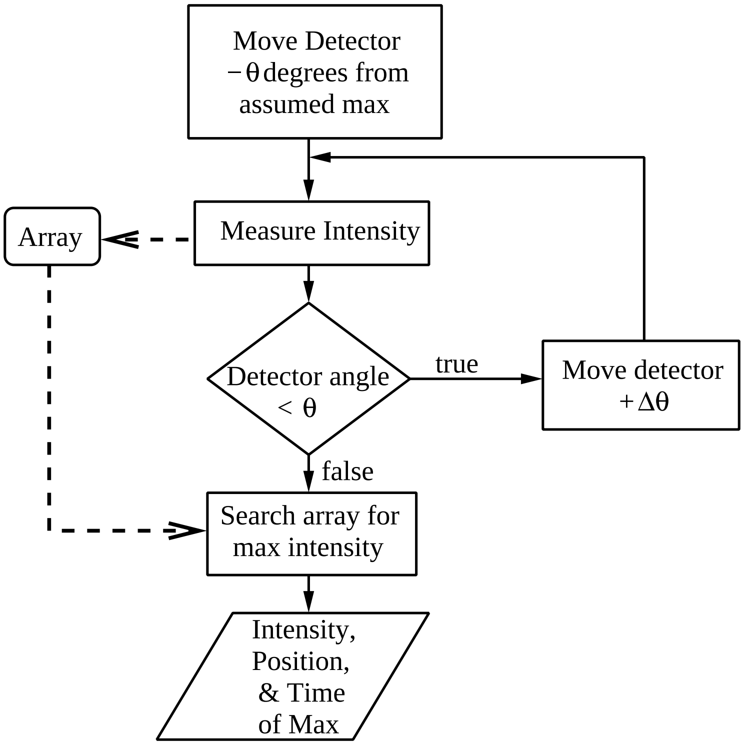

Figure 2.7: Flowchart of FindMax subVI. The dashed lines indicate the flow of data.

angle reflectance measurement. Figure 2.8 shows the process of making a $\theta\backslash 2\theta$ scan.

The VAR VI combines all these programs and is entirely automated after the mirror and detector are initially aligned. It checks the source intensity several times during the measurement and records the time when the measurements were made to take into consideration the time varying fluctuations of the source. It also calls other subVI's to perform data analysis and make graphics files. The data analysis is explained in Section 3.3. Figure 2.9 shows the process VAR.VI follows to take data.

All the LabVIEW programs may be found in Appendix C.3. They may also be found at http://xuv.byu.edu/thesis/MSthesis.pdf.

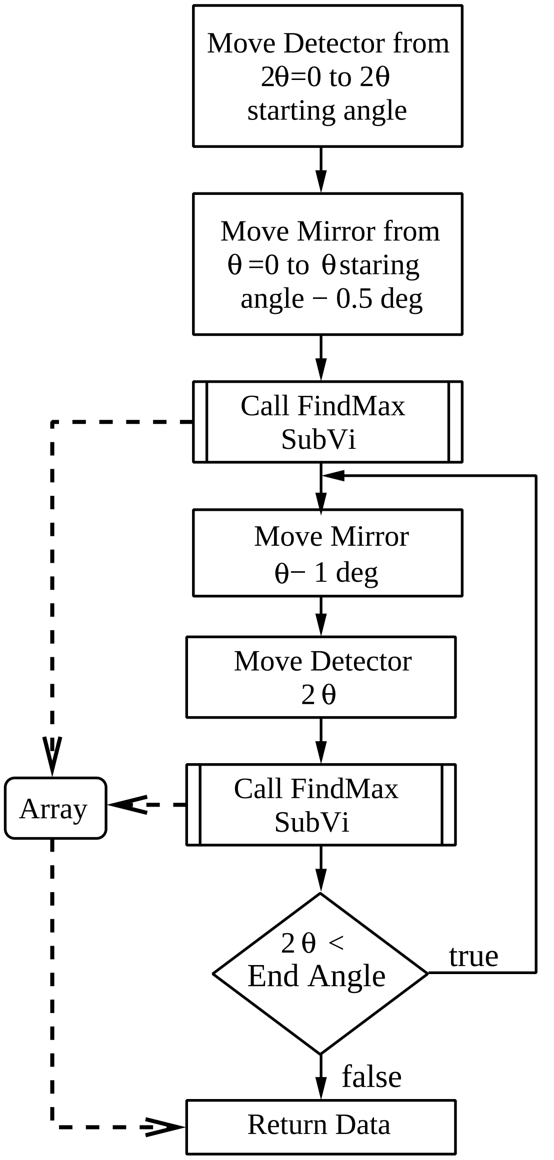

Figure 2.8: Flowchart of T2T subVI. The dashed lines indicate the flow of data.

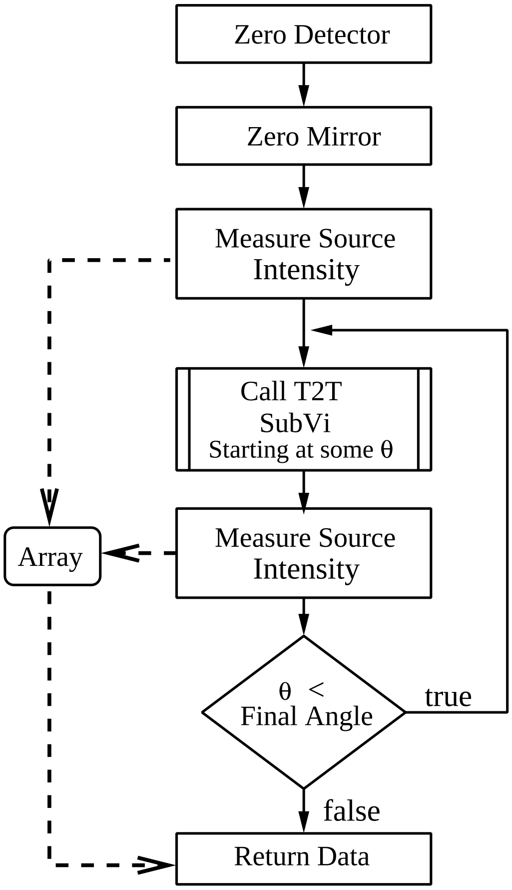

Figure 2.9: Flowchart of VAR subVI. The dashed lines indicate the flow of data.

Chapter 3

Analysis of Data Taken Using the VAR

This chapter will show a summary of the optical constants determined from the data taken using the VAR and will largely focus on the analysis used to calculate the optical constants from the measurements. Plots of the reflectance data and the confidence intervals are found in Appendix D. Figure 3.1 shows a typical reflectance measurement that has been used to fit the optical constants of the material. This data has been adjusted for irregularities in the surface of the diamond as will be explained in Section 3.2.2.

3.1 Summary of Measured Data

	diamond				HOPG			
λ (Å)	n	±	k	±	n	±	k	±
584	0.87	0.30	1.23	0.06	1.34	0.25	1.02	0.12
1025	1.38	err	1.22	err	1.42	0.15	0.63	0.11
1084	1.92	0.05	1.45	0.005	1.12	err	0.42	err
1134	1.98	0.07	1.32	0.02	1.63	0.05	0.17	0.12
1164	1.51	0.25	1.03	0.10	1.59	0.07	0.05	0.14
1199	2.08	0.06	0.99	0.02	1.43	0.07	0.20	0.14
1216	1.77	0.12	1.12	0.005	1.45	0.13	0.48	0.11
1640	2.05	0.29	1.07	0.10	0.97	0.17	0.40	0.10

Table 3.1: Summary of measured diamond and graphite optical constants measured at BYU using the variable angle reflectometer.

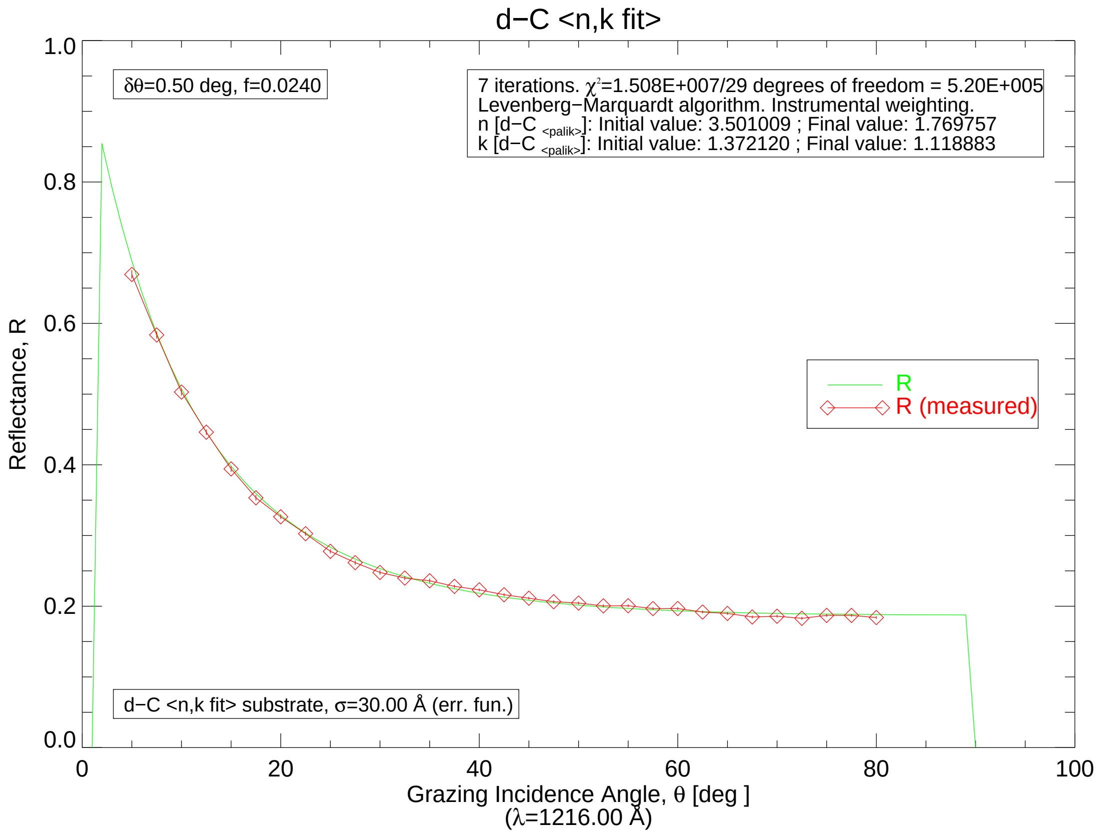

Figure 3.1: Example of variable angle reflectance data showing reflectance of diamond at 1216 Å. Statistical error bars are included but are smaller than the diamond marking the data.

3.2 Fitting Considerations

Fitting data to a complicated model is, at best, an art. Some of the "art" required may be avoided by making the model to be fit as simple as possible. This thesis was designed to use single bulk layers of a material to keep the fitting model simple. Carbon was also used in this thesis because carbon does not form an oxide that would complicate the fitting model by adding addition fitting parameters to the model.

There are other factors that should be considered when fitting the optical constants of a material. Measuring the reflectance at multiple angles is best suited for determining the real part of the index of refraction. The imaginary part may also be determined by using reflection measurements, but the absorptive properties of a material is best determined by measuring the transmission through a film of known thickness. Analysis of reflection data does a reasonable job at determining the imaginary part of the index of refraction (see Table 3.2). Data taken using a bulk sample will only give the optical constants for the bulk material. The optical constants of a thin film will differ from those of the bulk material, but that is not the object of this thesis. For more on the optical constants of thin films see Windt [12].

3.2.1 Uniqueness of Solution

It is important to address the question of uniqueness, because a reflectance curve fit to a data set may look good to the eye or even have a low χ^2, but there may be several combinations of n and k that will fit the data well. If there is more than one reflectance curve that will fit this data well then there is not a unique solution for one reflectance curve. If there is more than one solution, the best solution needs to be found. This problem has been addressed before and there are many known ways to find global extrema [13]. The global extrema in this case is the best n,k values that will fit the data assuming all n,k have been tried as possible fit parameters. A local extrema may be found if only a certain range of n,k values are used. Then it is possible that the best n,k are outside the chosen range. It is very difficult to verify that the "best" fit n,k values are truly the values that nature uses. Finding "best" fit n,k values can also be affected by systematic error in the model or data.

A simple way to see if there is one good solution to a set of data is to calculate a set of data using a well defined set of optical constants. Then put the calculated data back into IMD, but with the wrong initial conditions and fit the contrived data to see if it fits the same data to the original n and k. If the fit values of n and k match or are close to the original, even if initial conditions are obviously wrong, it may be assumed the n and k determined from the fit are unique. This is by no means a proof that the fit values are unique but it is a simple test to show how much a fit number may be trusted to be unique. The following table shows that in all cases, except for when $n = 0.601$ and $k = 0.010$, the fit optical constants match the original optical constants accurately to three decimal places. The initial n and k used for the fits are 1 and 1[1]. Table 3.2 covers a broad range

---

[1] Originally the initial value of k was zero, but IMD warned a small original value is a bad starting point. I tried it anyway, and it gave horrible fits, so I chose k to be the next positive integer, one.

Original		Fit		Original		Fit	
n	k	n	k	n	k	n	k
0.601	0.010	0.601000	0.009999	1.111	0.010	1.111000	0.010000
	0.111		0.111000		0.111		0.111000
	0.333		0.333000		0.333		0.333000
	1.111		1.111000		1.111		1.111000
	2.222		2.222000		2.222		2.222000
1.333	0.010	1.333000	0.010000	1.699	0.010	1.699000	0.010000
	0.111		0.111000		0.111		0.111000
	0.333		0.333000		0.333		0.333000
	1.111		1.111000		1.111		1.111000
	2.222		2.222000		2.222		2.222000

Table 3.2: Computational results of fitting dummy indices of refraction to contrived data, using the initial values $n, k = 1$. Some uncertainties are listed are err because the confidence interval was difficult to interpret.

	Original	Fit	Error in Fit
n	0.601	0.601294	0.05%
k	0.010	0.009626	3.74%

Table 3.3: Compare good reflectance data with erratic reflectance data.

and the results show that these initial conditions will fit any range of n and k to be found in the EUV. This is only shown for a single bulk material. Fitting the optical constants and thicknesses of various thin layers will not always yield a unique result.

The results of Table 3.2 are based on data that was calculated using IMD. In real life the data will not be smooth, but may have regions where there is significant error in the data. Ignoring the error bars that may be calculated, will the values of fit optical constants still be reasonable? To provide one possible answer to the question take one set of calculated data from Table 3.2 and convolute the original data with Gaussian noise. Then, as before, fit the data using the initial optical constants $n, k = 1$. The fit does not exacly match the original optical constants, but the data is flawed at several places. Data that is as obviously flawed as the data in Figure 3.2 should be remeasured. The error in n is acceptable, but there is quite a large error in k. The value of $\tilde{\chi}^2$ is 3.7×10^{-4} larger than the $\tilde{\chi}^2$ (9.9×10^{-11}) of a smooth set of data. But the $\tilde{\chi}^2$ of the data with Gaussian error is still much less than one indicating that the fit is reasonable (see Section 3.3.2).

3.2.2 Fitting Model

Surface Roughness

The surface roughness is one parameter of the fitting model that was measured using atomic force microscopy (AFM). Because the surface roughness has been measured using an external method it

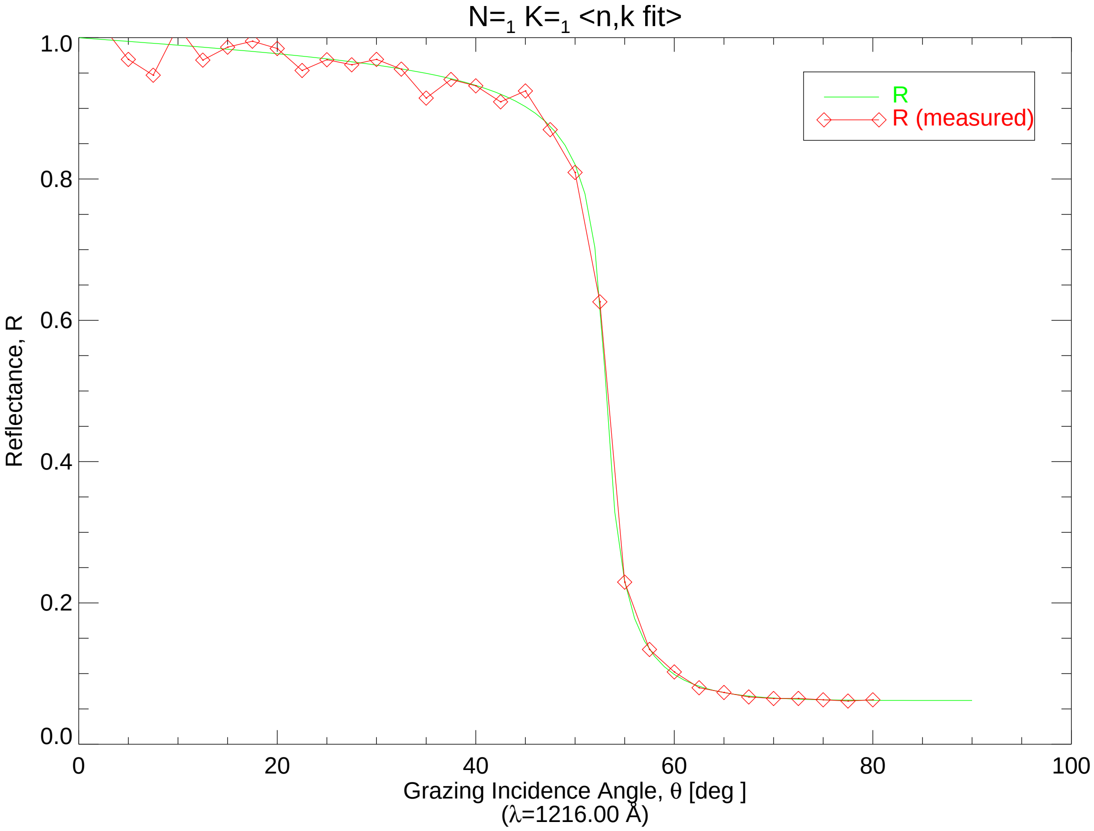

Figure 3.2: Fit of data that purposely had Gaussian error added and was then fit using initial parameters $n, k = 1$. The error was added by multiplying the original data by a random set of numbers that had a Gaussian distribution. Because the error was multiplied into the data the noise is more easily seen at points of higher reflectance.

does not have to be fit to the model. This reduces the number of fitting parameters, and AFM is the preferred method for quantifying the surface roughness at the sub nanometer level.

It is also important to know the surface roughness because it can make k appear to be larger than what it really is. If light is scattered into another direction by an irregularity on the surface it will not go into the detector, just the same as if it had been absorbed into the material. The surface roughness will also affect the determination of n because the surface will appear to be less reflective, giving the surface an effectively lower n. The relative changes in the surface roughness have to be on the order of tens of angstroms before the effect on the optical constants is large enough to be obviously wrong. But to accurately determine the optical constants it is important to include roughness in the model that will be used to determine the optical constants

The surface roughness is calculated from the calculated power spectral density (PSD). The PSD is calculated by taking the Fourier transform (FT) of the features on the surface of the sample. Because there is roughness over different length scales, there are semi-periodic fluctuations on the surface of the sample. The FT of the surface calculates what variations are periodic over multiple length scales. The PSD gives a measure of the roughness over large and small scales. The roughness is obtained by integrating the PSD. This is actually the two dimensional form [14].

$$\sigma^2 = 2\pi \int_0^\infty PSD(f)\, f\, df \tag{3.1}$$

Diamond (Industrial Fused)

Industrial diamond made from hot pressed, fused diamond micro-crystals was used for all the measurements in this thesis. After the diamond was fused together it is assumed the surface of the diamond was polished using a diamond paste. Because of the polishing a significant amount of roughness was expected. What was unexpected were deep pits that cover the surface of the sample (see Figure 3.3). The pits do not completely obscure the surface because the areas between the pits are flat from the polishing. The sides of the pits are sufficiently steep and the bottoms are rough so it is assumed that any light that enters a pit will be scattered into all directions. The effect of these pits is to reduce the area of the diamond that will reflect light.

The area of the sample that is covered with pits is calculated by importing the AFM image into MATLAB and counting the number of pixels that are black by calculating a histogram of the intensity of the pixels (see Figure 3.4.) This was done using a simple program that can be found in Appendix D.3. The pits cover about 2% of the surface of this image. This image is representative of the whole surface of the diamond.

All the diamond data was modified by the following function. The extra term is put in the denominator because the measured reflectance will be smaller than it should be if there are pits on the

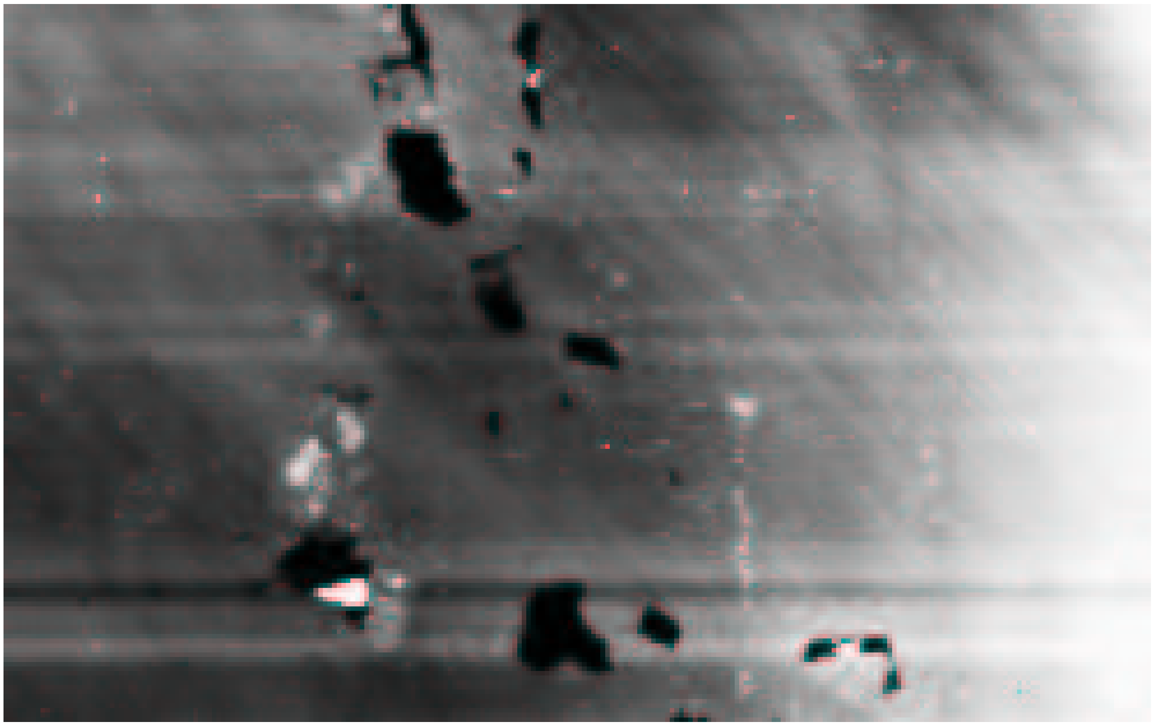

Figure 3.3: AFM image of diamond showing the pits on the surface. The pits take up approximately 2% of the surface. The lines that cross the image diagonally are assumed to be from polishing.

surface of the sample[2].

$$R_m = \frac{R}{(1 - 0.02)} \tag{3.2}$$

The surface roughness of the flat areas between the pits was determined by PSD to be about 30 Å rms roughness.

Graphite (HOPG)

The surface roughness of the graphite was small enough that the background noise was the significant contribution to the signal measured by the AFM. The resolution of the AFM is at worst 1–2 Å, so it is assumed that the roughness of the graphite is less than 2 Å. In the fitting models the roughness of the graphite was set to zero.

---

[2] The data used in the fitting was actually modified by

$$R_m = \frac{R}{(1 - 0.02 \sin\theta)}$$

It was later determined that that it would be better the remove the angular dependence. The calculated values of n and k should be *slightly* different, and given the systematic errors in the data this mistake is well contained within the error bars.

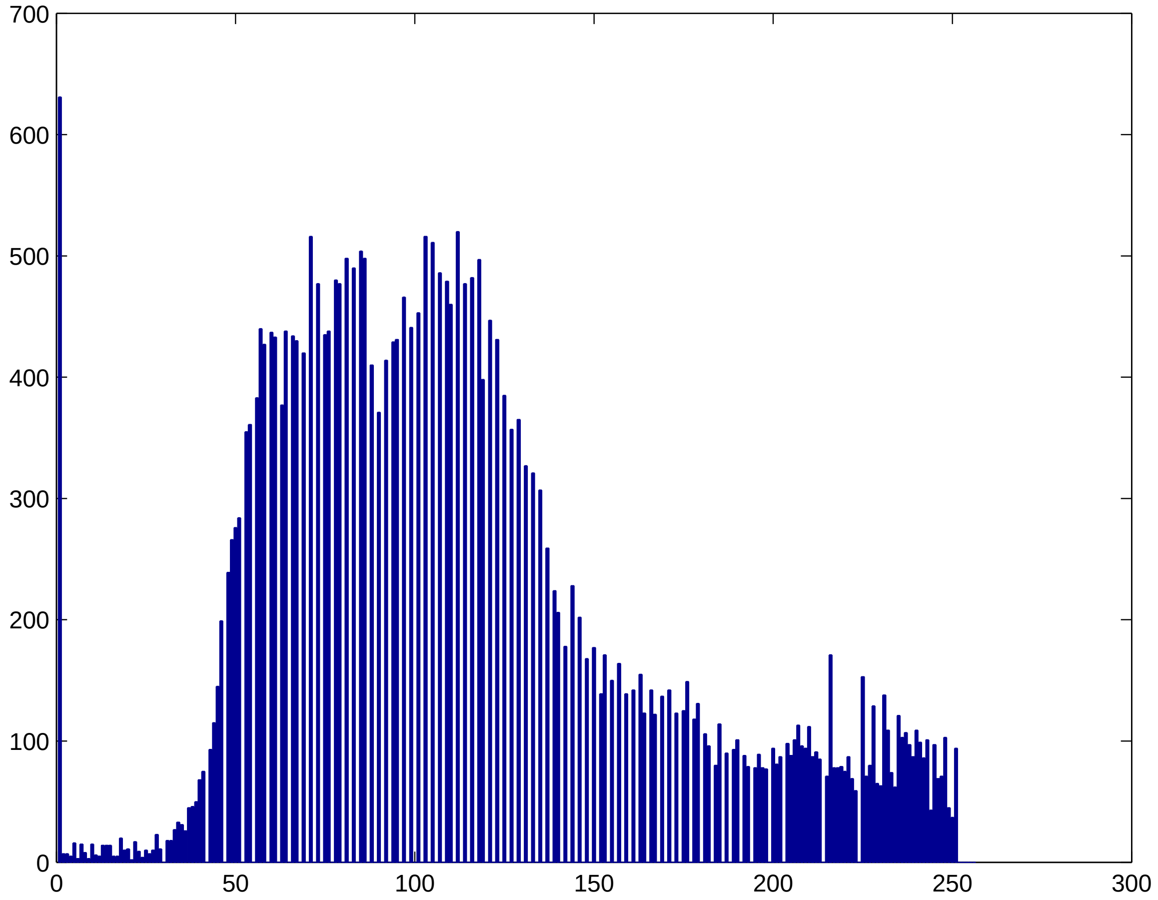

Figure 3.4: Histogram of AFM image to determine what fraction of the surface is covered by pits. The number of black pixels in the first bin is about 630 and the size of the image is 135 x 248, so about 2% of the surface is covered by pits.

3.3 Error Analysis

To accurately describe the optical properties of a material it is necessary to report the measured value and the error associated with the determination of the reported value. This thesis is not devoted to statistics, but it is important to explain the statistical methods used in fitting the optical constants. It is also important for anyone who wants to understand the statistics that is used in the LabVIEW VI's. The standard error, SE, will be used as an approximation to σ, the standard deviation in fitting the optical constants and calculating the confidence intervals. IMD will be used to fit the optical constants and calculate confidence intervals based on the χ^2 test to verify the reported error bars.

Two sources of error will be considered in calculating SE. Any other error due to misalignment of the apparatus is assumed to be negligible (see Appendix E for alignment details.) The first error is due to the counting of individual photons entering the detector during a beam intensity measurement. This type of error is often known as “shot noise” and is described by a Poisson distribution. For large numbers of counts ($n > 1000$) a Poisson distribution approaches a Gaussian distribution [15]. Assuming that there are enough counts and that Gaussian statistics are sufficient, the error contribution due to “shot noise” is given by

$$\sigma = \sqrt{n} \tag{3.3}$$

3.3.1 Time Dependent Source Variations

The second source of error is due to the time variations of the source intensity. For unknown reasons, the intensity of the source may be constant, increase, or decrease over time. In other measurement systems this is reconciled by using a second detector to measure the intensity of the beam before it reflects off the sample. This second detector is used to normalize the source intensity at the same time the reflected intensity is measured. In general this would be the preferred method for monitoring the fluctuations of the source intensity because the source intensity can be measured without moving the detector. This saves time and possible misalignment. Due to time and other constraints a second detector was never installed. To account for the time variations of the source, the source intensity is measured multiple times during the measurement of a sample. Then a quadratic function is fit to the variations in the source intensity so the intensity of the source can be interpolated for any time.

The General Polynomial Fit VI from the Mathematics, Fitting section of LabVIEW is used to fit the source intensity measurements to a line. The details about how it works may be found by going to the Help section in the LabVIEW program. The error associated with the fitting is calculated using inference for regression that is very similar to a weighted multiple regression [16]. The standard error is given by

$$SE = s\sqrt{\frac{1}{n} + \frac{(x^* - \bar{x})^2}{\sum(x - \bar{x})^2}} \tag{3.4}$$

Where n is the number of source intensity measurements, x^* is position that is being evaluated, and s is given by

$$s = \sqrt{\frac{1}{n-2} \sum (y - \hat{y})^2} \tag{3.5}$$

where $\hat{y}$ is the calculated source intensity.

The total error of the source intensity is combined with the "shot noise" error of the reflected intensity by summing the squares of the fractional standard deviations. This assumes the "shot noise" and fitting error are uncorrelated. This is a valid assumption because the source intensities and reflected intensities are measured at separate times. This would not be true if a two detector setup was used because the source intensity variations would be measured at the same time the reflected intensity was measured. The fractional standard deviation is

$$S = \frac{s}{X} \tag{3.6}$$

The combined standard deviation is then given by

$$S_{tot} = \sqrt{S_1^2 + S_2^2} \tag{3.7}$$

3.3.2 Test for Goodness of Fit

This section follows the discussion in Reference [17]. The χ^2 test is used to test if the error bars calculated using the standard deviation are reliable. The χ^2 test assumes the distribution is Gaussian and compares the relative difference between the fit reflectance and the measured reflectance to the standard deviation.

$$\chi^2 = \sum_{k=1}^{n} \frac{(O_k - E_k)^2}{E_k^2} \tag{3.8}$$

where n is the total number of measurements, O is an observed values, and E is the expected value. The fit is considered good if $\chi^2 < n$ and poor if $\chi^2 \gg n$.

Degrees of Freedom and Reduced χ^2

A better way of testing the goodness of a fit is to compare χ^2 to the degrees of freedom instead of n the number of data points. Depending on the data or the complexity of the fit there will fewer degrees of freedom compared to the number of data points. Another way to look at it to say each data point carries information. If a parameter is fit to a data point the information in that data point has been used, and it cannot be used again to calculate other parameters including χ^2. The number of degrees of freedom is easily calculated

$$d = n - c \tag{3.9}$$

where n is the number of data points and c is the number of constraints or parameters that are being fit to the data set. Using this definition the expected value of χ^2 should be d, the degrees of freedom.

$$\chi^2_{expected} = d \tag{3.10}$$

This may be taken a step further by dividing χ^2 by d to get the reduced chi squared or the chi squared per degree freedom.

$$\tilde{\chi}^2 = \chi^2/d \tag{3.11}$$

Now the expected value of $\tilde{\chi}^2$ should be 1 or smaller. This is only approximate; if $\tilde{\chi}^2 \sim 1$, the fit may still be good. But if $\tilde{\chi}^2 \gg 1$, then there is significant error in the fit. The reduced χ^2 of the fit n,k values is much greater than one. The fits appear to follow the data, but the error bars associated with the data only describe the statistical error in the data. There is still systematic error that is present in the data. The large value of the reduced χ^2 is indicative of systematic error in the data. The systematic error may be estimated to obtain a smaller reduced χ^2, but this was not done because of time constraints. Some systematic errors can be seen in the data (see Appendix D). These include having little data a grazing incidence because of the small size of the samples, jumps in the data where the source intensity was normalized, and dim spectral lines requiring longer integration times. The $\tilde{\chi}^2$ of the fits was very large because the error bars used to calculate the optical constants did not include the systematic errors. The $\tilde{\chi}^2$ for each fit can be read off the plots in Appendix D.

Chapter 4

Atomic Scattering Theory

The second purpose of this thesis is to determine what is the error associated with using atomic scattering factors (ASF) to determine the optical constants in the EUV. This can be done by seeing where the atomic scattering factors of graphite and diamond are significantly different. The definition of significantly different will depend on the application.

To compare data to a theory requires at least a working understand of the theories to be tested. Atomic scattering theory is very good at predicting the optical properties of a material in certain regimes of the electromagnetic spectrum. Most theories make assumptions to make it possible to find an analytic solution. Only a first principles calculation, that makes no assumptions, will accurately predict the optical properties of a material.

Only atomic scattering factors will be covered in the body of this thesis but Drude theory and Lorentz oscillator theory are covered in Appendix A.

4.1 Independent Particle Approximation

At high enough energies (typically > 50 eV) it is possible to assume that the core electrons will participate in the determination of the optical properties of a material. If the light has enough energy it will interact with a fixed number of core and valence electrons. If the light is higher or lower in energy different groups of core electrons will be involved in the interaction with the light. Eventually at high enough energies all the electrons in the atom will be involved in the interaction.

It would be desirable to determine how many electrons are participating in the interaction with the incoming light. It would be even better if at high energies the parameter the represents the index of refraction would equal the atomic number of the element. For example, carbon has six electrons so at high energies this parameter would be six. This means that all the electrons in a carbon atom are interacting with the light by reflecting or refracting the light. Besides using Kamers-Kronig relations (see Section 4.2.2) to check the validity of the calculated optical constants, a simple check would be to make sure the limit at high energy was six.

This theory is known as atomic scattering factors (ASF). It assumes the electrons are free to respond the the electric field, and is based on classical physics that describes each electron as a point charge that scatters light in many directions. For example, for a given atom at some energy four electrons are interacting with the light. Multiply the scattering effects of a classical electron scattering light by four to get the effective scattering of that particular atom.

The following is not a perfect example, but it illustrates the point. Imagine stirring gold spheres into a bucket of water and measuring the reflectance of the water and how much light it transmitted through the water. If more gold spheres are added to the water more light will be reflected and less light will pass through the water. This is similar to having a lot of electrons that scatter light. Each electron, in this situation, will strongly interact with the light by reflection or absorption.

What if, instead of gold, the spheres were made of glass? Even though there are many pieces of glass that can scatter the light not much is scattered because the glass is transparent to the light. This is very similar to high energy light interacting with some material that has a lot of electrons. Even though there are a lot of electrons that are influenced by the light, the electrons themselves do not scatter the light very much. So for the most part, the light passes through with little refraction, reflection, or absorption.

The following discussion closely follows the discussion in Reference [18].

4.1.1 Scattering Cross Sections

Before launching into the discussion of ASF it is important to review scattering cross sections. The ASF theory is based on comparing the scattering cross section of an atom to the scattering cross section of a single electron. Scattering cross sections have units of area. From a conceptual point of view, a scattering cross section describes how "wide" an object looks to something else that could hit it. A barn will have a larger scattering cross section than a fly because it is easier to hit. Unlike balls bouncing off the side of a barn, light scattering by an electron or atom will scatter into all directions including the forward direction.

The scattering cross section is defined as the scattered power divided by the intensity of the incident beam.

$$\sigma \equiv \frac{\bar{P}_{scatt}}{|\bar{S}_i|} \tag{4.1}$$

Where the bar means quantity is the time average. Power has units of watts, intensity has units of watts/m^2, so P/S has units of area. This relates the light scattered by an electron or atom to the apparent area of the electron or atom.

4.1.2 Scattering of a Single Free Electron

Start by looking at the scattering of a single free electron. Why free? The electrons in a material are bound to the atoms of the material. At high enough energies it is possible to have electrons that are bound to the atom by energies that are much smaller that the energy of the light. So the electron behaves as though it were free to the incident light. Akin to a car being able to move over a scratch in the pavement. Yes, the scratch is in the path of the car, but the effect it has on the moving car is negligible.

This assumption, that the electrons are free to respond to the incident light, breaks down around band edges where the binding energy of the electron is comparable to the energy of the incoming light. It also breaks down for low energy light because the energies of valence electrons are on the order of the energy of the incident light, and the energies of the valence electrons are significantly affected by the crystalline properties of the material. Quantifying how much the crystal properties make a difference over what range of incident light energy is purpose of this thesis.

As with most classical phenomena involving charges and electrons start with the Lorentz force law

$$\mathbf{f} = m\mathbf{a} = -e(\mathbf{E}_i + \mathbf{v} \times \mathbf{B}_i) \tag{4.2}$$

This can be simplified by assuming the electron does not approach relativistic speeds and remembering $\mathbf{B} = \mathbf{E}/c$. The acceleration on the electron due to the magnetic field is several orders of magnitude smaller that the acceleration due to the electric field.

The acceleration of the electron has the form

$$\mathbf{a} = -\frac{e}{m}\mathbf{E}_i \tag{4.3}$$

The amplitude of the scattered electric field depends on the transverse acceleration of the electron.

$$a_T = a\sin\theta = -\frac{e}{m}E_i\sin\theta \tag{4.4}$$

The scattered electric field depends on the acceleration of the charge.

$$E = -\frac{e^2 E_i \sin\theta}{4\pi\epsilon_0 mc^2 r}e^{-i\omega(t-r/c)} \tag{4.5}$$

Equation 4.5 can be simplified by introducing the classical electron radius

$$r_e = \frac{e^2}{4\pi\epsilon_0 mc^2} \tag{4.6}$$

Now relate $\bar{P}_{scatt}$ to the scattered electric field and $|\bar{S}_i|$ to the incident electric field. The dipole radiation of an accelerated electron is

$$P = \frac{8\pi}{3}(\frac{e^2|\mathbf{a}|^2}{16\pi^2\epsilon_0 c^3}) \tag{4.7}$$

The incident intensity may be calculated using the Poynting vector

$$\bar{\mathbf{S}} = \frac{1}{2}(\mathbf{E} \times \mathbf{H}^*) \tag{4.8}$$

Again using $\mathbf{E} = \mathbf{B}/c$ Equation 4.8 becomes

$$\bar{\mathbf{S}} = \frac{1}{2}\sqrt{\frac{\epsilon_0}{\mu_0}}|\mathbf{E}|^2 \tag{4.9}$$

Now put it all together using the acceleration given by Equation 4.4.

$$\sigma = \frac{\bar{P}_{scatt}}{|\bar{\mathbf{S}}_{\mathbf{i}}|} = \frac{8}{3}\frac{e^4}{16m^2\pi c^3}\sqrt{\frac{\mu_0}{\epsilon_0}} \tag{4.10}$$

With a little work using $c = (\epsilon_0\mu_0)^{-1/2}$ the last part of Equation 4.10 can be made to look like r_e. The scattering cross section of a free electron is given by

$$\sigma_e = \frac{8\pi}{3}r_e^2 \tag{4.11}$$

This result was first obtained by J.J. Thompson [19].

4.1.3 Scattering by a Multi-Electron Atom

To model the scattering by a multi-electron, one of two approaches may be taken. It may be assumed the wavelength of the light is large compared to the atomic distances. This assumption is also used in Appendix A.1 to make the electric field over a region be uniform so the calculation is easier. It effectively smears out the electronic distribution of the atom. Another way is to define the electron distribution within the atom. One way it may be expressed is to assume the electrons are distinct points represented by delta functions. This representation is not valid in the quantum mechanical limit, but in the end it still gives the correct result. It gives the correct result because at the end of this derivation the wavelength must be much larger than atomic dimensions to make the result be generally applicable. In this limit is it not unreasonable to ignore the quantum mechanical nature of the electrons. The why is a delta function then used to define the position of the electrons? The delta function will collapse the $\mathbf{r}$ integral making it possible to simply add the number of electrons to get the overall effect, which is one of the strengths of ASF theory.

$$\frac{N(\mathbf{r},t)}{R} = n(\mathbf{r},t) = -e\sum_{s=1}^{Z}\delta[\mathbf{r} - \Delta\mathbf{r}_s(t)] \tag{4.12}$$

The current density is found by multiplying the electron distribution by the velocity of the each of the electrons.

$$\mathbf{J}(\mathbf{r},t) = \sum_{s=1}^{Z}\delta[\mathbf{r} - \Delta\mathbf{r}_s(t)]\mathbf{v}_s(t) \tag{4.13}$$

It is assumed the $\mathbf{v}_s(t)$ term is driven by the incoming field and is not affected by fields scattered off of neighboring electrons. This assumption is known as the Born approximation.

The next several steps depend heavily on Fourier transforms (FT). For some problems it is easier to transform a problem from position space to momentum, or wave number space. On the surface

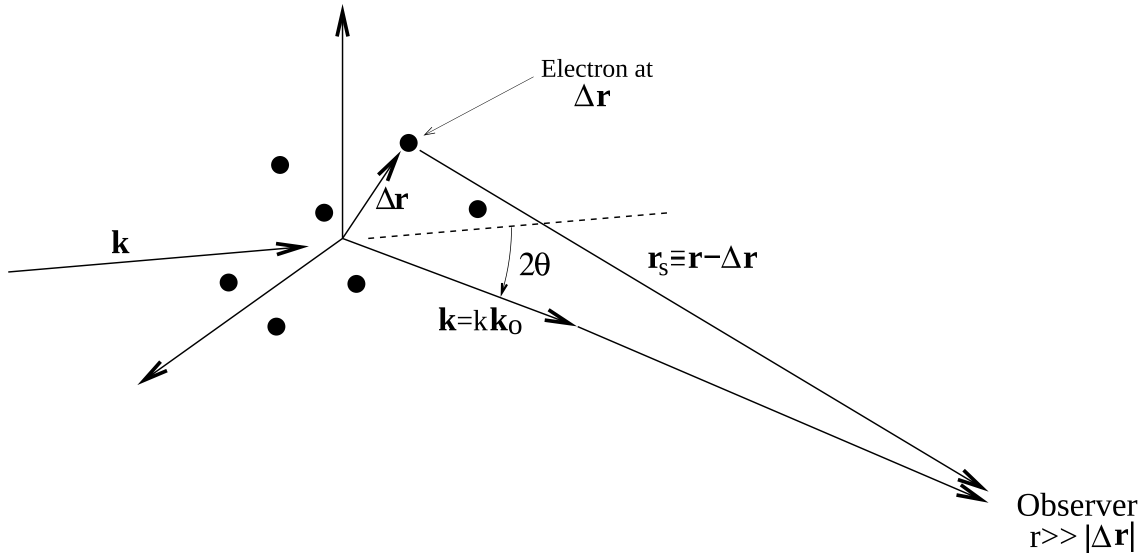

Figure 4.1: Scattering of light by an electron

it may seem to complicate the problem, but it actually makes it possible to solve the problem. Two transforms will be used to take $\mathbf{r} \rightarrow \mathbf{k}$ and $t \rightarrow \omega$. Use $\mathbf{J}(\mathbf{k}, t)$ to solve for $\mathbf{E}(\mathbf{k}, \omega)$. Then take the inverse Fourier transform to get $\mathbf{E}(\mathbf{r}, t)$.

First Fourier transform (FT) $\mathbf{J}(\mathbf{r}, t)$

$$\mathbf{J}(k, \omega) = \int \int \mathbf{J}(\mathbf{r}, t) e^{i(\omega t - \mathbf{k} \cdot \mathbf{r})} d\mathbf{r}\, dt \tag{4.14}$$

Now use the representation of the current density from Equation 4.13 in the above equation

$$\mathbf{J}(k, \omega) = -e \sum_{s=1}^{Z} \int \int \delta[\mathbf{r} - \Delta \mathbf{r}_s(t)] \mathbf{v}_s(t) e^{i(\omega t - \mathbf{k} \cdot \mathbf{r})} d\mathbf{r}\, dt \tag{4.15}$$

The delta function of $\mathbf{r}$ easily collapse the $\mathbf{r}$ integral. This does assume the time dependence of the $\Delta \mathbf{r}_s$ term is negligible compared to other time constraints in the integral. This also means the electrons move slowly in the atom compared to the oscillation of the field in the atom. Given these assumptions the current density now looks like

$$\mathbf{J}(k, \omega) = -e \sum_{s=1}^{Z} e^{-i\mathbf{k} \cdot \mathbf{\Delta r_s(t)}} \int \mathbf{v}_s(t) e^{i\omega t} dt \tag{4.16}$$

The remaining integral is a FT of the velocity from time space into frequency space.

$$\mathbf{J}_{k,\omega} = -e \sum_{s=1}^{Z} e^{-i\mathbf{k} \cdot \mathbf{\Delta r_s(t)}} \mathbf{v}_s(\omega) \tag{4.17}$$

Now solve for $\mathbf{E}(\mathbf{r},t)$ using $\mathbf{J}_{k,\omega}$. This expression can be found in Reference [18].

$$\mathbf{E}(\mathbf{r},t) = \frac{-i}{\epsilon_0(2\pi)^4}\int\int \frac{\omega\,\mathbf{J}_T(k,\omega)e^{-i(\omega t-\mathbf{k}\cdot\mathbf{r})}d\mathbf{k}\,d\omega}{\omega^2-k^2c^2} \tag{4.18}$$

where $\mathbf{J}_T(k\omega)$ is the transverse current density in the atom of interest. Only the electrons that are moving in the transverse direction to the observation point will produce fields that will be detected. Now explicitly write out the components in the current density and factor the denominator knowing the solution will require contour integration.

$$\mathbf{E}(\mathbf{r},t) = \frac{ie}{\epsilon_0(2\pi)^4}\sum_{s=1}^{Z}\int\int \frac{\omega\,e^{-i\mathbf{k}\cdot\boldsymbol{\Delta}\mathbf{r}}\mathbf{v}_s(\omega)e^{-i(\omega t-\mathbf{k}\cdot\mathbf{r})}d\mathbf{k}\,d\omega}{(\omega-kc)(\omega+kc)} \tag{4.19}$$

The radial parts in the exponents may be combined into a single expression by looking at the relative geometry of $\mathbf{r}$ and $\Delta\mathbf{r}_s$ (see Figure 4.1).

$$\mathbf{r}_s \equiv \mathbf{r} - \Delta\mathbf{r}_s \tag{4.20}$$

Using the above definition and combining the terms in the exponents Equation 4.19 may be written as where $\mathbf{r}_s$ points from the source to the observation point.

$$\mathbf{E}(\mathbf{r},t) = \frac{ie}{\epsilon_0(2\pi)^4}\sum_{s=1}^{Z}\int\int \frac{\omega\,e^{i(\mathbf{k}\cdot\mathbf{r}_s-\omega t)}\mathbf{v}_s(\omega)d\mathbf{k}\,d\omega}{(\omega-kc)(\omega+kc)} \tag{4.21}$$

This integration may be evaluated using contour integration. There are two simple poles of order 1 at $k=\pm\omega/c$. To complete the integral it must be assumed that k has an imaginary component. This makes the $e^{i\mathbf{k}\cdot\mathbf{r}}$ term in the numerator go to zero when $\mathbf{k}$ is large and imaginary during the contour integration. The contour is closed in the upper half plane to make the numerator go to zero[1]. The imaginary component of $\mathbf{k}$ also brings the poles off the real axis so the pole is completely enclosed in the contour. The pole being entirely enclosed is only makes the algebra slightly easier and is not crucial, assuming the integral did not blow up for large values of $\mathbf{k}$. There a several more details that are needed to finish the problem that may be found in Reference [18]. After the contour integration Equation 4.21 becomes

$$\mathbf{E}(\mathbf{r},t) = \frac{e}{\epsilon_0(2\pi)^4}\sum_{s=1}^{Z}\frac{1}{r_s}\int_{-\infty}^{\infty}(-i\omega)\mathbf{v}_s(\omega)e^{-i\omega(t-r/c)}\,d\omega \tag{4.22}$$

All that is left is to evaluate the ω integral. First recognize that the $-i\omega$ comes from taking the derivative of the exponent. Because $\mathbf{v}_s(\omega)$ does not depend on t Equation 4.22 may be written as

$$\mathbf{E}(\mathbf{r},t) = \frac{e}{\epsilon_0(2\pi)^4}\sum_{s=1}^{Z}\frac{1}{r_s}\int_{-\infty}^{\infty}\frac{d}{dt}(\mathbf{v}_s(\omega)e^{-i\omega(t-r/c)})\,d\omega \tag{4.23}$$

---

[1] If there was an extra negative sign in the exponent the contour could be closed in the lower half plane with the same result.

This is verified by taking the derivative. Now let $t' = t - r/c$ and pull the derivative out of the integral[2]. Equation 4.23 now becomes

$$\mathbf{E}(\mathbf{r}, t) = \frac{e}{\epsilon_0 (2\pi)^4} \sum_{s=1}^{Z} \frac{1}{r_s} \frac{d}{dt} \int_{-\infty}^{\infty} (\mathbf{v}_s(\omega) e^{-i\omega(t')})\, d\omega \tag{4.24}$$

which is the inverse Fourier transform back into a retarded time domain. The extra r/c comes from the extra time it takes the fields to reach the observation point. The electric field as a function of space and time is now

$$\mathbf{E}(\mathbf{r}, t) = \frac{e}{(4\pi)\epsilon_0 c^2} \sum_{s=1}^{Z} \frac{1}{r_s} \frac{d}{dt} \mathbf{v}_s(\omega(t - r/c)) \tag{4.25}$$

Evaluate the time derivative to get the acceleration and use $t' = t - r/c$.

$$\mathbf{E}(\mathbf{r}, t) = \frac{e}{\epsilon_0 (2\pi)^4} \sum_{s=1}^{Z} \frac{\mathbf{a}_{T,s}(\omega(t'))}{r_s} \tag{4.26}$$

The term inside the sum is the electric field radiated by an accelerated electron [21]. The sum allows the influence of more than one electron to taken account of.

Several things can now be said about the analysis so far. First start by defining the positions of the electrons inside the atom using delta functions. Then define **J**, the FT of **J** and use it to calculate the FT of the electric field. Solve the inverse FT to get **E** as a function of **r** and t, and what comes out? An expression for the electric field. This same result could have been obtained by summing the field coming from individual electrons, accounting for the distance of each electron. What this really means is that each electron is behaving as though it was in a vacuum. This is sometimes called the independent particle approximation. This should be what was expected because the interaction between neighboring electrons was assumed to be small and was ignored. So the definition of **J** is what really makes the electrons behave like isolated charged particles. This is very similar to Appendix A.1.1 where the electrons are assumed to be driven by the incident electric field and the interactions between the electrons is negligible. These approximations still allow for a good result because of the positive nuclei that help screen out the repulsive Coulombic forces. For high energies this is a good approximation for ASF because each electron is essentially free compared to the binding energies of the electrons. In the EUV this is not true. The energies of the electrons and their bonds becomes more important than it is for ASF in the x-ray portion of the spectrum.

Equations of Motion

Now write out the equation of motion. Assume there is a damping term that is proportional to γ and a restoring force that is proportional to ω_s^2. Physically γ is related to the energy lost during collisions and ω_s^2 is related to the Colombic attraction that holds the electrons to the atom. The electric field provides the driving force. As always, any contribution to the force from the magnetic

---

[2] Switching the order of integration and differentiation of two variables is not always this easy, but it can be done in a general way [20].

field is ignored. It may seem odd to be including the damping and restoring forces when it was completely ignored in the discussion of ASF. ASF are useful away from resonances or places where the damping and restoring forces plays a significant role in the optical response of the material, but to relate ASF and oscillator strengths it is necessary to introduce the damping and restoring forces.

$$m\frac{d^2\mathbf{x}_s}{dt^2} + m\gamma\frac{d\mathbf{x}_s}{dt} + m\omega_s^2\mathbf{x}_s = -e\mathbf{E}_i \tag{4.27}$$

This equation can be solved by assuming the motion is oscillatory and at the same frequency as the incoming wave.

$$\mathbf{x}_s(t) = \mathbf{x}_s e^{-i\omega t} \tag{4.28}$$

Putting this into Equation 4.27 and taking the derivatives

$$m(-i\omega)^2\mathbf{x}_s(t) + m\gamma(-i\omega)\mathbf{x}_s(t) + m\omega_s^2\mathbf{x}_s(t) = -e\mathbf{E}_i \tag{4.29}$$

Explicitly write out the spatial and time dependent parts of $\mathbf{E}_i$.

$$\mathbf{E}_i(\mathbf{r}, t) = \mathbf{E}_i e^{-i(\omega t - \mathbf{k}_i \cdot \Delta\mathbf{r}_s)} \tag{4.30}$$

Combine Equations 4.29 and 4.30, and solve for $\mathbf{x}_s(t)$.

$$\mathbf{x}_s(t) = \frac{1}{\omega^2 - \omega_s^2 + i\gamma\omega}\frac{e}{m}\mathbf{E}_i e^{-i(\omega t - \mathbf{k}_i \cdot \Delta\mathbf{r}_s)} \tag{4.31}$$

Take two time derivative to get the acceleration.

$$\mathbf{a}_s(t) = \frac{-\omega^2}{\omega^2 - \omega_s^2 + i\gamma\omega}\frac{e}{m}\mathbf{E}_i e^{-i(\omega t - \mathbf{k}_i \cdot \Delta\mathbf{r}_s)} \tag{4.32}$$

Multiply this result by $\sin\theta$ to get $\mathbf{a}_{T,s}$. Then substitute into Equation 4.26

$$\mathbf{E}(\mathbf{r}, t) = \frac{e^2}{4\pi\epsilon_0 mc^2}\sum_{s=1}^{Z}\frac{\omega_s^2 E_i \sin\theta}{\omega^2 - \omega_s^2 + i\gamma\omega}\frac{1}{r_s}e^{-i[\omega(t - r_s/c) - \mathbf{k}_i \cdot \Delta\mathbf{r}_s]} \tag{4.33}$$

The front term may be recognized as the classical electron radius (see Equation 4.6). From Figure 4.1 it can be seen that if $r \gg \Delta r_s$ then the angle between r and r_s will be very small. Any correction may be approximated as subtracting the projection of $\Delta\mathbf{r}_s$ from r. This should almost always be a good correction because most experimental measurements are much larger than the beam spot on the sample.

$$r_s \simeq r - \mathbf{k}_0 \cdot \Delta\mathbf{r}_s \tag{4.34}$$

Now gather like terms, and make the further simplification that the correction to r_s is most important in the calculating the relative phase. The amplitude term can be simplified as r assuming the slight change in distance will not significantly change the amplitude.

$$\mathbf{E}(\mathbf{r},t) = \frac{e^2}{4\pi\epsilon_0 mc^2}\sum_{s=1}^{Z}\frac{\omega_s^2 E_i \sin\theta}{\omega^2-\omega_s^2+i\gamma\omega}\frac{1}{r}e^{-u[\omega(t-r/c)+\omega(\frac{\mathbf{k}_0\cdot\Delta\mathbf{r}_s}{c})-\mathbf{k}_i\cdot\Delta\mathbf{r}_s]} \tag{4.35}$$

Write $k\mathbf{k}_0 = \mathbf{k}$ and remember that $\omega/c = k$ to simplify the phase term that depends on $\mathbf{k}$.

$$\mathbf{E}(\mathbf{r},t) = \frac{e^2}{4\pi\epsilon_0 mc^2}\sum_{s=1}^{Z}\frac{\omega_s^2 E_i \sin\theta}{\omega^2-\omega_s^2+i\gamma\omega}\frac{1}{r}e^{-i[\omega(t-r/c)+(\mathbf{k}-\mathbf{k}_i)\cdot\Delta\mathbf{r}_s} \tag{4.36}$$

The phase term may be simplified further by defining

$$\Delta\mathbf{k} = \mathbf{k} - \mathbf{k}_i \tag{4.37}$$

Where $\Delta\mathbf{k}$ is related to the material scattering the light into specific directions that depend on the structure of the material. From Figure 4.2 it is possible to write Bragg's law of diffraction

$$|\Delta\mathbf{k}| = 2k_i \sin\theta \tag{4.38}$$

How does Bragg's law of diffraction come out of trying to calculate optical properties of materials? By defining $\Delta\mathbf{k}$ it was implicitly stating that this material would not scatter light into all direction, but into specific directions depending on how the electrons were bunched together. It is also stating that the electron bunches were not uniformly distributed though the material, but that they could be found in periodic bunches centered around specific points (i.e. nuclei) in the solid.

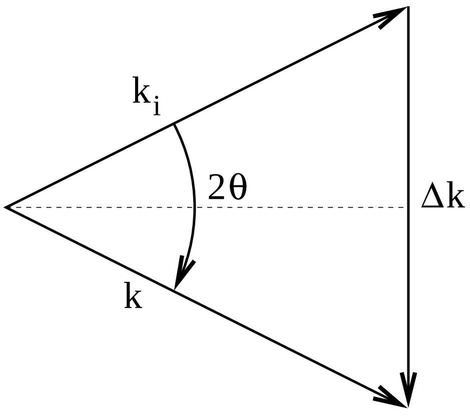

Figure 4.2: Bragg diffraction is $\mathbf{k}$ space. This version of Bragg diffraction is often used in solid state physics.

One last time write out all the details of the electric field

$$\mathbf{E}(\mathbf{r},t) = -\frac{r_e}{r}\left[\sum_{s=1}^{Z}\frac{\omega^2 e^{-\Delta\mathbf{k}\cdot\Delta\mathbf{r}_s}}{\omega^2-\omega_s^2+i\gamma\omega}\right]E_i\sin\theta e^{-i\omega(t-r/c)} \tag{4.39}$$

The term in square brackets becomes the complex atomic scattering factor

$$f(\Delta\mathbf{k},\omega) = \sum_{s=1}^{Z}\frac{\omega_s^2 e^{-\Delta\mathbf{k}\cdot\Delta\mathbf{r}_s}}{\omega^2-\omega_s^2+i\gamma\omega} \tag{4.40}$$

Write the electric field in terms of the ASF.

$$E(\mathbf{r},t) = -\frac{r_e f(\Delta\mathbf{k},\omega)E_i \sin\theta}{r} e^{-i\omega(t-r/c)} \tag{4.41}$$

The scattering cross section of a single free electron, E_{e^-}, is given in Section 4.1.2.

$$E_{e^-} = -\frac{r_e E_i \sin\theta}{r} e^{-i\omega(t-r/c)} \tag{4.42}$$

By combining Equations 4.41 and 4.42 the field scattered by a multi-electron can be written as

$$E(\mathbf{r},t) = f(\Delta\mathbf{k},\omega)E_{e^-} \tag{4.43}$$

It is easy to see the ASF is a unitless parameter that relates the scattering of a multi-electron atom to the fields scattered by a single free electron.

Using Equation 4.1 the scattering cross section of a multi-electron atom is

$$\sigma(\omega) = \frac{8\pi}{3}|f|^2\mathbf{r}_e^2 \tag{4.44}$$

where f is the complex ASF.

The ASF as currently written is still difficult to use because the $\Delta\mathbf{k}\cdot\Delta\mathbf{r}_s$ does not simplify and can take on many values depending on the particular details of the situation.

Use Equation 4.38 with $k_i = 2\pi/\lambda$ to get

$$\Delta k = \frac{4\pi a_0}{\lambda}\sin\theta \tag{4.45}$$

Now take the dot product of $\Delta\mathbf{k}$ and $\Delta\mathbf{r}$ and assume the magnitude of Δr is about the size of an atom. For convenience use the Bohr radius a_0.

$$|\Delta\mathbf{k}\cdot\Delta\mathbf{r}| \leq \frac{4\pi a_0}{\lambda}\sin\theta \tag{4.46}$$

The phase dependence will be negligible in two cases

$$a_0/\lambda \ll 1 \tag{4.47}$$

$$\theta \ll 1 \tag{4.48}$$

If either one or both of these two situations are satisfied, the phase dependence drops out of the equation so the ASF may be expressed as

$$f^0 = \sum_{s=1}^{Z} \frac{\omega^2}{\omega^2 - \omega_s^2 + i\gamma\omega} \tag{4.49}$$

Where the zero superscript means this from of ASF is only valid for situations where the phase dependence is negligible.

Other Regions where f^0 is not valid

The simplified expression of f^0 is a good approximation when the two previous conditions are met. Either the angle must be small or the wavelength must be larger than about the size of an atom. This approximation is not valid around atomic resonance because the mechanics of the transitions are not adequately described by the semi-classical model that was used to derive f^0. Even though Equation 4.47 may hold for visible light ASF do not adequately describe the optical properties of a material at visible wavelengths because the energy of the light is on the order of the energy of the bonds in the material. Changes in the bonds of the material will significantly affect the way the material responds to visible light.

Relating ASF to n,k

The real and imaginary parts of atomic scattering factors are very similar to the real and imaginary parts described by the Lorentz oscillator model (see Appendix A.2). In Section A.2 the optical constants n and k were derived by assuming there were oscillators in the material that interacted with the light at different and specific frequencies. The behavior of each oscillator contributed to the overall shape and behavior of the optical constants. By comparing Equations A.64, derived using Lorentz oscillators, and 4.49 there a simple relationship that relates the complex index of refraction to the atomic scattering factors.

$$n(\omega) = 1 - \delta + i\beta = 1 - \frac{n_a r_e \lambda^2}{2\pi}(f_1^0 - i f_2^0) \tag{4.50}$$

4.2 Sum Rules and Kramers-Kronig Relations

The theory of sum rules and Kramers-Kronig relations is different from the other theories in this thesis. ASF, Drude theory, and Lorentz oscillators are used to better understand or predict the optical properties of materials at various wavelengths of light. Sum rules are used to check the validity of optical constant by “counting” the number of electrons that are involved in interactions with light. Kramers-Kronig relations are used to calculate the imaginary part of the index of refraction using the real part of the index of refraction or visa versa. Both of these methods are extremely useful in test the validity of a set of optical constants.

4.2.1 Sum Rules

The discussion of sum rules follows directly from the discussion of atomic scattering factors (see Section 4.1 and closely follows the discussion in [18]. The last equation in Section 4.1 showed the ASF being a sum of oscillators.

$$f^0 = \sum_{s=1}^{Z} \frac{\omega^2}{\omega^2 - \omega_s^2 + i\gamma\omega} \tag{4.51}$$

At low energies the sum will only include those electrons that are influenced by the light and will not include the influence of the core electrons because the light does not have sufficient energy. Equation 4.49 may be written as

$$f^0 = \sum_{s=1}^{N(\omega)} \frac{\omega^2}{\omega^2 - \omega_s^2 + i\gamma\omega} \tag{4.52}$$

where $N(\omega)$ denotes the number of electrons that will be involved in the scattering depends on the frequency of the light used to probe the material.

Closely related to the oscillators at each ω_s is an oscillator strength, g_s, that corresponds to the effective number of electrons associated with each ω_s. In the semi-classical model that is being used in this thesis g_s is an integer value that represents the number of electrons that are involved in a given resonance frequency.

$$f^0 = \sum_s g_s = Z \tag{4.53}$$

As an example, in carbon there are two K shell electrons, or two electrons that are more tightly bound to the nucleus than the other electrons. The ω_s associated with this resonance occurs at 284 eV (see Figure 4.3.) Above this energy both electrons will be able to scatter light, so the g_s associated with this resonance is 2. It can also be seen in Figure 4.3 that below this energy a carbon atom has four electrons ($N(\omega < \omega_K) = 6 - 2$) that participate in the scattering of light.

Only allowing g_s to take on integer values is an ideal case and can be made more general by allowing g_s to take on non-integer values. This corresponds to transition probabilities in quantum mechanics that themselves are not integer values (An atom is *slightly* more complicated than a collection of free electrons.) The sum rule still holds but the oscillator strengths are summed over the states in the atom

$$f^0 = \sum_n g_{kn} = Z \tag{4.54}$$

where k is the initial state and k is the final state. This is known as the Thomas-Reich-Kuhn sum rule [22, 23, 24]. The ASF can now be written in terms of g_s

$$f^0 = \sum_s^Z \frac{g_s\omega^2}{\omega^2 - \omega_s^2 + i\gamma\omega} \tag{4.55}$$

For $\omega^2 \gg \omega_s^2$ Equation 4.55 will simplify to

$$f^0(\omega) = \sum_s g_s \frac{\omega^2}{\omega^2} = \sum_s g_s \tag{4.56}$$

Integrating or summing over all frequencies is necessary if the real part of the index of refraction is going to be determined from the imaginary part, but it is not a useful form for determining where data is the measured spectrum is wrong. Partial sum rules may be used to calculate the effective number of electrons that are involved in the scattering of light up to a certain energy.

$$N_{eff}(\omega) = \frac{2}{\pi} \frac{m\epsilon_0}{n_a e^2} \int_0^\omega \omega' \epsilon_2(\omega')\, d\omega' \tag{4.57}$$

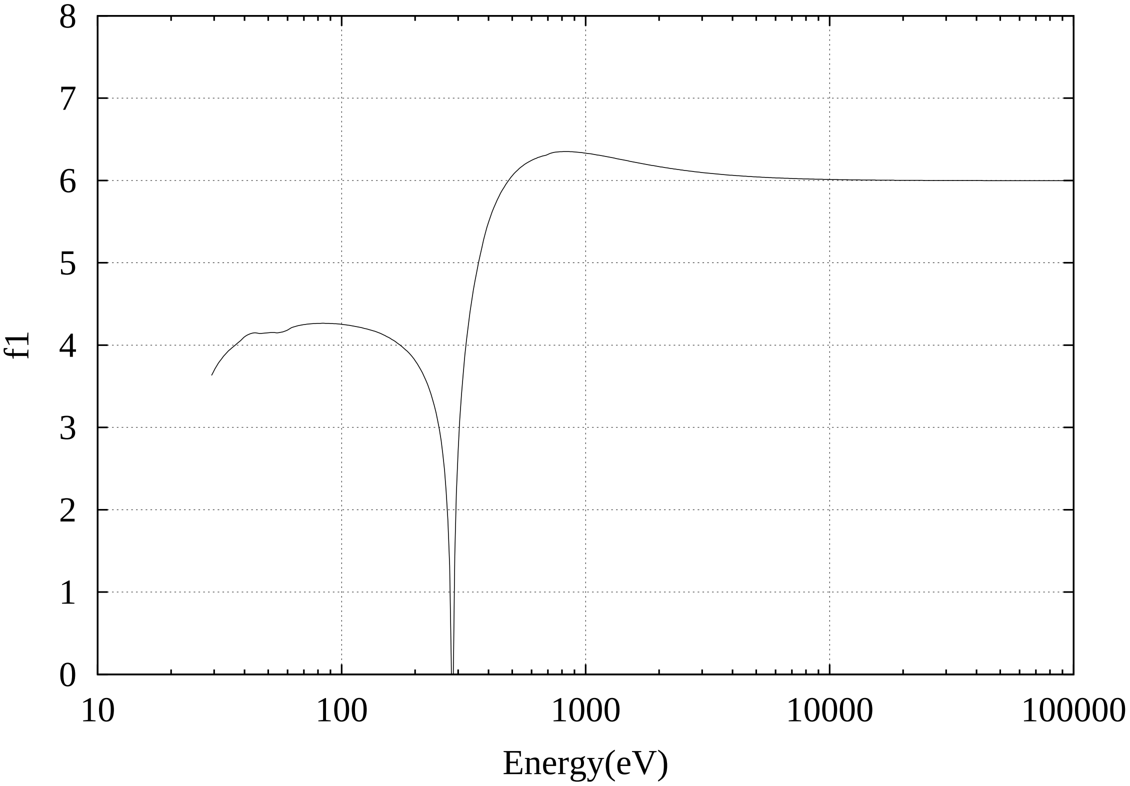

Figure 4.3: At high enough energies the value of f_1^0 of carbon (Z=6) goes to six. This shows that at high enough energies the atoms scatters light six times more than the light scattered by a single electron. That is what should be expected because there are six electrons in a carbon atom.

where $\epsilon_2 = 2nk$.

As the frequency of light sweeps through a resonance, the N_{eff} of the atom should increase by the number of electrons that are involved in the transition. Because most atoms have multiple resonance it is important that the resonances are sufficiently far apart for this analysis to be well defined. Otherwise it will be difficult to separate the effects of the two resonances. This principle can be seen in Figure 4.3. Between 40 and 200 eV the f_1 of carbon hovers around four before going through a resonance around 280 eV and jumping up to six. If the resonance at 280 eV was farther away f_1 would taper off to four because of the four electrons that are involved in the scattering around 100 eV.

There are other forms of sum rules that may be used to test the validity of a set of ASF. An explanation of the various sums rules and their relationships can be found in Reference [4].

4.2.2 Kramers-Kronig Relations

Kramers-Kronig relations are a mathematical argument involving functions that have coupled real and imaginary parts. The real and imaginary parts of optical constants are coupled because it is the same electrons that are involved in determining the optical properties of a solid. This is known as causality, or that the physical response described by optical constants is caused by the same physical mechanism. There are more subtle arguments that involve causality, but for the purposes of this thesis it is satisfactory to understand that if the way an electron scatters light can be described by n, then the same electron will also absorb light, described by k, in a way that is related to the way the electron scatters light. The two optical constants describe different material properties but they are fundamentally related because it is the same electrons involved in the scattering and absorption. The analysis in this thesis will not involve Kramers-Kronig relations, but for completeness the forms of the integrals will be given. More details about evaluating Kramers-Kronig relations may be found in Reference [4].

First assume the complex index of refraction is $\mathcal{N} = n + ik$. The Kramers-Kronig relations relating the real and imaginary parts are

$$\Re[\mathcal{N}^2(\omega_0) - 1] = \frac{2}{\pi} P \int_0^\infty \frac{\omega \Im[\mathcal{N}^2(\omega) - 1]}{\omega^2 - \omega_0^2}\, d\omega \tag{4.58}$$

$$\Im[\mathcal{N}^2(\omega_0) - 1] = -\frac{2}{\pi} P \int_0^\infty \frac{\omega_0 \Re[\mathcal{N}^2(\omega) - 1]}{\omega^2 - \omega_0^2}\, d\omega \tag{4.59}$$

Notice that to get a single value of n or k at a fixed ω_0 it is necessary to know the values of optical constants at nearby ω's. That is why it is important to know the optical constants for all frequencies, because to truly use the Kramers-Kronig relations over measurements must be made at all frequencies.

The compilation of ASF by Henke, et al. is based on the Kramers-Kronig relations. The real part of the ASF was calculated using Kramers-Kronig relations from the imaginary part of the

ASF. This method is used in other wavelength regimes to determine the optical properties of a material. Depending on the region of focus and the available data different parts of the spectrum are approximated by functions to patch holes in the data set. For this reason ASF and other optical constants calculated using Kramers-Kronig are not the exact optical properties of the material but an approximation using the data that is available.

Chapter 5

Data

The industrial diamond and graphite (HOPG) data reported in Chapter 3.1 will not be used in the analysis section of this thesis, because the data does not cover important features in the atomic scattering of carbon. But it will be displayed for comparison. Data from previously published data sets will be used for the analysis.

5.1 Summary of Optical Constants

Before calculating the relative difference between the ASF of diamond and graphite first examine the atomic scattering factors of several references to determine which data set is the best to use for the analysis. To determine which data set to use, plot the calculated atomic scattering factors of diamond, graphite, and amorphous carbon. Most of this data was found digitized and gathered in IMD [25].

Diamond and graphite have been measured previously and the optical properties are most often tabulated as n and k values or f_1 and f_2 values. The most common reference for n and k values is The Handbook of Optical Constants (HBOC) ed. E. Palik [5]. Optical constants are for cubic carbon (c-C, diamond) are tabulated in HBOC I and range between 600–10,000 Å. The optical constants for graphite (g-C) in HBOC II and range between 150–10,000 Å.

Atomic scattering factors (f_1 and f_2) were first compiled in a comprehensive way by B.L. Henke et al [26]. The ASF tables have been updated since they were first published [27]. The data for the updates may be found in References [28, 29, 30, 31] and are cited in this thesis as taken from CXRO\LLNL [27]. ASF have also been calculated by Chantler within a self-consistent Dirac-Hartree-Fock framework [32].

Data from Henke [26] and Chantler [32] are reported as f_1 and f_2 data, but all other references report their data as n,k values. For the purposes of this thesis n,k values are converted to f_1 and f_2 values by inverting Equation 4.50. In general this conversion assumes the atomic scattering factors are independent of the density of the material. Here that assumption is ignored in the conversion because the f_1 and f_2 values will not be used for calculating the optical properties of a material for a real application but for the purpose of comparison.

$$f_1 + i f_2 = \frac{\beta}{\lambda^2}(1 - n + ik) \tag{5.1}$$

where λ is the wavelength in meters and β is given by

$$\beta = \frac{2\pi W}{r_e \rho A}\left(1 \times 10^{-2}\right)^3 \tag{5.2}$$

where W is the atomic weight in grams/mole, the cubed factor of 10^{-2} is to convert cm to m, r_e is the classical electron radius in meters, ρ is the density of the material in grams/cm^3, and A is Avogadro's number. This is the equation for a material made from one element. It is possible to calculate the optical constants of a compound by summing the indices of refraction weighted by their densities [18].

There are two preexisting references for the optical constants of diamond, but there is not good agreement between the two data sets. By comparing the optical constants of diamond to those of amorphous carbon and graphite it is possible to see the Palik data is more reliable. The optical constants of diamond measured by Windt were determined from a thin film sample of chemical vapor deposition (CVD) diamond. The difference in the optical properties may be due to the difference between measuring a bulk film and thin film, but the surface of the diamond sample is reported in Reference [12] to have visible surface irregularities.

Amorphous carbon is not used in the data analysis but it is useful for comparison because there are very few references that report the phase specific optical constants of carbon.

5.2 Data Analysis

The second purpose of this thesis is focused on determining the errors associated with using ASF to estimate the optical properties of materials in the EUV. That is done by calculating the relative difference between the optical constants of diamond and graphite (HOPG).

As previously mentioned in Section 4.1 the atomic scattering factors give a measure of how many electrons are participating in some interaction with light. At high energies all the electrons are involved in the scattering of light, so it is expected that f_1 will approach Z. But at low energies the number of electrons involved in the interaction with the light depends on the crystal properties of the material. ASF can still be calculated but they will be unique to the material that was measured and will not be easily transferable to another crystal phase of a similar material, even if the difference between the densities of the materials is taken into consideration (see Equation 5.1.)

The difference may be shown by calculating the relative difference between the ASF of one crystal

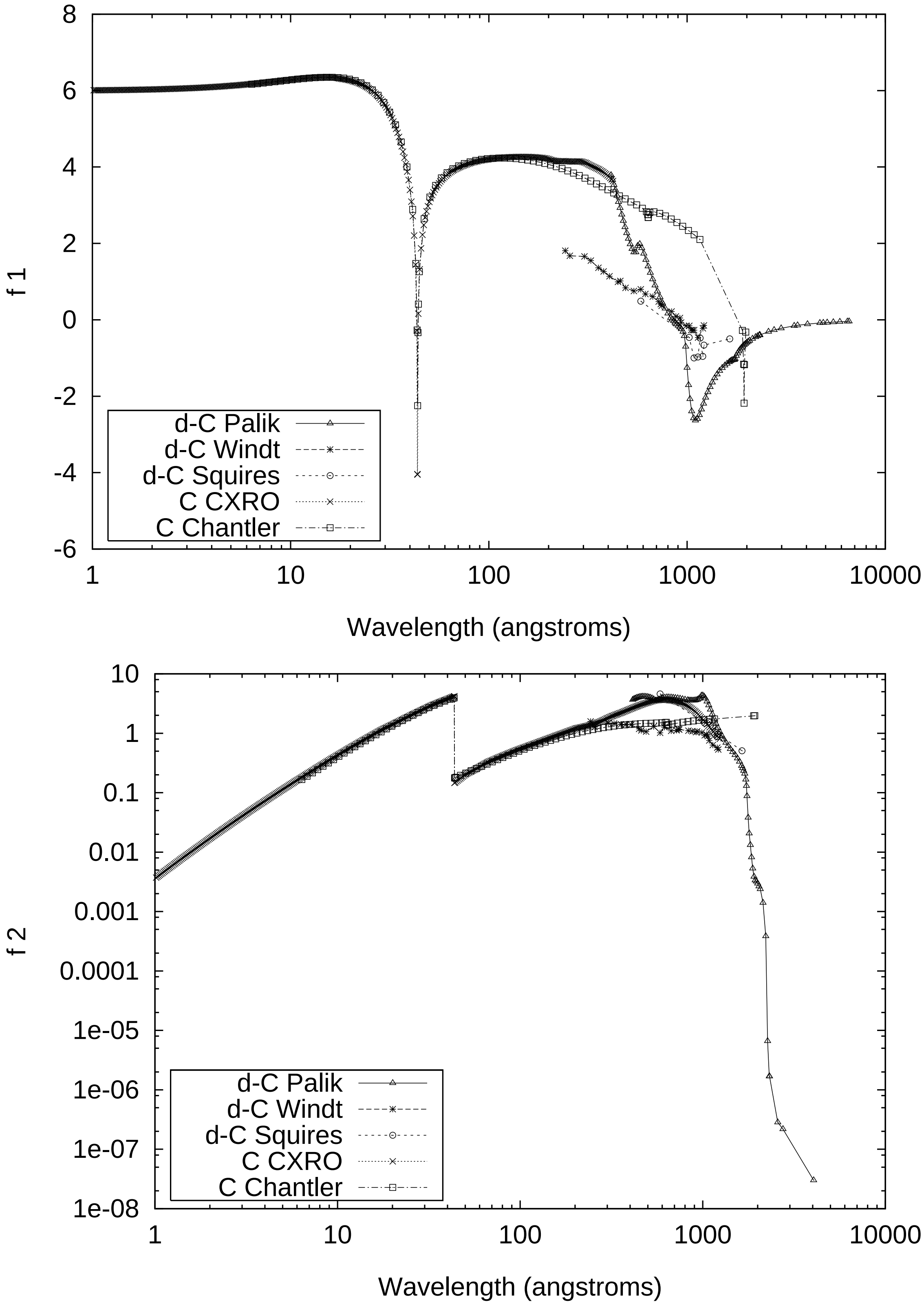

Figure 5.1: Summary of atomic scattering factors of diamond from various references between 10–10000 Å [5, 12, 27, 32]. Notice the low absorption of diamond at long wavelengths.

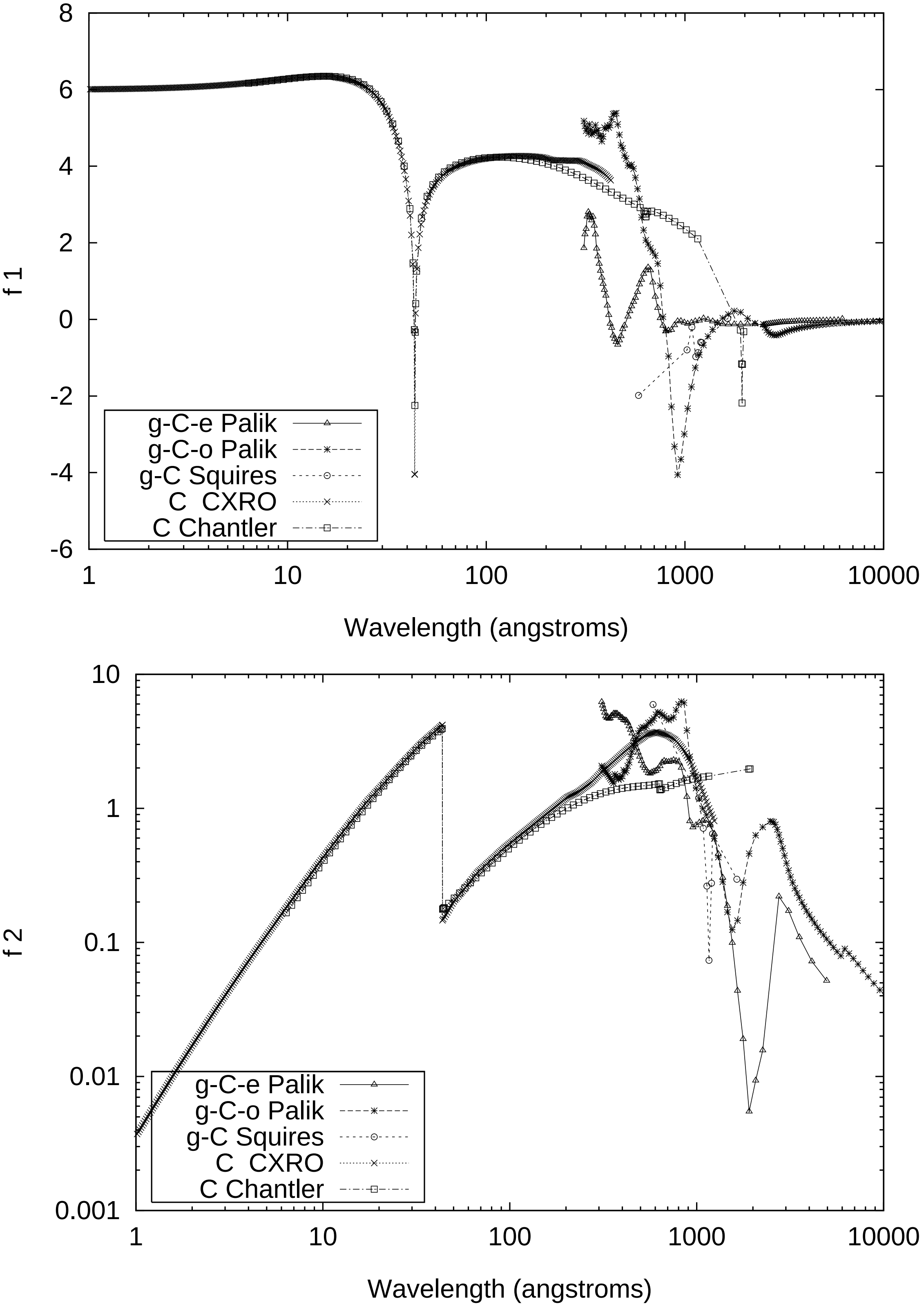

Figure 5.2: Summary of atomic scattering factors of graphite from various references between 10–10000 Å [6, 27, 32].

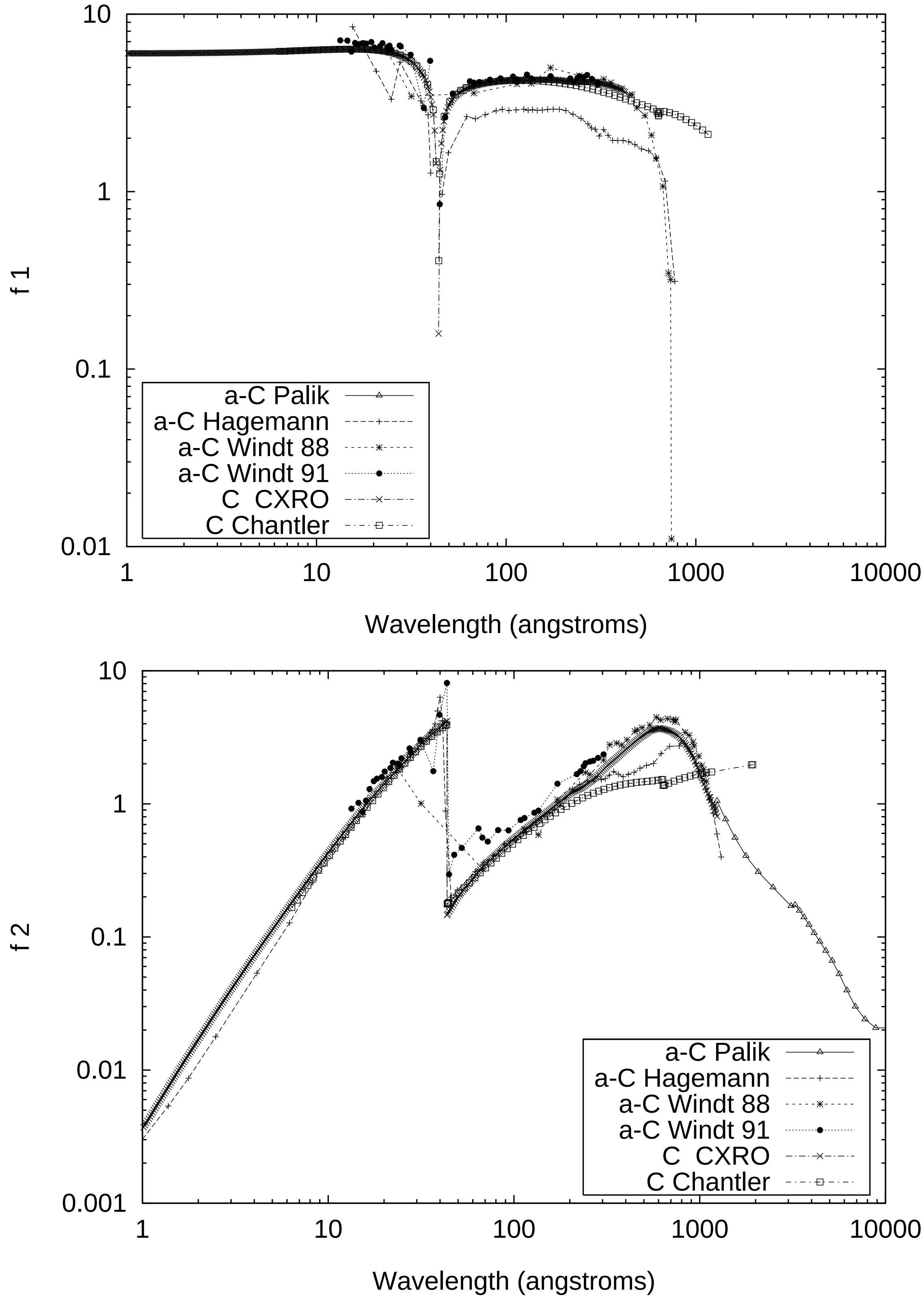

Figure 5.3: Summary of atomic scattering factors of amorphous carbon from various references between 10–10000 Å [6, 33, 34, 35, 27, 32].

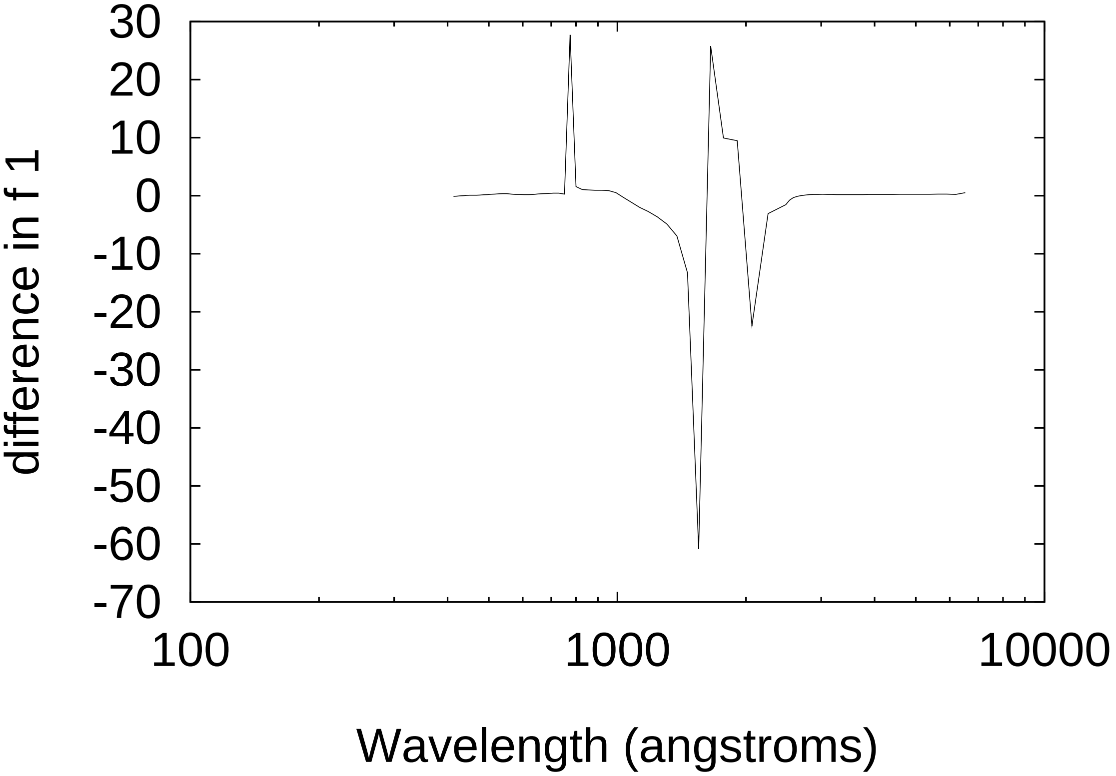

Figure 5.4: Relative difference in f_1 30-160 nm. The difference appears to be zero for wavelengths less than 750 Å, but because of the large vertical scale it is difficult to see if the relative difference is zero or if it only approaches zero.

phase to another. The relative difference is calculated as may be expected

$$\Delta = \frac{f_{diamond} - f_{graphite}}{f_{graphite}} \tag{5.3}$$

The graphite data is used to normalize that data because as currently tabulated in HBOC II it has data tabulated farther into the EUV than diamond. Because graphite is an anisotropic material it has two sets of n,k values that depend on what direction the light is incident on the material.

Graphite data is tabulated for extraordinary and ordinary axis of the crystal in HBOC II [6]. Other References [34, 33] have measured the optical properties of amorphous carbon, but not a graphite crystal. Because graphite is anisotropic it is not possible to compare the n,k values for diamond directly to the optical constants of graphite, because graphite has two n,k data sets of its own. For this thesis the optical constants of graphite will be "averaged." But not using a straight average because there are three orthogonal directions in a crystal. Two axis are described by the ordinary direction and one axis is described by the extraordinary direction. For example the "average" n is calculated by

$$n_{ave} = \frac{2n_o + n_e}{3} \tag{5.4}$$

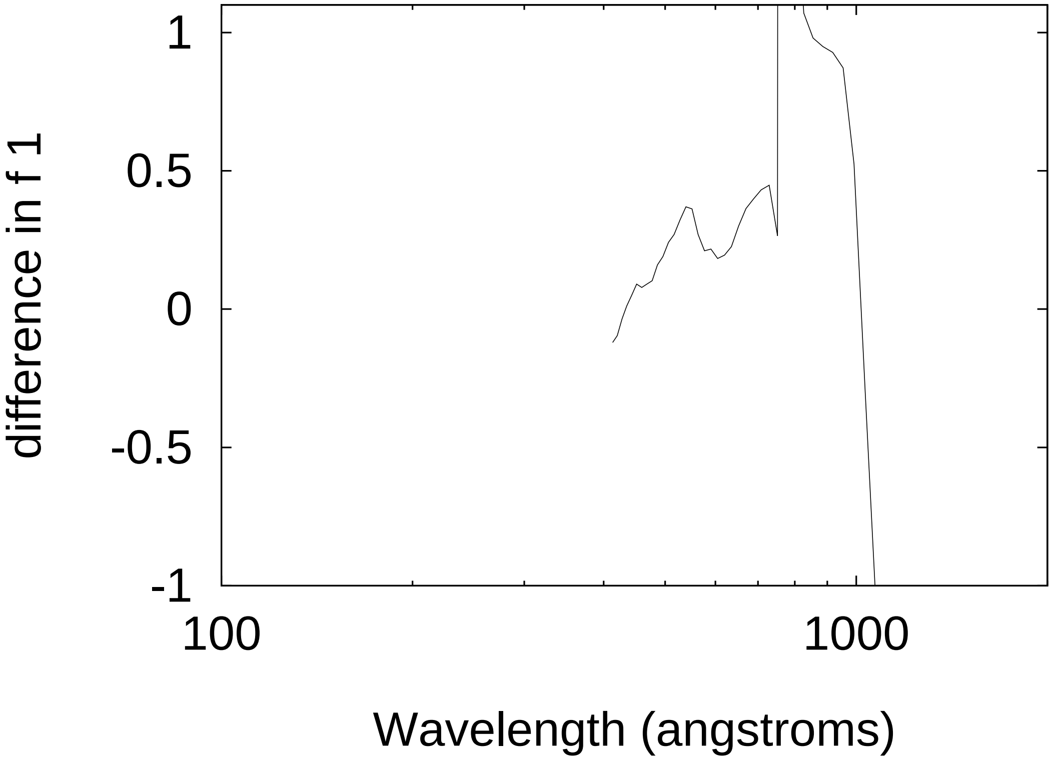

Figure 5.5: Relative difference in f_1 30–110 nm. The large discontinuity at 80 nm is due to the merger of two diamond data sets that were used in the *Handbook of Optical Constants*. The error is still about 25 % on average between 50–80 nm, and then decreases to zero around 40 nm. However there is little data at and beyond the point where the relative difference goes to zero. It is impossible, without more data at or below 40 nm, to determine if the difference goes to zero as expected or if there is some "ringing" about zero.

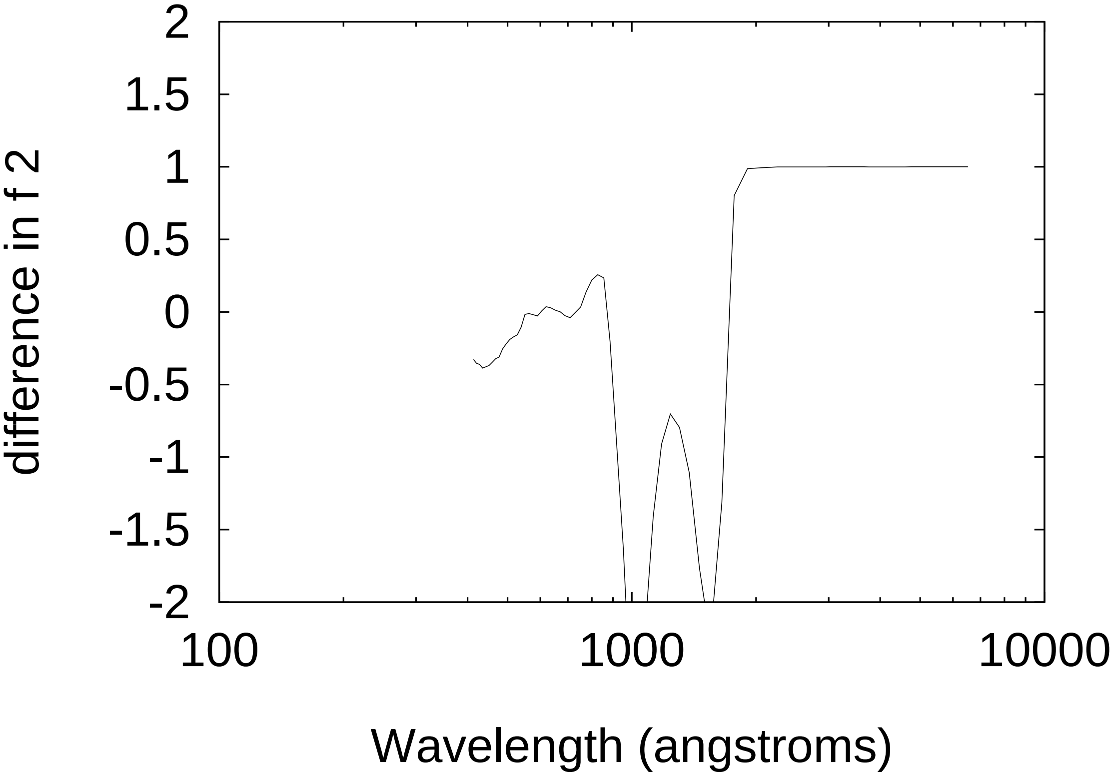

Figure 5.6: Relative difference in f_2 30-160 nm. The relative difference in f_2 goes to one at wavelengths greater than about 1100 Å. That wavelength corresponds to the band gap energy of diamond at about 10 eV. At energies less than 10 eV the relative difference must be one because the f_2 of diamond is essentially zero.

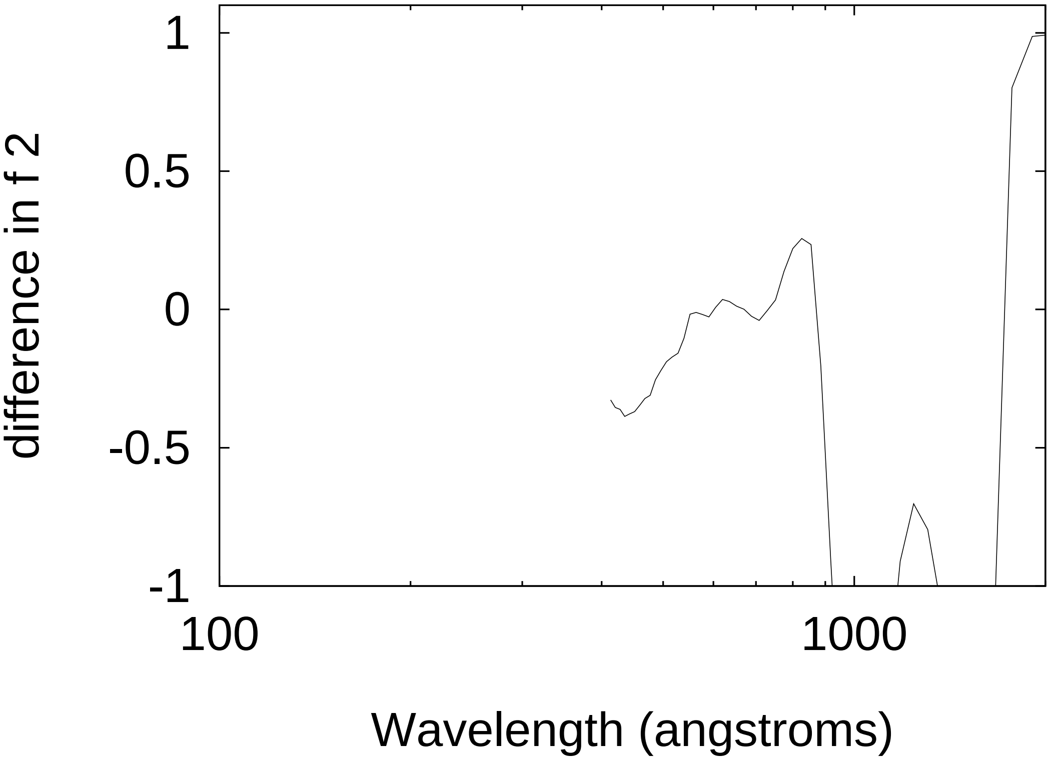

Figure 5.7: Relative difference in f_2 30–110 nm. The relative error in f_2 is less than that of f_1. This may be due to the different mechanisms that determine the dispersive nature and the absorptive nature. It is probably why f_2 in reported to 30 eV in the Henke tables and f_1 is reported to 50 eV.

These figures show that the greatest difference can be seen in the difference between the f_1 values of the different materials. In the case of carbon, the difference is pronounced above 750 Å or 16.5 eV. This difference should be material dependent to some extent.

Chapter 6

Conclusions

A variable angle reflectometer was built to measure the absolute reflectance of surfaces between 2.5° and 85°. The usefulness of this chamber has been demonstrated by measuring the optical properties of industrial diamond and HOPG at multiple wavelengths in the EUV. The reflectance measurements have been automated using LabVIEW to control the stepper motors and calculate the reflectance.

Atomic scattering factors are very useful for calculating the optical constants for soft and hard x rays. The assumptions used to simplify the calculations at high energies are not valid in the visible and IR portion of the spectrum. This is not a surprise because the theory is based on the assumption that the atoms are independent of the crystal phase of the material. The relative difference in the ASF of the material has been quantified by calculating the ASF of diamond and graphite from tabulated values found in References [5, 6].

There is still a 20-40% relative difference between the ASF of diamond and graphite between 400-700 Å (about 30–17 eV). That is 5–10 times greater than the average energy of a carbon to carbon bond. This shows that the configuration of the valence electrons still plays a significant role in the optical properties of a material at energies greater than 10 eV.

The effect of this difference can be seen by looking at the reflectance of light normal to a surface in a vacuum given by

$$R = \frac{n-1}{n+1} \tag{6.1}$$

This assumes there is not absorption. Now assume that the index of refraction is actually $n + \Delta n$. Now Equation 6.1 becomes

$$R = \frac{n+\Delta n-1}{n+\Delta n+1} \tag{6.2}$$

Expand the denominator using the binomial expansion to get back equation 6.1.

$$R = \frac{n-1}{n+1} + \frac{\Delta n}{n+1} + \frac{\Delta n(1-n-\Delta n)}{(n+1)^2} \tag{6.3}$$

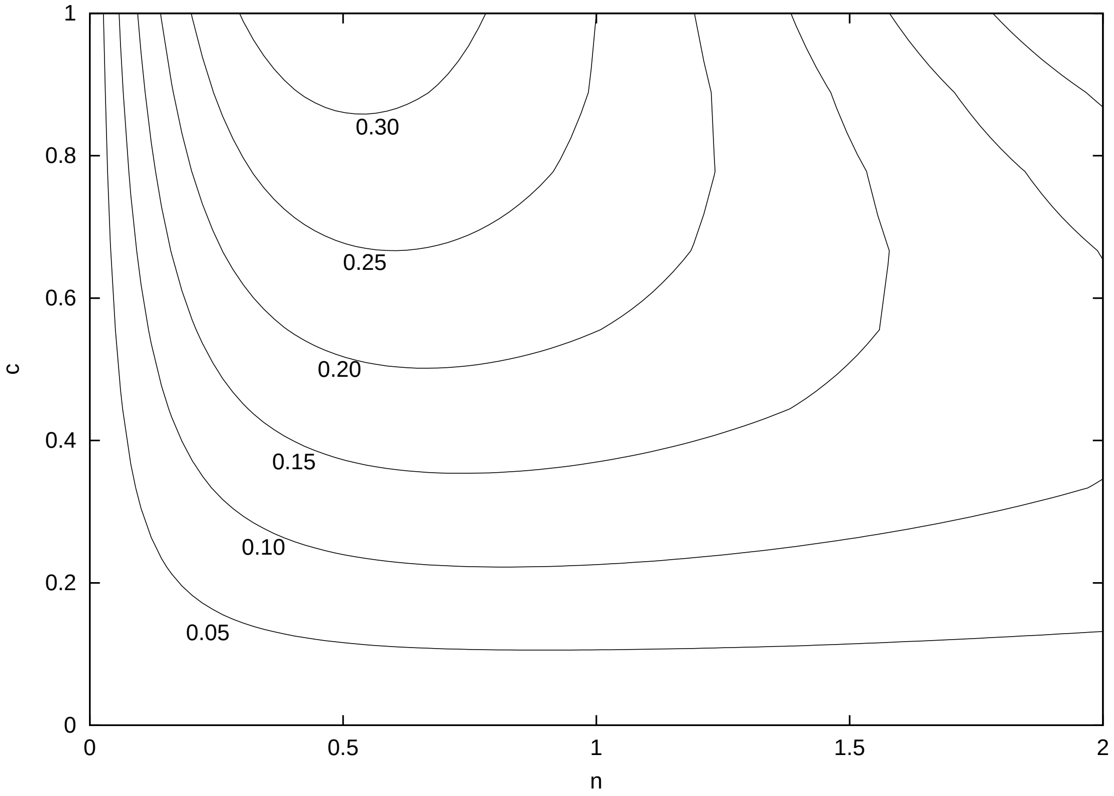

Figure 6.1: General fractional first order correction in reflectance as a function of the index of refraction and the fraction of change in the index of refraction. The vertical axis, c, denotes the relative difference between the ASF and the horizontal axis denotes the real part of the index of refraction, n.

If the correction term is some fraction of the original index of refraction, $\Delta n = cn$ it is possible to calculate the error in the reflectance as a function of the index and the fractional difference in the optical constants.

The work in this thesis does not show where the ASF of diamond and graphite converge. Because of time and physical constraints it was not possible to measure the optical constants of diamond to 40 eV. The trend of the relative difference in f_1 (see Figure 5.5) tends toward zero around 300 Å. However, because of the lack of data for diamond at higher energies, it is impossible to tell if the relative difference is monotonically decreasing, if the relative difference will oscillate about zero, or if there is more structure to be seen in the relative difference at higher energies. There will be some structure around absorption edges, but is there structure far from absorption edges that makes it difficult to use ASF.

This thesis has only focused on elemental carbon because it has two well defined crystal phases and there are no surface oxides that will make the determination of the optical properties more difficult. Carbon is also a light element with only six electrons. There are no “inner” core electrons that may be less affected by the crystal structure of the material. This may be determined by studying other materials.

This work may be most applicable to lighter elements that have electrons that are not shielded by other electrons in the atom. Oxygen is a light element with eight electrons. Oxygen forms compounds with most metals, and can be the bane or miracle of high reflectance. Because it is a lighter element this analysis may be applicable in determining at what energies atomic scattering theory may be used to accurately predict the optical properties of oxides.

Appendix A

Classical Theories of Optical Constants

A.1 Drude Theory

This discussion mostly follow the discussions in References [36] and [37].

With the advent of the kinetic theory of gases in the 19th century there was a great deal of physics that was able to use the results of the kinetic theory of gases to describe other phenomena. Three years after the development of the kinetic theory Drude used the kinetic theory of gases to describe the conductivity of metals and the transparency of metals in the ultraviolet. The Drude theory was successful at describing DC and AC conductivity. Because it was successful at describing AC conductivity the Drude theory was also successful at predicting the dielectric properties or optical properties of a metal.

Drude theory describes the behavior of electrons in a metal, but graphite and diamond are not metals. Carbon is known as a semi metal, and graphite is conductive along certain directions, so the Drude theory is a little related to the optical properties of carbon. The Drude theory is very conceptual and is a good place to start a study of optical properties.

Drude theory works very well despite many incorrect approximations that are made to make the problem easier. The number of approximations made is amazing, and the theory only works because two bad approximations cancel. There are many approximations and I will first discuss the obvious approximations, and then more subtle approximations in the theory.

A.1.1 Approximations

Review of Ideal Gas Theory

In the ideal gas theory all the particles are assumed to be small hard spheres with a negligible size. Between the collisions it is assumed there are no forces acting on the particles, so they travel in straight lines according to Newton's laws. When two particles collide it is assumed the collision is instantaneous, or at least the time scale is small compared to other times involved in the problem. It is also assumed that the gas is a low pressure so the volume of the particles does not significantly effect the volume of the container. The actual electron density and pressure in a metal are much greater than pressures and densities that the ideal gas law is good at predicting. Despite that the ideal gas approximation works surprisingly well.

Drude's Approximations

Besides using the ideal gas law Drude made several other approximations in developing his theory. The first was to assume the electrons were bound to positive ions in the metal by coulombic forces. The positive ions were assumed to be massive and move little. Electrons that are close the ion cores are called core electrons and are not involved in the conductivity of the metal. Electrons not strongly bound to the core are called valence electrons and are free to move in the metal. The number of valence electrons in an atom is Z.

When an electric field is applied to a metal the valence electrons acquire a net velocity opposite the electric field. The freedom of the electrons to move due to an applied electric field is denoted by σ the conductivity. The conductivity is not infinite because the electrons scatter off the ion cores, acquiring a random direction with each collision. The direction the electrons leaves the ion core does not depend on the conditions before the collision. It is assumed that electrons do not scatter off each other.

The electrons come into thermal equilibrium with the ions only through collisions. The velocity an electrons leaves an ion core depends on the thermal properties of the ion core. No velocity distribution is assumed, and would not significantly change the result of the Drude theory.

The average time between collisions is τ, and is known as the relaxation time. It is also known as the collision time or the mean free time. The probability of a collision is given by τ^{-1}. Much of the information describing the collision is hidden in τ.

A.1.2 DC Conductivity

The goal is to derive the AC conductivity (eventually relating it to the optical properties of a material), but the derivation of the DC conductivity is a good introduction for the AC conductivity.

Given that background, start with Ohm's law $V = IR$. A more general form of Ohm's law is

$$\mathbf{J} = \sigma \mathbf{E} \tag{A.1}$$

where σ the conductivity is related to τ the relaxation time. As a reminder $\mathbf{J} = \frac{\mathbf{I}}{A}$. The current density $\mathbf{J}$ is related to the net velocity of the electrons.

$$\mathbf{J} = ne\mathbf{v} \tag{A.2}$$

Where n is the number of electrons per unit volume, e is the fundamental charge, and $\mathbf{v}$ is the net velocity of the electrons due to external forces. The net velocity of the electrons is also called the drift velocity. When $\mathbf{E} = 0$ the electrons are still moving but the velocities are randomly distributed and cancel any net movement of the electrons.

To start solving for σ first solve for the velocity of the electron as a function of $\mathbf{E}$ and τ. The force on an electron is

$$\mathbf{F} = -e(\mathbf{E} + \mathbf{v} \times \mathbf{B}) \tag{A.3}$$

Ignore $\mathbf{B}$ because the magnitude of $\mathbf{B}$ is negligible compared to $\mathbf{E}$. The acceleration is simply

$$\mathbf{a} = -\frac{e\mathbf{E}\tau}{m_e} \tag{A.4}$$

Assuming the initial velocity after the collision is zero, the velocity of an electron some time t after the collision is

$$\mathbf{v(t)} = -\frac{e\mathbf{E}\tau}{m_e}t \tag{A.5}$$

The average time an electron has to accelerate is τ, so the average velocity of an electron is

$$\mathbf{v_{ave}} = -\frac{e\mathbf{E}\tau}{m_e}\tau \tag{A.6}$$

Plug this back into Equation 4.20 to get

$$\mathbf{J} = (-\frac{e^2 n\tau}{m_e})\mathbf{E} \tag{A.7}$$

The term in parenthesis is the DC conductivity of a metal using Drude Theory

$$\sigma = \frac{ne^2\tau}{m_e} \tag{A.8}$$

The conductivity σ is actually a second rank tensor, but Drude assumed the metal was isotropic. Though graphite is anisotropic there is no good reason to make a simple theory harder than it needs to be. Especially when Drude theory is very good a conceptually understand how light interacts with a metal.

Now look at the mean free path of an electron to get a little better understanding about the behavior of electrons in metals. The mean free path is the distance an electron will travel between collisions.

Assume it depends on the relaxation time τ and it's velocity v between collisions.

$$\ell = v_o t \tag{A.9}$$

Ignore the contribution by **E** for simplicity and because its contribution is negligible. Solve for v_o using the classical equipartition of energy assuming three degrees of freedom.

$$\frac{1}{2} m v_o^2 = \frac{3}{2} k_b T \tag{A.10}$$

The relaxation time τ is estimated using the measured conductivity of common metals. At room temperature $v_o \sim 10^7$cm/sec, so $\ell \sim$1–10Å. About the distance between atoms, fortifying the concept that electrons scatter off ion cores. Another way to think about it is the electron clouds are large enough to overlap between atoms. This makes it easy for electrons to move through the metal because the electron cloud is shared over multiple atoms [38].

DC Conductivity Fails

When a metal is cooled its conductivity increases. The temperature dependence of the conductivity is not predicted by Drude theory. Also at low temperatures and not predicted by Drude theory, the mean free path also increases to ∼1 cm! This means the electrons are scattering off of something besides the ion cores because they are spaced every few angstroms. There are other interactions that dominate at other temperatures that must be described by quantum mechanics. Drude theory works reasonably well in regions when the quantum mechanical nature of materials does not dominate, but its limitations can be seen in regions where quantum mechanics plays a more visible role in the behavior of a material. Despite the failure of Drude theory, τ is still used to describe some phenomena. It can be used to describe the behavior of conductors in large magnetic fields and the AC behavior of metals.

Momentum Considerations

Now find the average momentum of an accelerated electron between collisions. This becomes important when solving for the AC properties of the conductivity. Between collisions the electron will accelerate or change momentum if there is an applied electric field. Assume at time t the electron has momentum $\mathbf{p}$, and at some infinitesimal time later the momentum is given by $\mathbf{p} + \mathbf{dt}$. The increased momentum is

$$\Delta \mathbf{p}(t) = \mathbf{f}(t)dt + \mathcal{O}(dt^2) \tag{A.11}$$

Ignore the second order terms. The momentum after a time dt the momentum is given by

$$\mathbf{p}(t + dt) = \mathbf{p} + \mathbf{f}(t)dt \tag{A.12}$$

A fraction of the electrons will be scattered in the time dt and will lose all memory of their previous speed and direction. The fraction of the electrons that are scattered in a time dt is dt/τ. The remaining electrons will gain momentum and will be able to move with the applied electric field. The number of remaining electrons that contribute to the average momentum is

$$1 - \frac{dt}{\tau} \tag{A.13}$$

Now put it all together to find the momentum after a time dt

$$\begin{aligned} \mathbf{p}(t+dt) &= (1 - \frac{dt}{\tau})(\mathbf{p}(t) + \mathbf{f}(t) + \mathcal{O}(dt)^2) \\ &= \mathbf{p}(t) - \frac{dt}{\tau}\mathbf{p}(t) + \mathbf{f}(t)dt - \mathbf{f}(t)\frac{dt^2}{\tau} + \mathcal{O}(dt)^2 \end{aligned} \tag{A.14}$$

Put all the dt^2 terms into $\mathcal{O}(dt)^2$. The collisions between electrons is grouped in the $\mathcal{O}(dt)^2$ term and will eventually be thrown out. For more details on why the second order term is small see pg 11 of Reference [36]. Gather all the momentum terms that are not multiplied by other terms on the left side and all remaining terms on the right.

$$\mathbf{p}(t+dt) - \mathbf{p}(t) = -\frac{dt}{\tau}\mathbf{p}(t) + \mathbf{f}(t)dt - \mathbf{f}(t)\frac{dt^2}{\tau} + \mathcal{O}(dt)^2 \tag{A.15}$$

Divide by dt and take the limit as $dt \to 0$.

$$\frac{d}{dt}\mathbf{p}(t) = -\frac{\mathbf{p}(t)}{\tau} + \mathbf{f}(t) \tag{A.16}$$

The negative in front of the first term is the damping term. This comes from the $(1 - \frac{dt}{\tau})$ term that is multiplied into the Equation 4.20 to account for the electrons that are involved in collisions.

A.1.3 AC Conductivity

Now assume the electric field is varying in time instead of the static field assumed in the section on DC conductivity. Start by assuming the electric field is uniform over the surface and has a form

$$\mathbf{E}(t) = Re(\mathbf{E}(\omega)e^{-i\omega t}) \tag{A.17}$$

Equation A.16 now becomes

$$\frac{d}{dt}\mathbf{p}(t) = -\frac{\mathbf{p}(t)}{\tau} - e\mathbf{E}(t) \tag{A.18}$$

Also assume the momentum has the form

$$\mathbf{p}(t) = Re(\mathbf{p}(\omega)e^{-i\omega t}) \tag{A.19}$$

Taking the derivatives and cancelling all terms with the form $e^{-i\omega t}$ the previous equation becomes

$$i\omega\mathbf{p}(\omega) = \frac{\mathbf{p}(\omega)}{\tau} + e\mathbf{E}(\omega) \tag{A.20}$$

Now it is possible to solve for the frequency dependent momentum and by extension the velocity imparted to the electrons in the material by the electric field.

$$\mathbf{p}(\omega) = -\frac{e\mathbf{E}(\omega)}{\frac{1}{\tau} - i\omega} \tag{A.21}$$

The current density is defined to be

$$\mathbf{j} = -ne\mathbf{v} = -\frac{ne}{m}\mathbf{p} \tag{A.22}$$

where n is the number of electrons per unit volume. Combine Equations A.17 and A.21, and once again, to remove the exponent from the equations, assume the current density is frequency dependent and has the familiar form

$$\mathbf{j}(t) = Re[\mathbf{j}(\omega)e^{-i\omega t}] \tag{A.23}$$

Ohm's law now looks like

$$\mathbf{j} = -\frac{e}{\frac{1}{\tau} - i\omega}\mathbf{E}(\omega) \tag{A.24}$$

By comparing Equations A.1 and A.24 it is possible to recognize the frequency dependent conductivity to be

$$\sigma(\omega) = \frac{ne^2}{m(\frac{1}{\tau} - i\omega)} = \frac{\sigma_o}{1 - i\omega\tau} \tag{A.25}$$

where

$$\sigma_o = \frac{ne^2\tau}{m} \tag{A.26}$$

More may be done with the conductivity, but simplifying the conductivity will not illuminate the optical properties any more than simplifying the final results. More details may be found in Reference [37].

A.1.4 Maxwell's Equations in Free Space

Maxwell's equations are used with $\mathbf{J}$ found previously to solve for the dielectric properties of an electron gas in a metal. The following are Maxwell's equations in free space.

$$\nabla\cdot\mathbf{E} = 0 \tag{A.27}$$

$$\nabla\cdot\mathbf{H} = 0 \tag{A.28}$$

$$\nabla\times\mathbf{E} = -\frac{1}{c}\frac{\partial\mathbf{H}}{\partial t} \tag{A.29}$$

$$\nabla\times\mathbf{H} = \frac{4\pi}{c}\mathbf{J} + \frac{1}{c}\frac{\partial\mathbf{E}}{\partial t} \tag{A.30}$$

A.1.5 Dielectric Properties

Now use the frequency dependent current in Maxwell's equations to find the form of the dielectric constant. Getting to Maxwell's equations is the crux of explicitly solving for the dielectric and optical properties of a material. Assume the electric and magnetic fields have the form

$$\mathbf{E} = \mathbf{E}_o e^{-i\omega t} \tag{A.31}$$

$$\mathbf{H} = \mathbf{H}_o e^{-i\omega t} \tag{A.32}$$

Now any time derivative will bring down a $i\omega t$ to the derivative term.

Then, as is commonly done, take the curl of Equation A.29 to start solving for the wave equation.

$$\nabla\times(\nabla\times\mathbf{E}) = -\frac{1}{c}\nabla\times(\frac{\partial\mathbf{H}}{\partial t}) \tag{A.33}$$

Using the following vector identity

$$\nabla\times(\nabla\times\mathbf{E}) = \nabla\cdot\mathbf{E} - \nabla^2\mathbf{E} \tag{A.34}$$

simplify the left hand side of the previous equation. This will further simplify by recognizing that Equation A.27 makes the first term be zero. Now use the time derivative of Equation A.30 get Equation A.33 entirely in terms of **E**.

$$\begin{aligned} -\nabla^2\mathbf{E} &= \frac{i\omega}{c}\nabla\times\mathbf{H} \\ &= \frac{i\omega}{c}\left[\frac{4\pi\sigma}{c} - \frac{i\omega}{c}\right]\mathbf{E} \\ &= \frac{\omega^2}{c^2}\left[1 + \frac{4\pi i\sigma}{\omega}\right]\mathbf{E} \end{aligned} \tag{A.35}$$

Equation A.35 is now in the form of the wave equation. The dielectric constant may then be recognized to

$$\epsilon(\omega) = 1 + \frac{4\pi i\sigma(\omega)}{\omega} \tag{A.36}$$

A.1.6 Plasma Frequency

Solving for the dielectric constant is only the beginning of understanding the optical properties of a material. One property that may be derived is what is known as the plasma frequency. It is used to estimate at what frequency a metal will become transparent. Start by explicitly writing out the conductivity part of Equation A.36.

$$\epsilon(\omega) = 1 + \frac{4\pi i\sigma_o}{\omega(1 - i\omega\tau)} \tag{A.37}$$

Separate the real from the imaginary parts by multiplying the second term by the complex conjugate of the denominator. This yields

$$\epsilon(\omega) = 1 + \frac{4\pi\sigma_o}{1+\omega^2\tau^2} + i\frac{4\pi\sigma_o}{\omega(1+\omega^2\tau^2)} \tag{A.38}$$

For notational convenience label the real and imaginary parts.

$$\epsilon(\omega) = \epsilon_1 + i\epsilon_2 \tag{A.39}$$

At a high enough frequency $\omega\tau \gg 1$ it is possible to simplify the denominator without losing too much information. Explicitly include σ_o (equation A.26.)

$$\epsilon(\omega) \simeq 1 - \frac{4\pi n e^2 i\tau}{\omega^2 m i\tau} \tag{A.40}$$

Cancel terms and group all the constants.

$$\epsilon(\omega) \simeq 1 - \frac{\omega_p^2}{\omega^2} \tag{A.41}$$

$$\omega_p^2 \equiv \frac{4\pi n e^2}{m} \tag{A.42}$$

This result has significance when it is put back into the wave equation. One form of $\mathbf{E}(\omega)$ that satisfies the equation A.35 is

$$\mathbf{E}(\omega) = \mathbf{E}_o e^{\sqrt{\epsilon(\omega)} i\omega\mathbf{r}/c} \tag{A.43}$$

If $\omega < \omega_p$ then the exponent of Equation A.43 will be imaginary making the electric field oscillatory. This means radiation will propagate though the medium, or the material will be transparent. If $\omega < \omega_p$ then the exponent will be real and negative and the electric field decay inside the material. No radiation will be transmitted through the medium. The energy may be absorbed by the medium or it may be reflected[1].

A.1.7 Index of Refraction

The dielectric constant by itself adequately describes the optical behavior of a material, but Fresnel equations use the complex index of refraction $\tilde{\mathcal{N}}$ to describe the optical properties of the material. The tilde denotes $\mathcal{N}$ is a complex number.

$$\tilde{\mathcal{N}} = n + ik \tag{A.44}$$

---

[1] The ionosphere of the earth is a plasma with a plasma frequency. The frequency of AM radio waves is less than the plasma frequency of ionosphere, so the AM waves will bounce off the ionosphere and back to the earth. That is why AM stations from two states away can be heard during different times of the day. The frequency of FM stations is greater than the plasma frequency of the ionosphere. So as far as FM waves are concerned the ionosphere is a big window and they pass though out into the depths of outer space.

The dielectric constant also has a real and imaginary part. No tilde will be used with ϵ because it is assumed the complex nature of ϵ is implicit.

$$\epsilon = \epsilon_1 + i\epsilon_2 \tag{A.45}$$

Conversion between ϵ and $\tilde{\mathcal{N}}$ is simple (see Section A.2).

$$\tilde{\mathcal{N}}^2 = \epsilon \tag{A.46}$$

$$\epsilon_1 = n^2 - k^2 \tag{A.47}$$

$$\epsilon_2 = 2nk \tag{A.48}$$

A.2 Lorentz Oscillators

Drude theory assumes that the electrons are free to "slosh" around inside the metal like water in a glass. But that concept is only valid for metals, and more specifically alkali metals. What if the material is not a metal, how could the optical properties be understood? A model that works well is to assume an electron is harmonic coupled to a fixed nucleus. The electron is considered to be coupled to the nucleus by a spring with a spring constant of k_s (different than the wavenumber k or absorptive constant k.) There will be a natural harmonic frequency ω_0 that depends on k_s. A physical interpretation of the spring is the coulombic force that binds the electron to the nucleus. There is also a damping force, γ, that is proportional to the velocity of the electron around the nucleus.

$$m\frac{d^2\mathbf{x}_s}{dt^2} + m\gamma\frac{d\mathbf{x}_s}{dt} + m\omega_s^2\mathbf{x}_s = -e\mathbf{E}_i \tag{A.49}$$

where $\mathbf{E}_i$ is the incident electric field that is driving the oscillations. Assuming the oscillations are small and harmonic the displacement x can be represented by

$$x(t) = xe^{i\omega t} \tag{A.50}$$

Also assume the electric field has a similar form

$$\mathbf{E}(t) = E_0 e^{i\omega t} \tag{A.51}$$

Each time derivative of $x(t)$ will bring down an ωt making it possible to easily solve Equation A.49 for $x(t)$.

$$\tilde{\mathbf{x}}(t) = \frac{(e)}{m[(\omega_0^2 - \omega^2 - i\gamma\omega)]}\mathbf{E_0}e^{-i\omega]} \tag{A.52}$$

The tilde signifies the value is complex, which comes from the damping term.

As the electrons oscillate around the ion cores a dipole moment is created due to a displacement of charged ion cores from the electrons.

$$\mathbf{p} = q\mathbf{d} \tag{A.53}$$

where q is the amount of charge that has been separated and $\mathbf{d}$ is the distance between the centers of the positive and negative charges.

The frequency that the electron rotates around the nucleus depends on the distance from the nucleus. The distance of the electron from the nucleus is related to the energy of the electron while bound to the nucleus. The nucleus is assumed to be fixed and motionless because of its large mass. The spacing of the nuclei determines the density of electrons in a material.

It is assumed that each electron in an atom has a resonating frequency, ω_0, that is associated with the energy of the electron in the atom.

The interaction of light with frequency, ω, and a single electron with an oscillating frequency, ω_0, can be described by Maxwell's equations. The displacement of the electron by the electric field component of the light creates a dipole moment in the atom. The time-dependent dipole moment

$\tilde{\mathbf{p}}(t)$ created by the movement of the electron is

$$\tilde{\mathbf{p}}(t) = \frac{(e^2)/m_e}{(\omega_0^2 - \omega^2 - i\gamma\omega)}\mathbf{E_0}e^{-i\omega t} \tag{A.54}$$

where m_e is the mass of an electron, e is the charge of an electron, γ is a damping factor, and $\mathbf{E_0}$ is the amplitude of the light's electric field. In a real material electrons may oscillate at one of several different oscillating frequencies that are material specific. These specific frequencies are due to the energy spacings within the atom. If there are N atoms per unit volume, and there is a fraction, f_j, of the electrons with frequency ω_j and damping factor γ_j the net polarization of the material is

$$\tilde{\mathbf{P}} = \frac{Ne^2}{m_e}\sum_j \frac{f_j}{(\omega_j^2 - \omega^2 - i\gamma_j\omega)}\tilde{\mathbf{E}} \tag{A.55}$$

where $\tilde{\mathbf{P}}$ and $\tilde{\mathbf{E}}$ are complex amplitudes. $\tilde{\mathbf{P}}$ and $\tilde{\mathbf{E}}$ are related by

$$\tilde{\mathbf{P}} = \epsilon_0\chi_e\tilde{\mathbf{E}} \tag{A.56}$$

for an isotropic material. The complex susceptibility, χ_e, is related to the complex permittivity, ϵ, by

$$\epsilon = \epsilon_0(1 + \chi_e) \tag{A.57}$$

By modelling the interaction of light with an electron in an atom as a damped harmonic oscillator, the complex permittivity takes the form

$$\epsilon = \epsilon_0\left[1 + \frac{Ne^2}{m_e\epsilon_0}\sum_j \frac{f_j}{(\omega_j^2 - \omega^2) - i\gamma_j\omega}\right] \tag{A.58}$$

Even though ϵ is a complex number it is not written with a tilde because ϵ is explicitly complex. Following standard convention, the complex permittivity is expressed as ϵ_1 and ϵ_2. They are defined to be

$$\epsilon = \epsilon_1 + i\epsilon_2 = Re\left\{\epsilon\right\} + iIm\left\{\epsilon\right\} \tag{A.59}$$

The wave equation can still be solved with a complex ϵ and has a solution

$$\tilde{\mathbf{E}}(x,t) = \tilde{\mathbf{E}}_0e^{i(\mathcal{K}x - \omega t)} \tag{A.60}$$

where $\mathcal{K}$ is the complex wavenumber that can be expressed as

$$\mathcal{K}^2 = \frac{\omega^2}{c^2}\left[1 + \frac{Ne^2}{m_e\epsilon_0}\sum_j \frac{f_j}{(\omega_j^2 - \omega^2) - i\gamma_j\omega}\right] \tag{A.61}$$

The wavenumber is often expressed in terms of the real and imaginary parts as

$$\mathcal{K} = k + i\alpha = Re\left\{\mathcal{K}\right\} + iIm\left\{\mathcal{K}\right\} \tag{A.62}$$

Because $\mathcal{K} = \frac{\omega}{c}\mathcal{N}$ the complex index of refraction is defined as

$$\mathcal{N} = n + ik = Re\left\{\mathcal{N}\right\} + iIm\left\{\mathcal{N}\right\} \tag{A.63}$$

$\mathcal{N}$ can now be expressed as

$$\mathcal{N} = \left[1 + \frac{Ne^2}{m_e \epsilon_0} \sum_j \frac{f_j}{(\omega_j^2 - \omega^2) - i\gamma_j \omega}\right] \tag{A.64}$$

Appendix B

Plots of Spectral Line Radiation

The following tables show the relative intensities of spectral emissions from various gases that may be used in the hollow cathode. Not every gas that is shown was used in this thesis, but the information should be useful for future work. Any intensity below 150 has be excluded to avoid data overload.

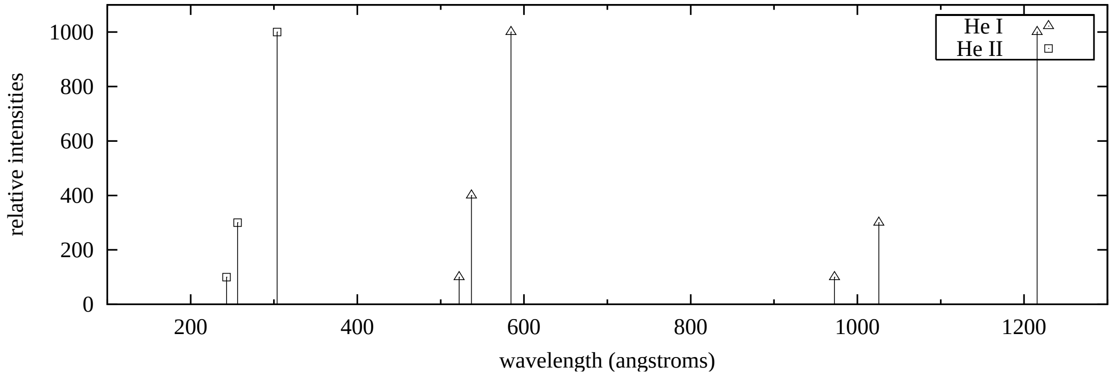

Figure B.1: Line Radiation of helium gas between 100–1300 Å taken from Reference [39].

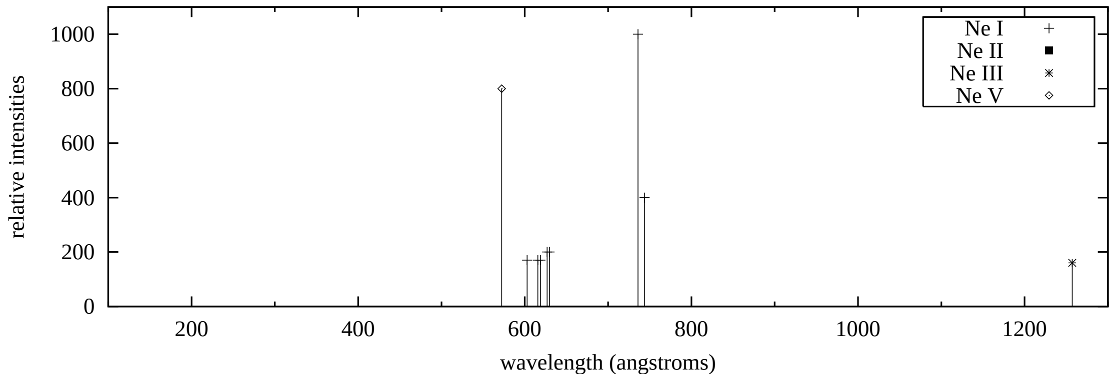

Figure B.2: Line Radiation of neon gas between 100–1300 Å taken from Reference [39].

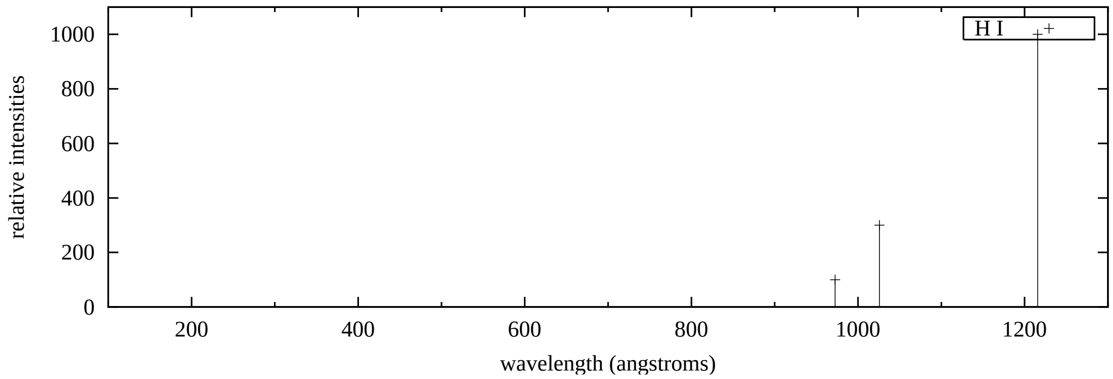

Figure B.3: Line Radiation of hydrogen gas between 100–1300 Å taken from Reference [39].

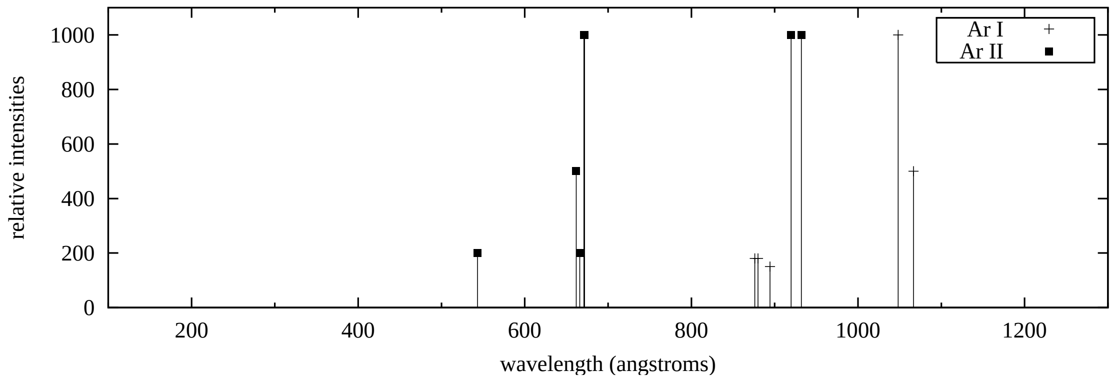

Figure B.4: Line Radiation of argon gas between 100–1300 Å taken from Reference [39].

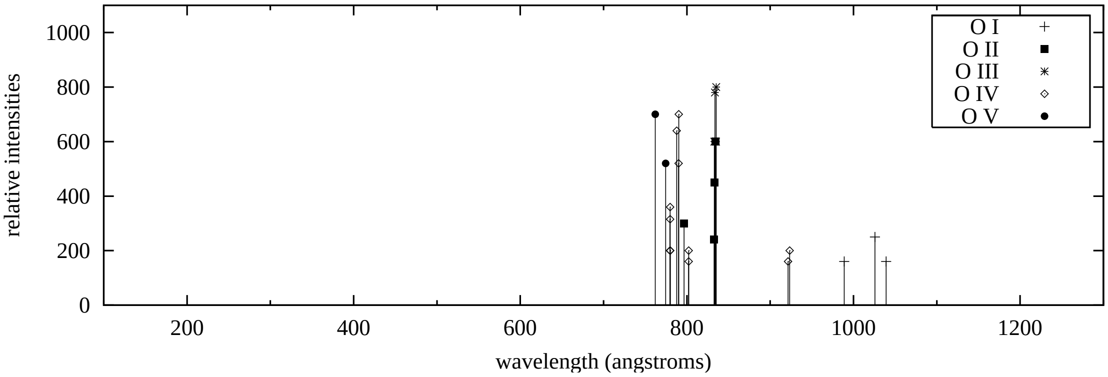

Figure B.5: Line Radiation of oxygen gas between 100–1300 Å taken from Reference [39].

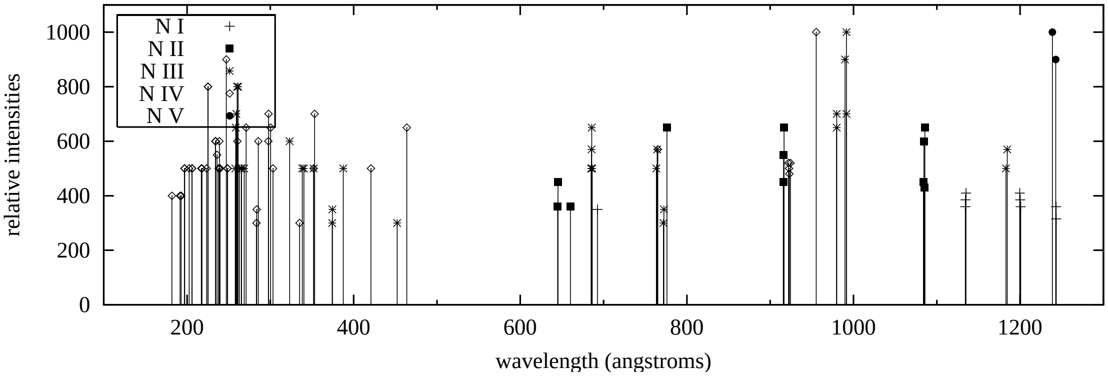

Figure B.6: Line Radiation of nitrogen gas between 100–1300 Å taken from Reference [39].

Appendix C

O-Chamber Details

C.1 LabVIEW Programs

This is the output obtained by printing all the documentation on the VI's in LabVIEW. The following files are documented in this Appendix:

1. VAR
    (a) Combines all SubVI's to make $\theta/2\theta$ measurements while checking the source intensity several times
2. T2T
    (a) Performs a simple $\theta/2\theta$ once
3. StageControlSpring
    (a) Sends pulses to the NIDAQ board that move the stepper motors. It is assumed the motors are spring loaded so there is no reason to correct for backlash.
4. CalcR
    (a) Takes an array of reflectance and source measurements and calculates the reflectance
5. FindMax
    (a) Measures the intensity over a range of angles or positions and returns the most intense counts and its position
6. InferenceForRegression
    (a) Calculates the statistical error of the measurements

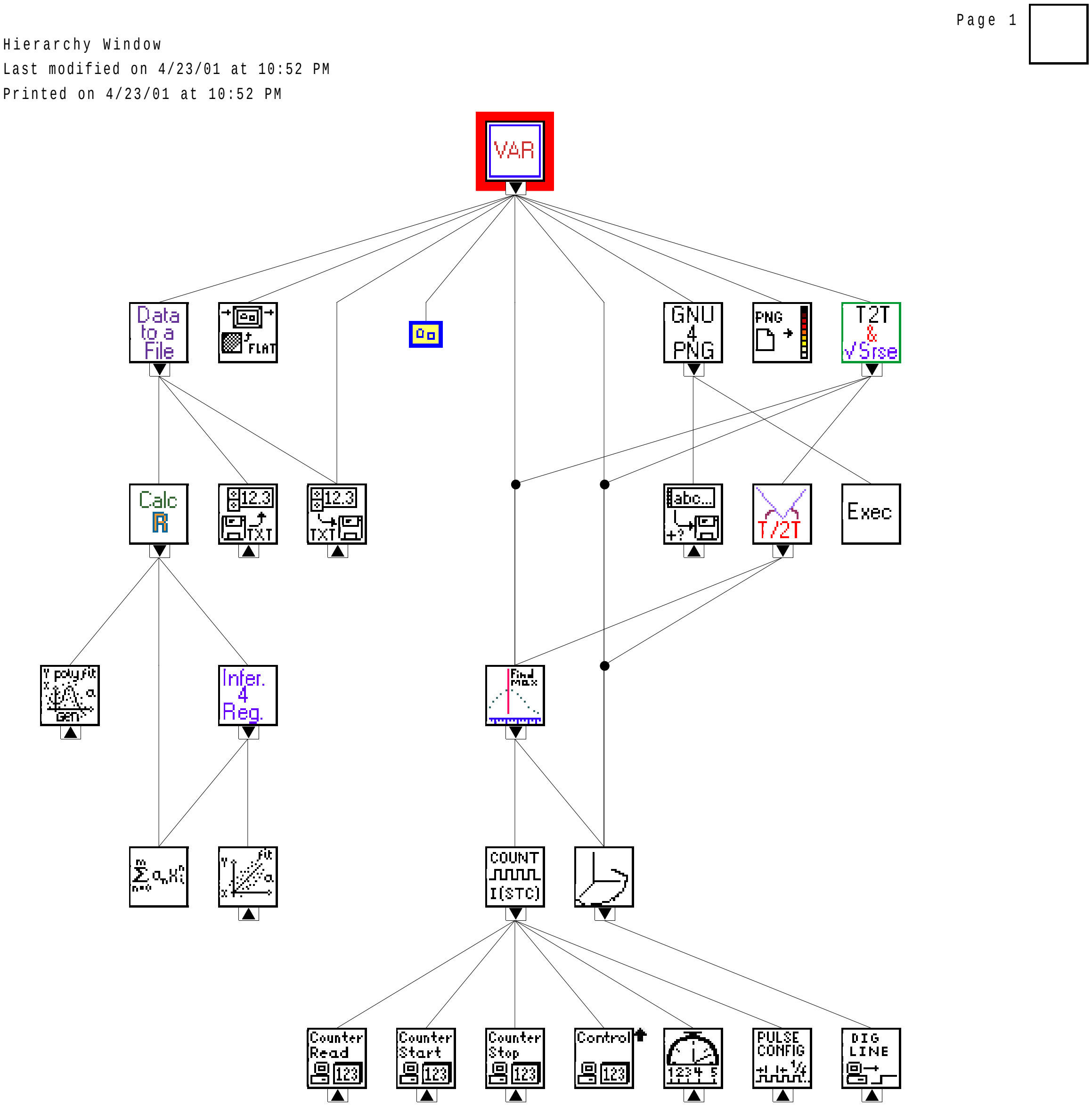

Page 1

Hierarchy Window
Last modified on 4/23/01 at 10:52 PM
Printed on 4/23/01 at 10:52 PM

Figure C.1: Hierarchy of SubVI's for the VAR VI page 1.

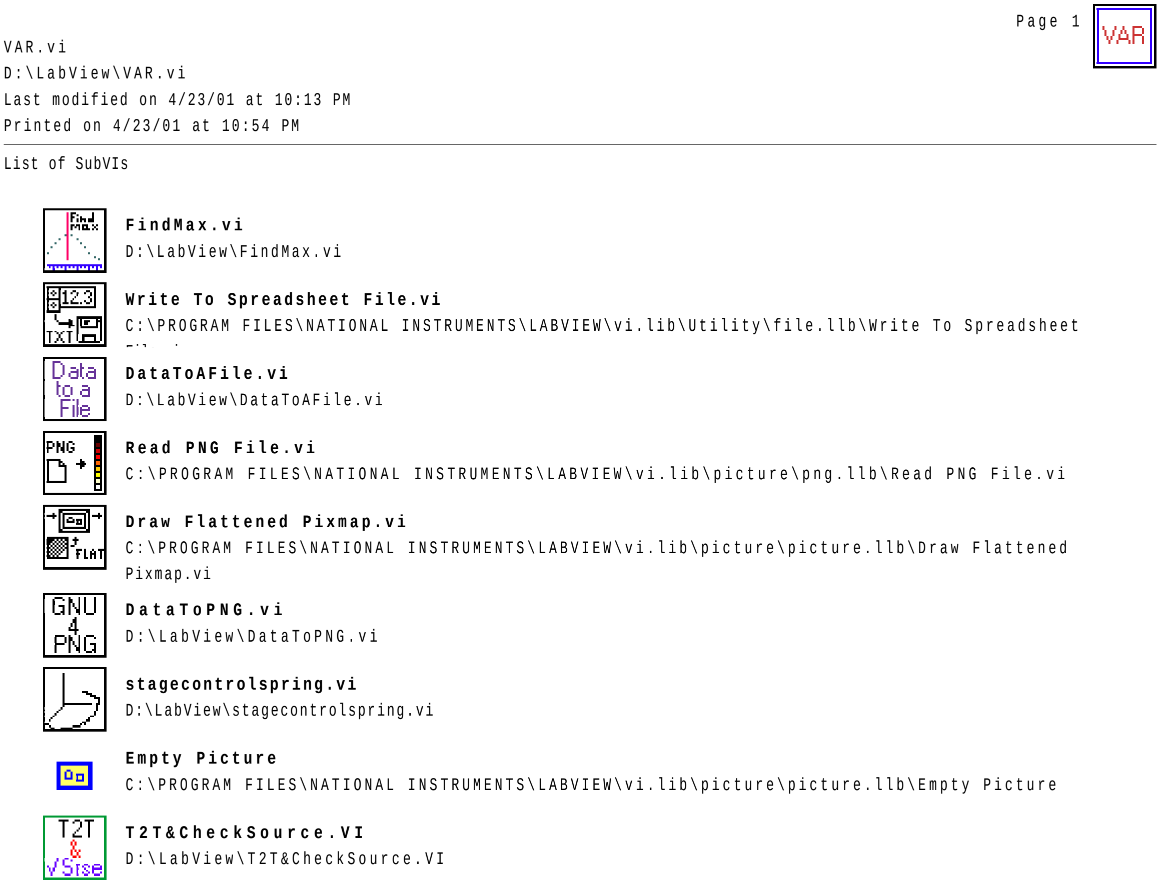

Page 1

VAR.vi
D:\LabView\VAR.vi
Last modified on 4/23/01 at 10:13 PM
Printed on 4/23/01 at 10:54 PM

List of SubVIs

FindMax.vi
D:\LabView\FindMax.vi

Write To Spreadsheet File.vi
C:\PROGRAM FILES\NATIONAL INSTRUMENTS\LABVIEW\vi.lib\Utility\file.llb\Write To Spreadsheet

DataToAFile.vi
D:\LabView\DataToAFile.vi

Read PNG File.vi
C:\PROGRAM FILES\NATIONAL INSTRUMENTS\LABVIEW\vi.lib\picture\png.llb\Read PNG File.vi

Draw Flattened Pixmap.vi
C:\PROGRAM FILES\NATIONAL INSTRUMENTS\LABVIEW\vi.lib\picture\picture.llb\Draw Flattened Pixmap.vi

DataToPNG.vi
D:\LabView\DataToPNG.vi

stagecontrolspring.vi
D:\LabView\stagecontrolspring.vi

Empty Picture
C:\PROGRAM FILES\NATIONAL INSTRUMENTS\LABVIEW\vi.lib\picture\picture.llb\Empty Picture

T2T&CheckSource.VI
D:\LabView\T2T&CheckSource.VI

Figure C.2: List of SubVI's for the VAR VI page 1.

Page 1

VAR.vi
D:\LabView\VAR.vi
Last modified on 4/23/01 at 10:04 PM
Printed on 4/23/01 at 10:04 PM

Front Panel

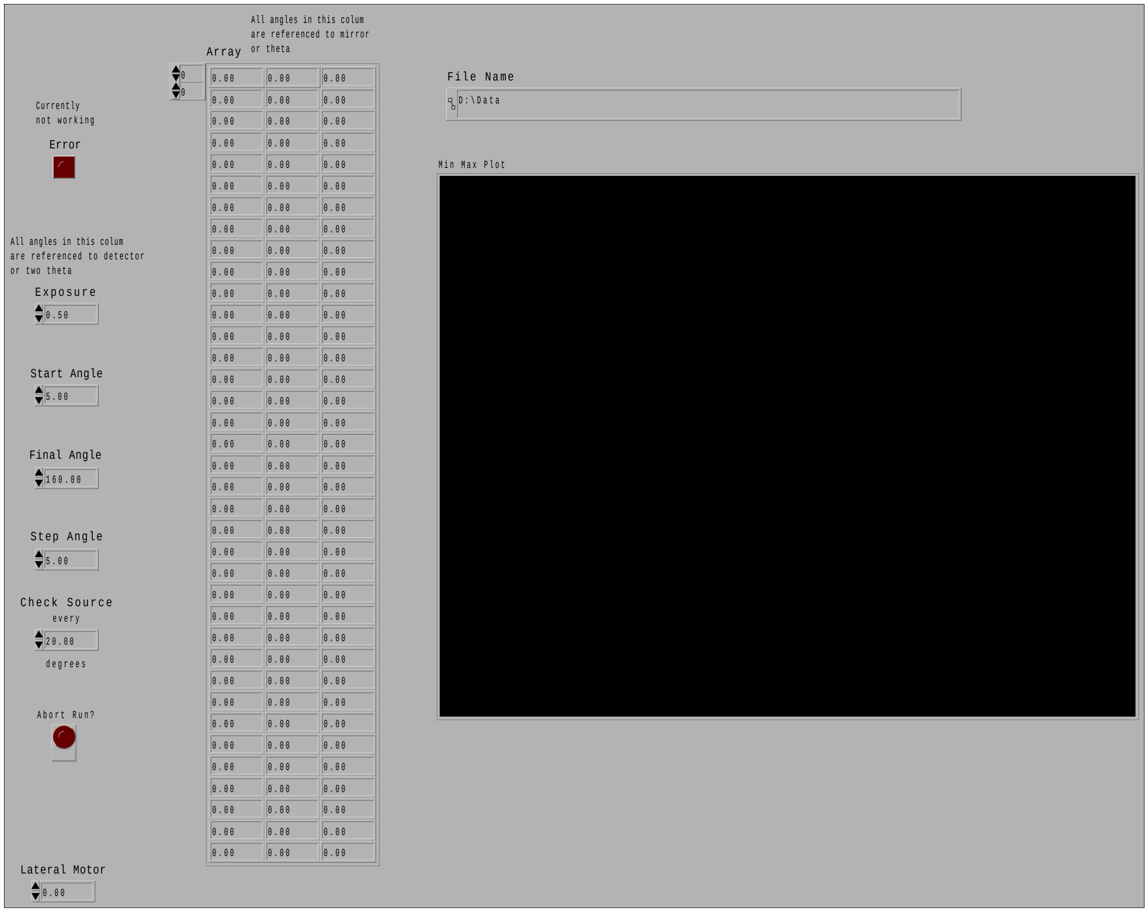

Exposure 0.50

Start Angle 5.00

Final Angle 160.00

Step Angle 5.00

Check Source every 20.00 degrees

Lateral Motor 0.00

File Name D:\Data

Array (index 0, 0)

0.00	0.00	0.00
0.00	0.00	0.00
0.00	0.00	0.00
0.00	0.00	0.00
0.00	0.00	0.00
0.00	0.00	0.00
0.00	0.00	0.00
0.00	0.00	0.00
0.00	0.00	0.00
0.00	0.00	0.00
0.00	0.00	0.00
0.00	0.00	0.00
0.00	0.00	0.00
0.00	0.00	0.00
0.00	0.00	0.00
0.00	0.00	0.00
0.00	0.00	0.00
0.00	0.00	0.00
0.00	0.00	0.00
0.00	0.00	0.00
0.00	0.00	0.00
0.00	0.00	0.00
0.00	0.00	0.00
0.00	0.00	0.00
0.00	0.00	0.00
0.00	0.00	0.00
0.00	0.00	0.00
0.00	0.00	0.00
0.00	0.00	0.00
0.00	0.00	0.00
0.00	0.00	0.00
0.00	0.00	0.00
0.00	0.00	0.00
0.00	0.00	0.00
0.00	0.00	0.00
0.00	0.00	0.00
0.00	0.00	0.00

Figure C.3: Documentation on VAR VI page 1.

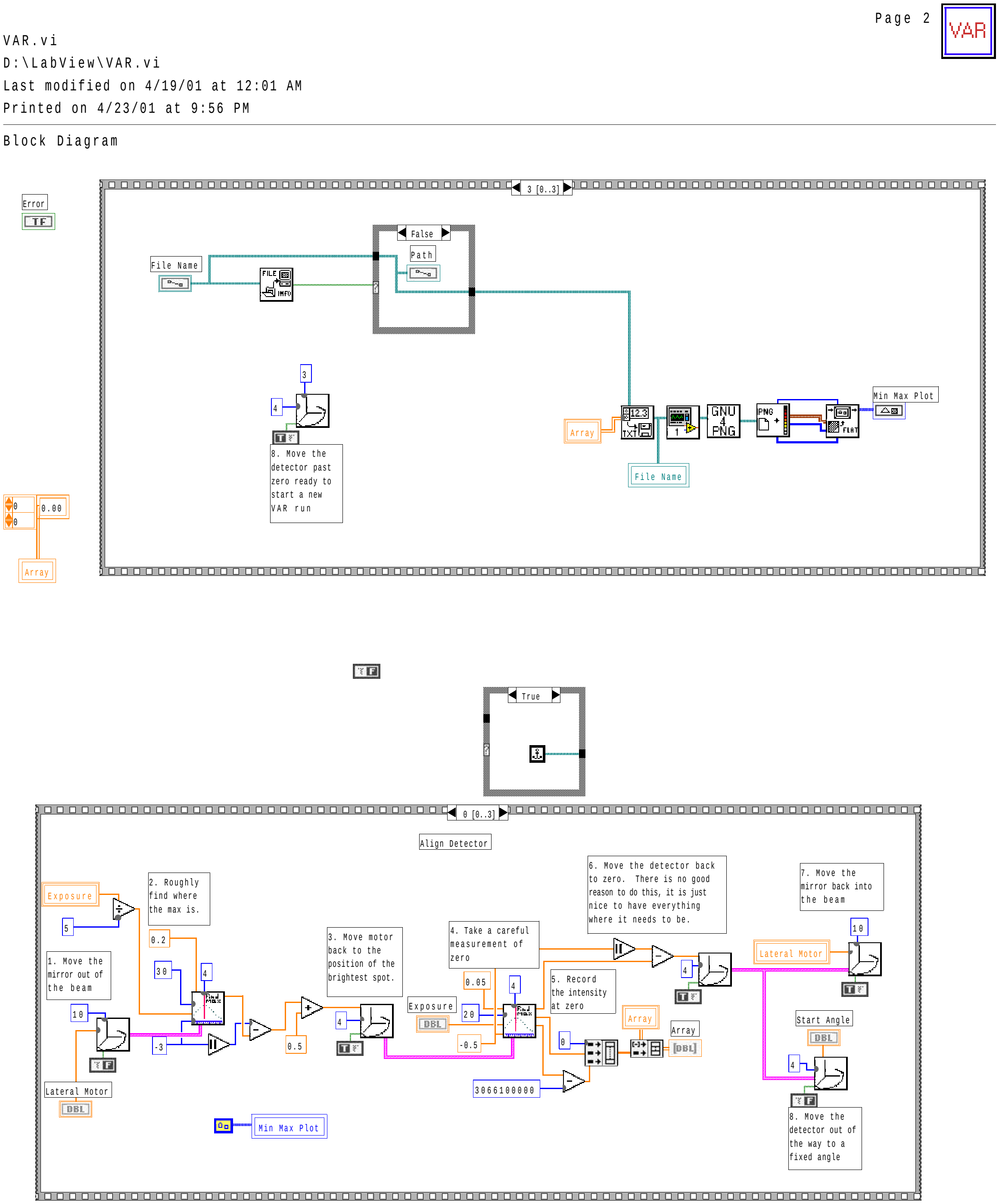

Page 2

VAR.vi
D:\LabView\VAR.vi
Last modified on 4/19/01 at 12:01 AM
Printed on 4/23/01 at 9:56 PM

Block Diagram

8. Move the detector past zero ready to start a new VAR run

2. Roughly find where the max is.

1. Move the mirror out of the beam

3. Move motor back to the position of the brightest spot.

4. Take a careful measurement of zero

5. Record the intensity at zero

6. Move the detector back to zero. There is no good reason to do this, it is just nice to have everything where it needs to be.

7. Move the mirror back into the beam

8. Move the detector out of the way to a fixed angle

Figure C.4: Documentation on VAR VI page 2.

Page 3

VAR.vi
D:\LabView\VAR.vi
Last modified on 4/19/01 at 12:01 AM
Printed on 4/23/01 at 9:56 PM

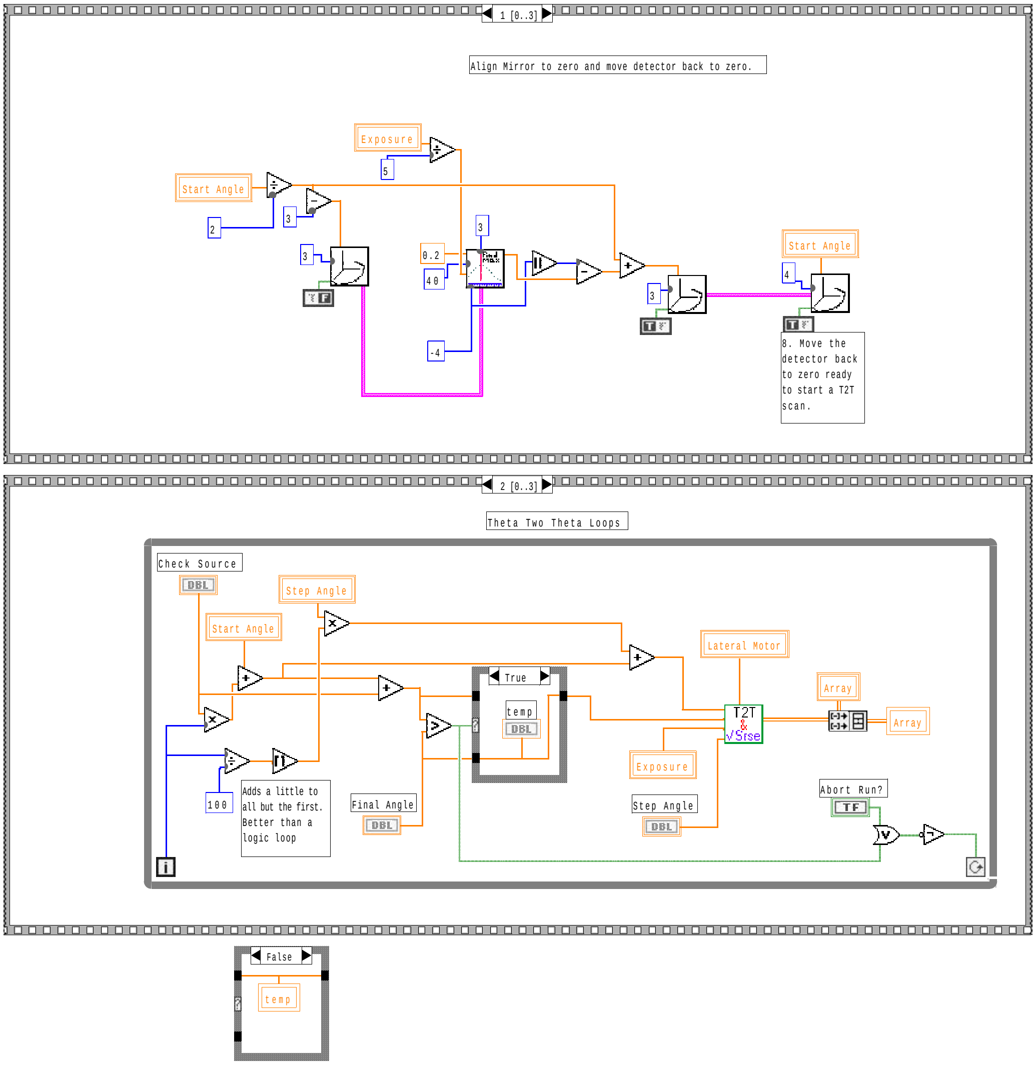

Align Mirror to zero and move detector back to zero.

8. Move the detector back to zero ready to start a T2T scan.

Adds a little to all but the first. Better than a logic loop

Figure C.5: Documentation on VAR VI page 3.

Page 1

T2T.vi
D:\LabView\T2T.vi
Last modified on 4/16/01 at 1:22 PM
Printed on 4/23/01 at 10:20 PM

Front Panel

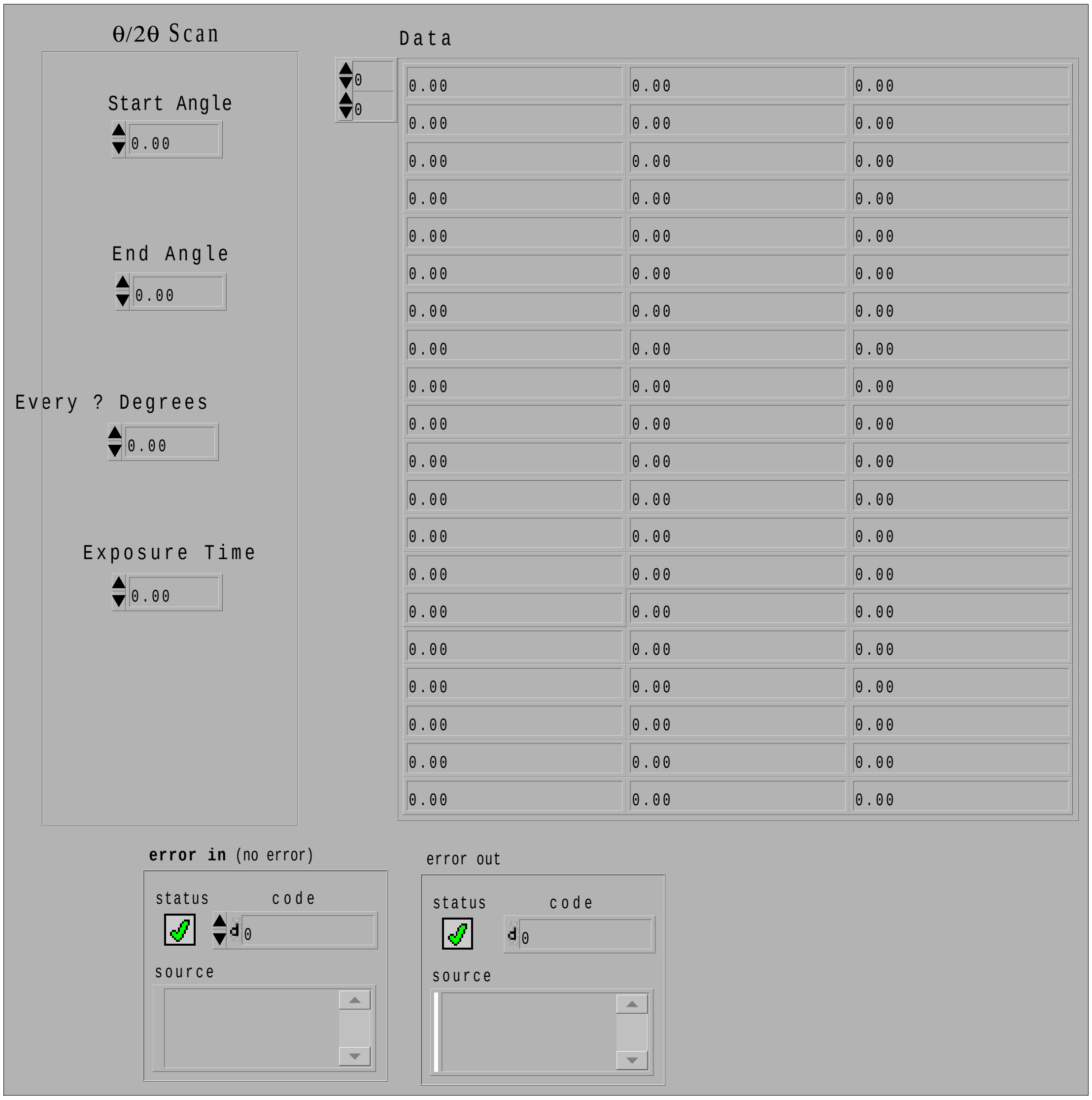

θ/2θ Scan

Start Angle: 0.00

End Angle: 0.00

Every ? Degrees: 0.00

Exposure Time: 0.00

Data: 0, 0

0.00	0.00	0.00
0.00	0.00	0.00
0.00	0.00	0.00
0.00	0.00	0.00
0.00	0.00	0.00
0.00	0.00	0.00
0.00	0.00	0.00
0.00	0.00	0.00
0.00	0.00	0.00
0.00	0.00	0.00
0.00	0.00	0.00
0.00	0.00	0.00
0.00	0.00	0.00
0.00	0.00	0.00
0.00	0.00	0.00
0.00	0.00	0.00
0.00	0.00	0.00
0.00	0.00	0.00
0.00	0.00	0.00
0.00	0.00	0.00

error in (no error)
status: ✓ code: d 0
source:

error out
status: ✓ code: d 0
source:

Figure C.6: Documentation on T2T VI page 1.

Page 2

T2T.vi
D:\LabView\T2T.vi
Last modified on 4/16/01 at 1:22 PM
Printed on 4/23/01 at 10:21 PM

Block Diagram

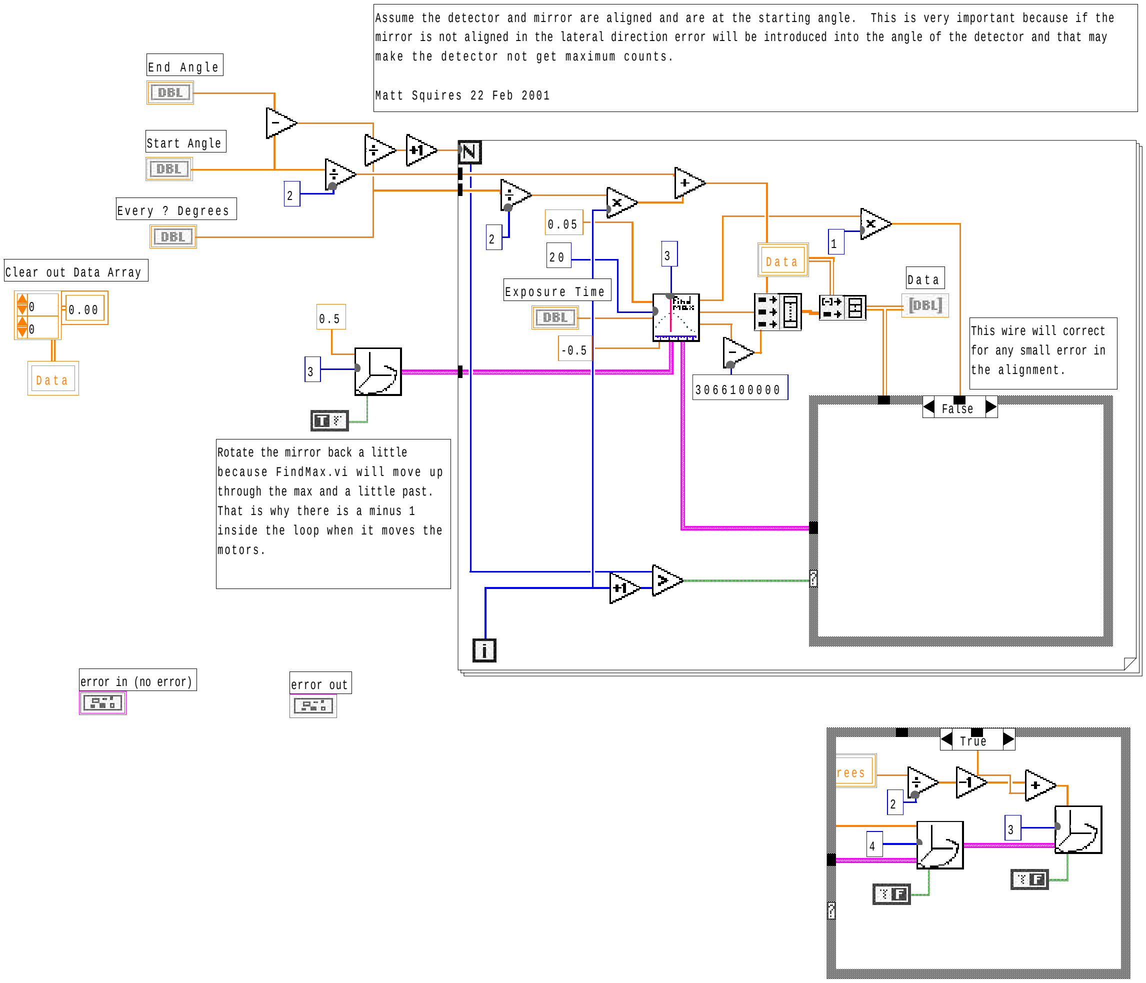

Assume the detector and mirror are aligned and are at the starting angle. This is very important because if the mirror is not aligned in the lateral direction error will be introduced into the angle of the detector and that may make the detector not get maximum counts.

Matt Squires 22 Feb 2001

Rotate the mirror back a little because FindMax.vi will move up through the max and a little past. That is why there is a minus 1 inside the loop when it moves the motors.

This wire will correct for any small error in the alignment.

Figure C.7: Documentation on T2T VI page 2.

Page 1

stagecontrolspring.vi
D:\LabView\stagecontrolspring.vi
Last modified on 11/29/00 at 8:33 PM
Printed on 4/23/01 at 10:17 PM

This VI moves the stage that it is sent the distance inputed in the direction inputed

Front Panel

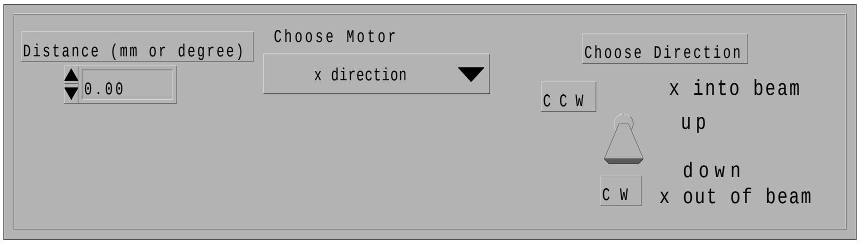

Block Diagram

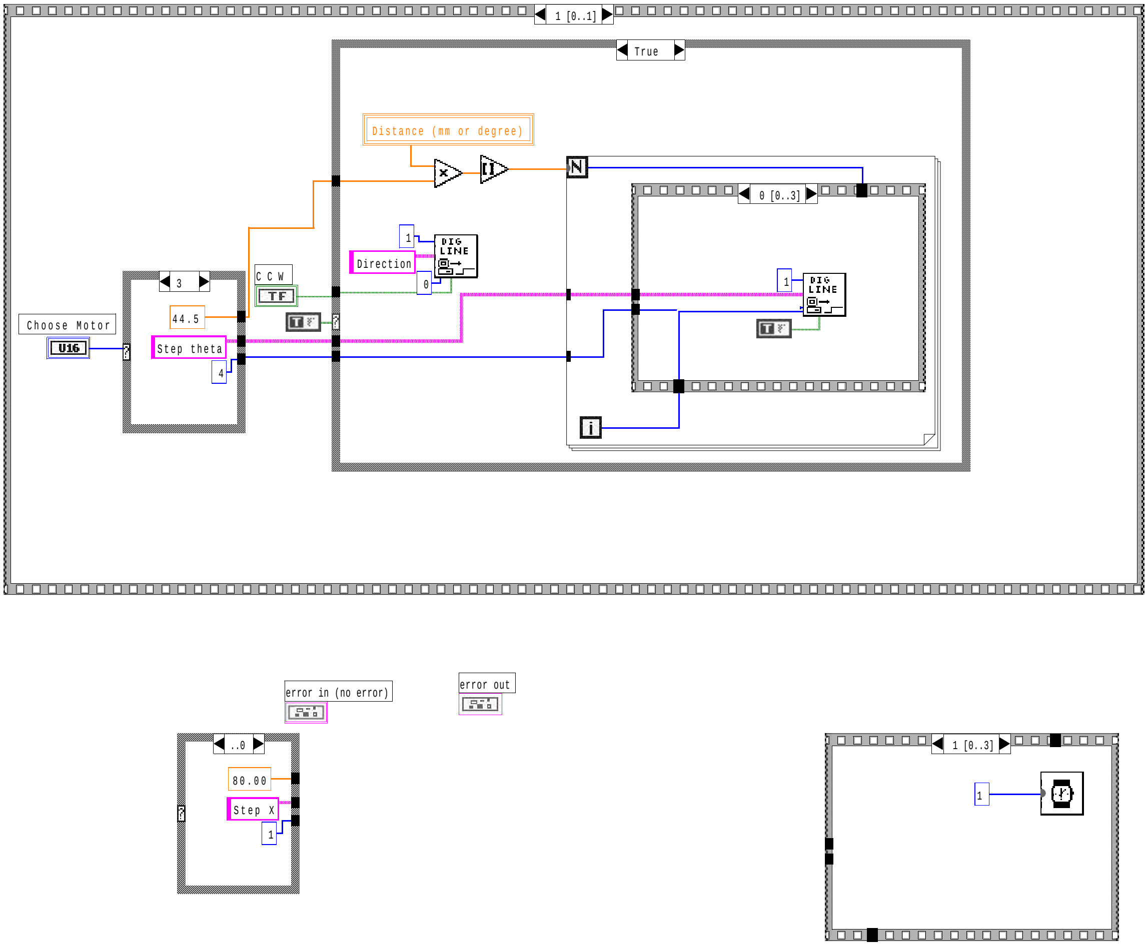

Figure C.8: Documentation on StageControlSpring VI page 1.

Page 2

stagecontrolspring.vi
D:\LabView\stagecontrolspring.vi
Last modified on 11/29/00 at 8:33 PM
Printed on 4/23/01 at 10:18 PM

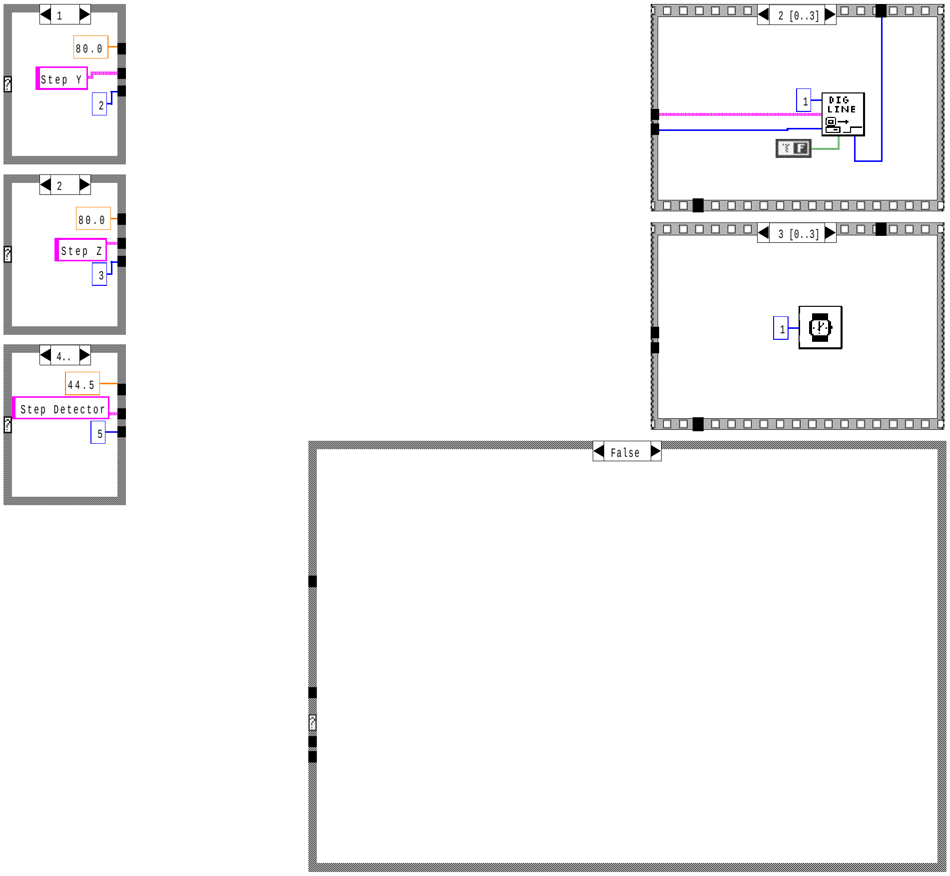

Figure C.9: Documentation on StageControlSpring VI page 2.

Page 3

stagecontrolspring.vi
D:\LabView\stagecontrolspring.vi
Last modified on 11/29/00 at 8:33 PM
Printed on 4/23/01 at 10:19 PM

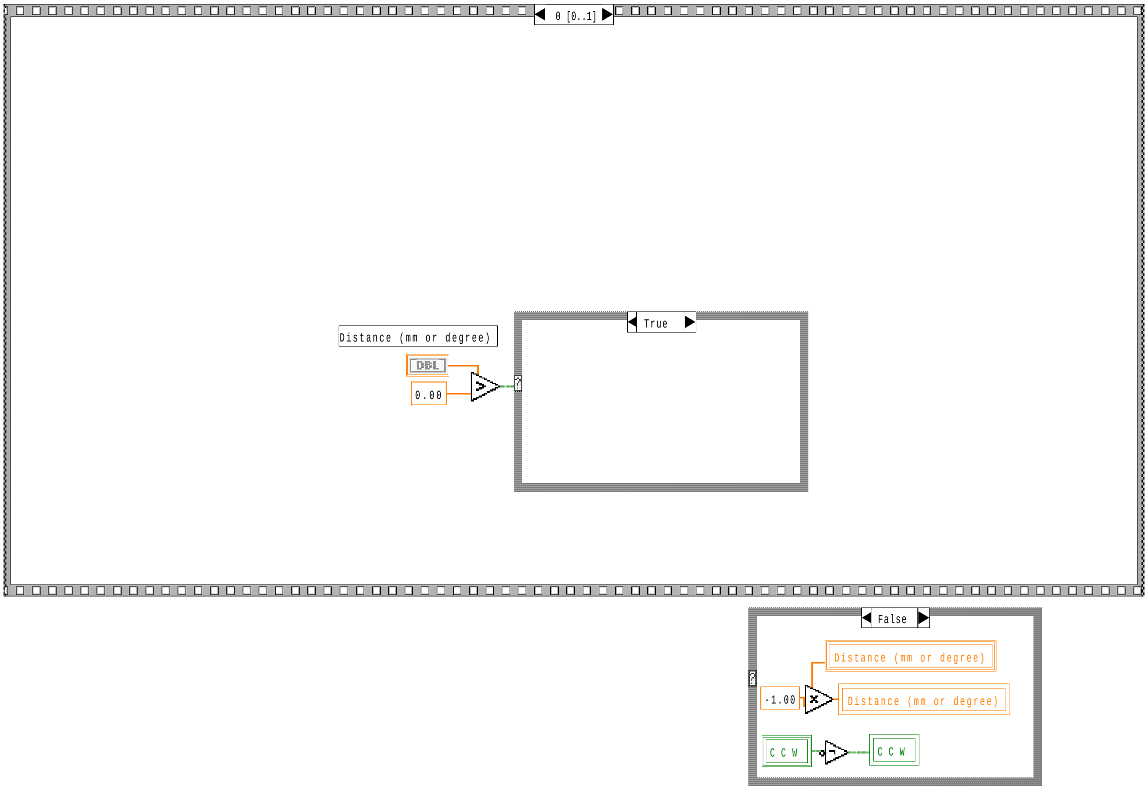

Figure C.10: Documentation on StageControlSpring VI page 3.

Page 1

CalculateReflectance.vi
D:\LabView\CalculateReflectance.vi
Last modified on 4/5/01 at 7:40 PM
Printed on 4/23/01 at 10:45 PM

Front Panel

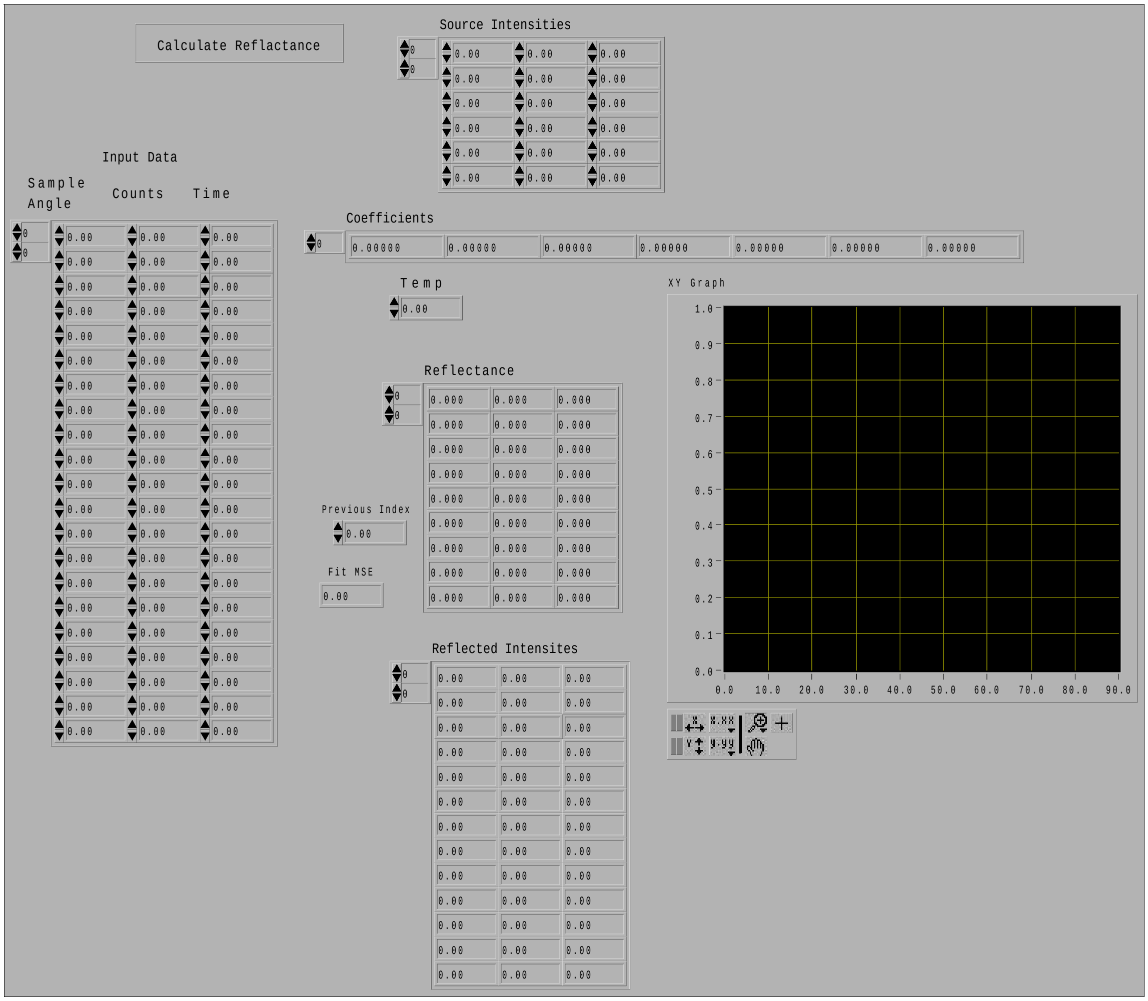

Figure C.11: Documentation on CalcR VI page 1.

Page 2

CalculateReflectance.vi
D:\LabView\CalculateReflectance.vi
Last modified on 4/5/01 at 7:40 PM
Printed on 4/23/01 at 10:47 PM

Block Diagram

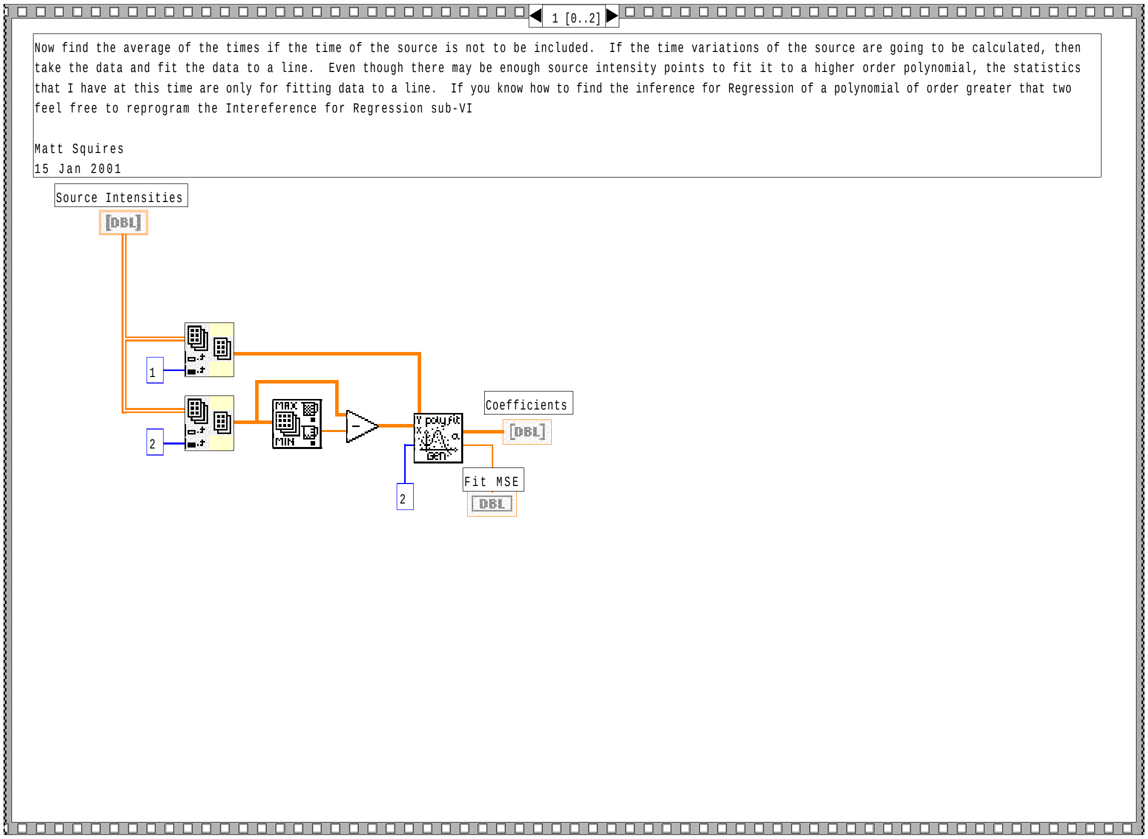

Now find the average of the times if the time of the source is not to be included. If the time variations of the source are going to be calculated, then take the data and fit the data to a line. Even though there may be enough source intensity points to fit it to a higher order polynomial, the statistics that I have at this time are only for fitting data to a line. If you know how to find the inference for Regression of a polynomial of order greater that two feel free to reprogram the Intereference for Regression sub-VI

Matt Squires
15 Jan 2001

Figure C.12: Documentation on CalcR VI page 2.

Page 3

CalculateReflectance.vi
D:\LabView\CalculateReflectance.vi
Last modified on 4/5/01 at 7:40 PM
Printed on 4/23/01 at 10:48 PM

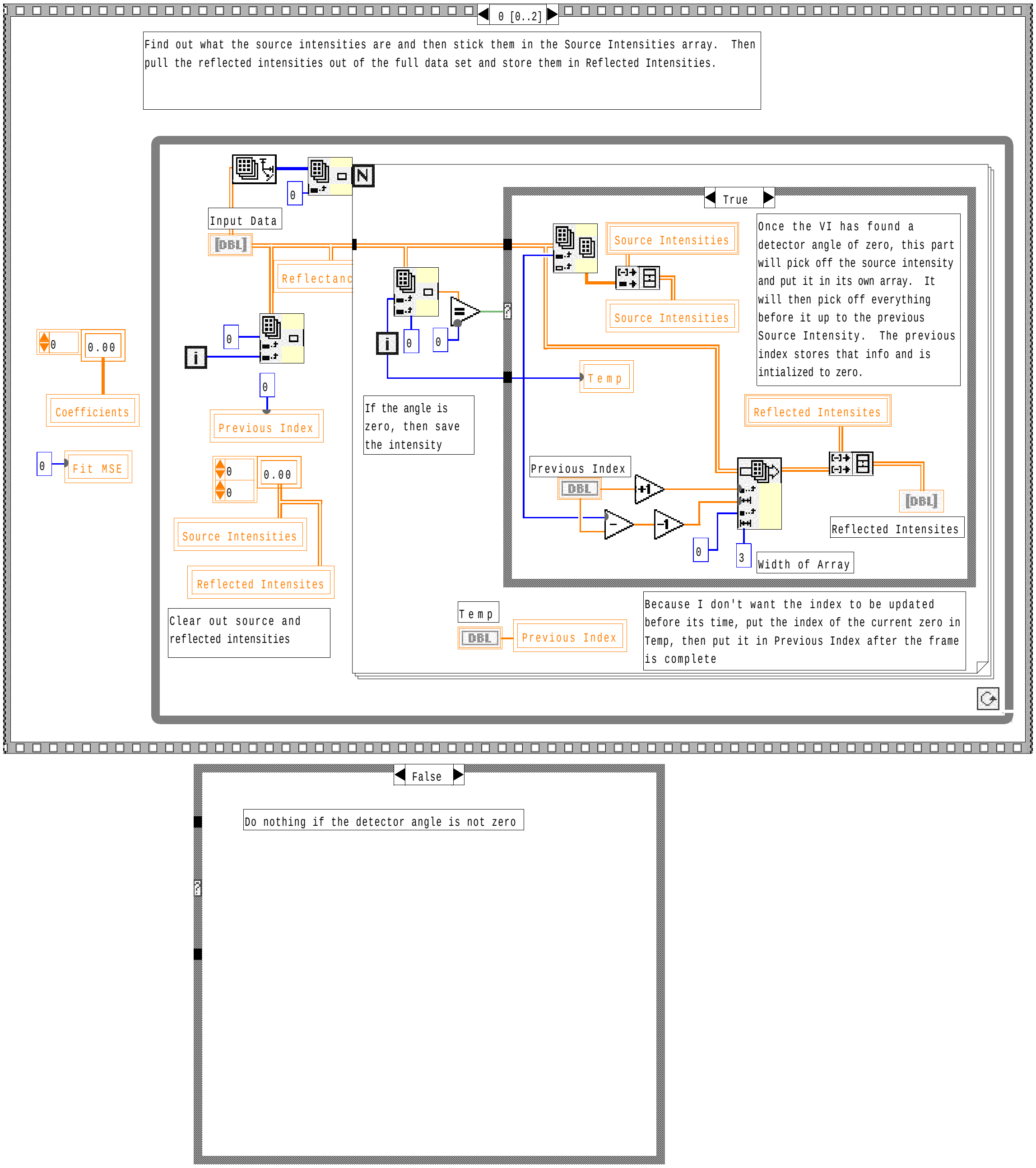

Find out what the source intensities are and then stick them in the Source Intensities array. Then pull the reflected intensities out of the full data set and store them in Reflected Intensities.

Once the VI has found a detector angle of zero, this part will pick off the source intensity and put it in its own array. It will then pick off everything before it up to the previous Source Intensity. The previous index stores that info and is intialized to zero.

If the angle is zero, then save the intensity

Clear out source and reflected intensities

Because I don't want the index to be updated before its time, put the index of the current zero in Temp, then put it in Previous Index after the frame is complete

Do nothing if the detector angle is not zero

Figure C.13: Documentation on CalcR VI page 3.

Page 4

CalculateReflectance.vi
D:\LabView\CalculateReflectance.vi
Last modified on 4/5/01 at 7:40 PM
Printed on 4/23/01 at 10:48 PM

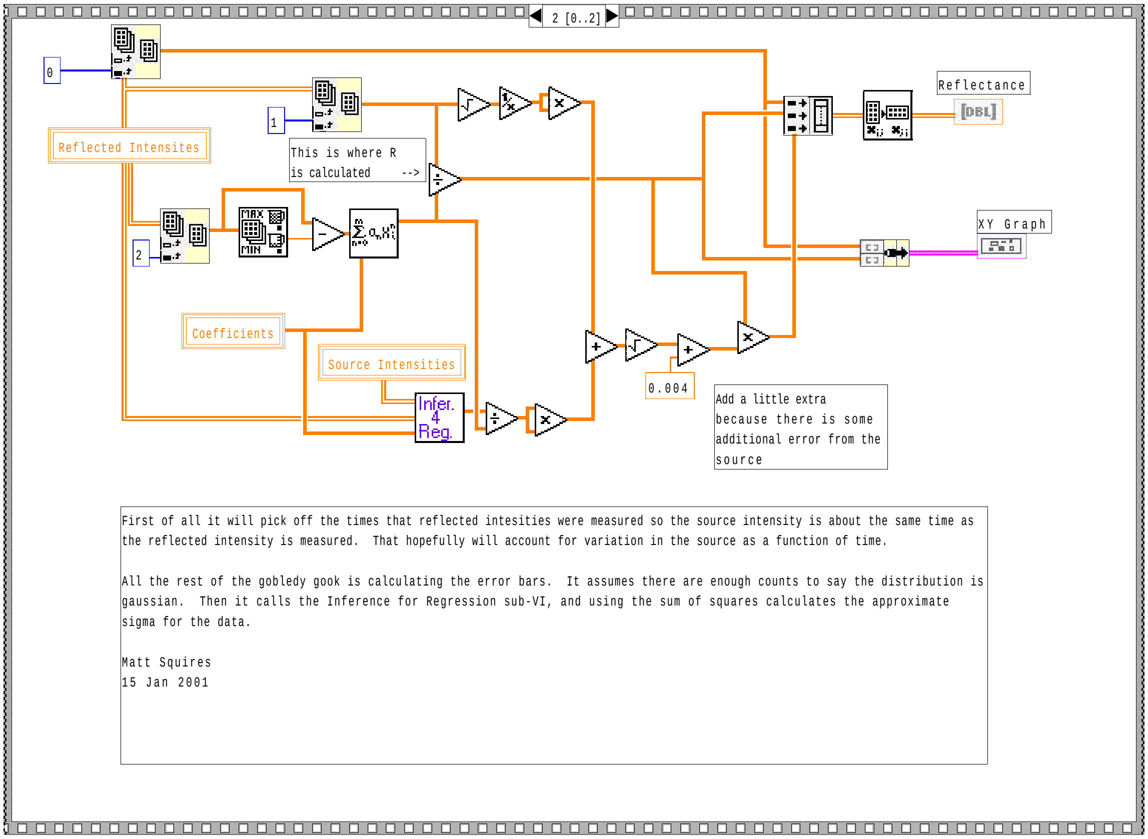

This is where R is calculated -->

Add a little extra because there is some additional error from the source

First of all it will pick off the times that reflected intesities were measured so the source intensity is about the same time as the reflected intensity is measured. That hopefully will account for variation in the source as a function of time.

All the rest of the gobledy gook is calculating the error bars. It assumes there are enough counts to say the distribution is gaussian. Then it calls the Inference for Regression sub-VI, and using the sum of squares calculates the approximate sigma for the data.

Matt Squires
15 Jan 2001

Figure C.14: Documentation on CalcR VI page 4.

Page 1

FindMax.vi
D:\LabView\FindMax.vi
Last modified on 3/8/01 at 9:08 AM
Printed on 4/23/01 at 10:28 PM

Front Panel

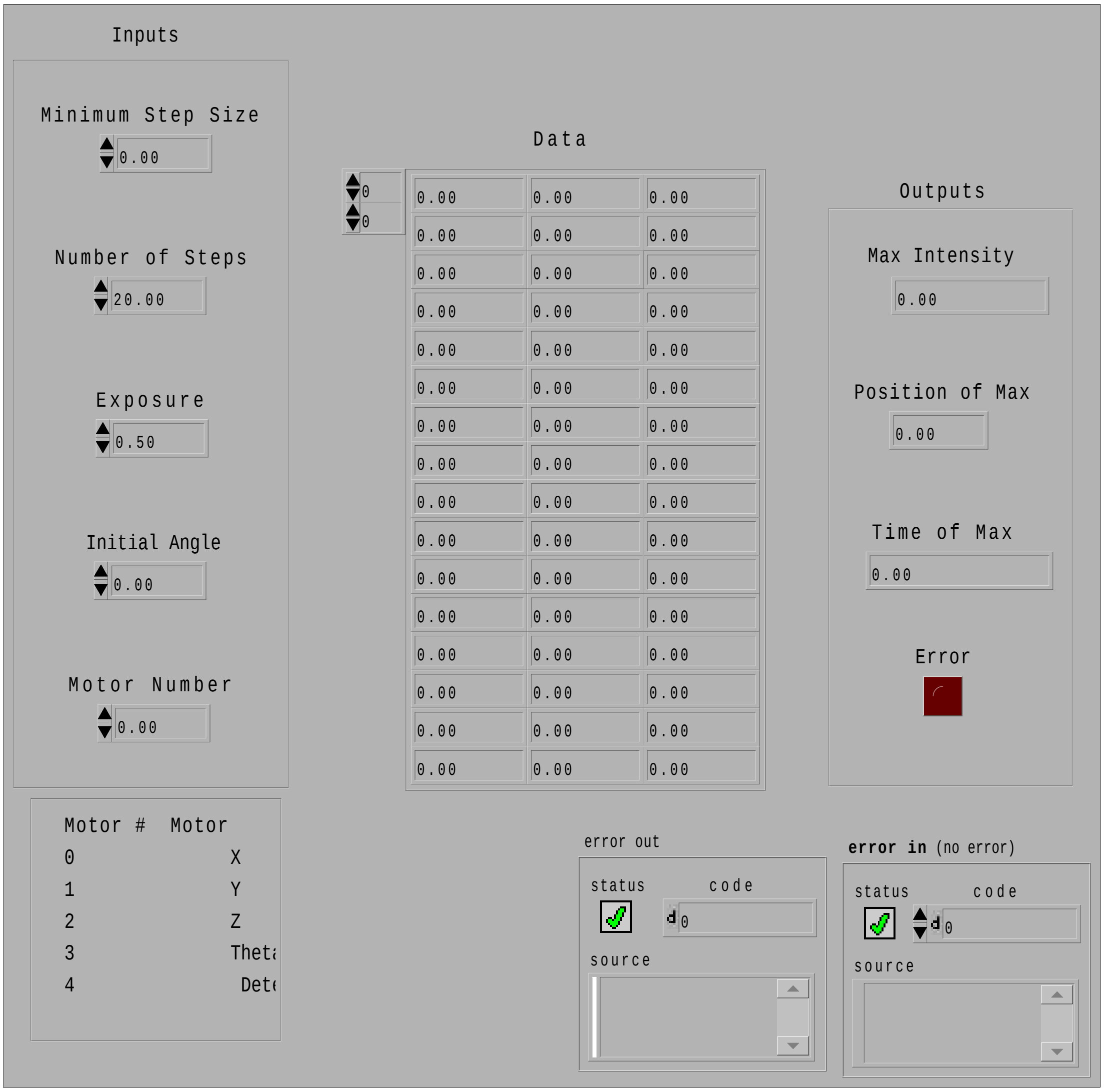

Inputs

Minimum Step Size: 0.00

Number of Steps: 20.00

Exposure: 0.50

Initial Angle: 0.00

Motor Number: 0.00

Motor #	Motor
0	X
1	Y
2	Z
3	Thet
4	Det

Data (index 0, 0)

0.00	0.00	0.00
0.00	0.00	0.00
0.00	0.00	0.00
0.00	0.00	0.00
0.00	0.00	0.00
0.00	0.00	0.00
0.00	0.00	0.00
0.00	0.00	0.00
0.00	0.00	0.00
0.00	0.00	0.00
0.00	0.00	0.00
0.00	0.00	0.00
0.00	0.00	0.00
0.00	0.00	0.00
0.00	0.00	0.00
0.00	0.00	0.00

Outputs

Max Intensity: 0.00

Position of Max: 0.00

Time of Max: 0.00

Error

error out
status: ✓
code: 0
source:

error in (no error)
status: ✓
code: 0
source:

Figure C.15: Documentation on FindMax VI page 1.

Page 2

FindMax.vi
D:\LabView\FindMax.vi
Last modified on 3/8/01 at 9:08 AM
Printed on 4/23/01 at 10:28 PM

Block Diagram

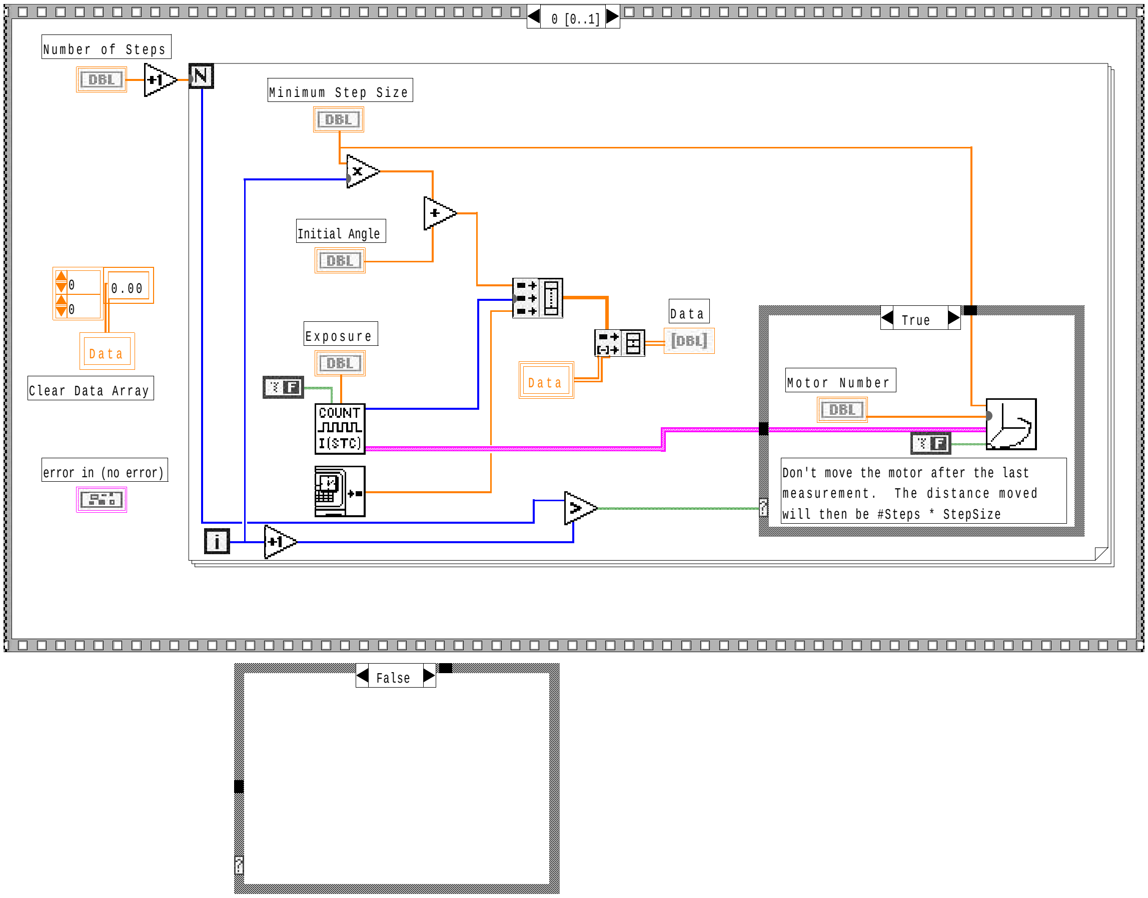

Don't move the motor after the last measurement. The distance moved will then be #Steps * StepSize

Figure C.16: Documentation on FindMax VI page 2.

Page 3

FindMax.vi
D:\LabView\FindMax.vi
Last modified on 3/8/01 at 9:08 AM
Printed on 4/23/01 at 10:29 PM

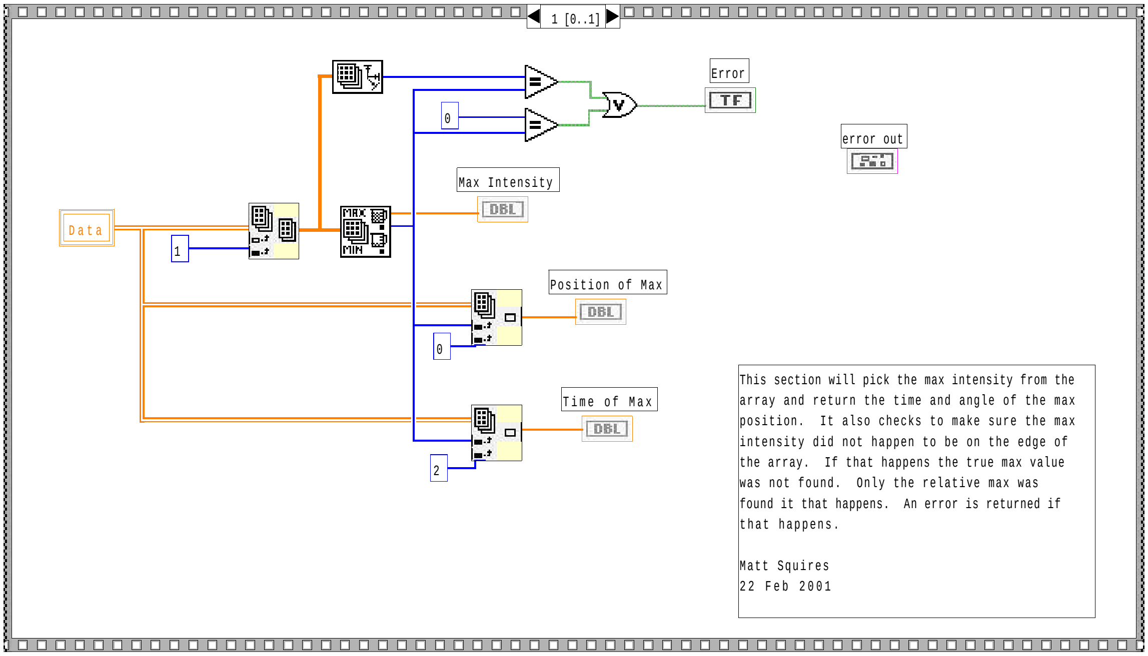

This section will pick the max intensity from the array and return the time and angle of the max position. It also checks to make sure the max intensity did not happen to be on the edge of the array. If that happens the true max value was not found. Only the relative max was found it that happens. An error is returned if that happens.

Matt Squires
22 Feb 2001

Figure C.17: Documentation on FindMax VI page 3.

Page 1

InferenceForRegression.vi
D:\LabView\InferenceForRegression.vi
Last modified on 4/5/01 at 6:24 PM
Printed on 4/23/01 at 10:26 PM

Front Panel

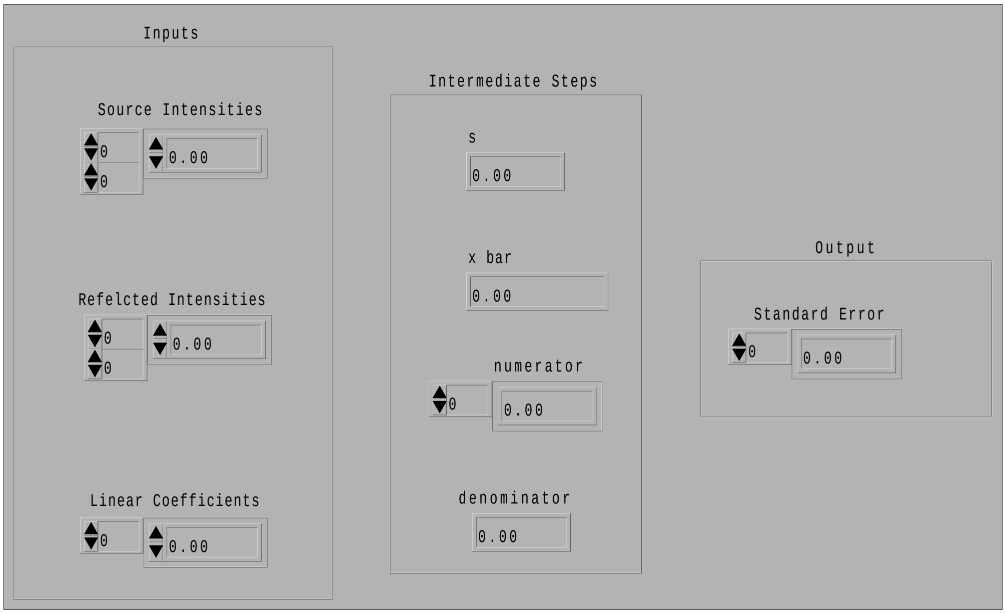

Block Diagram

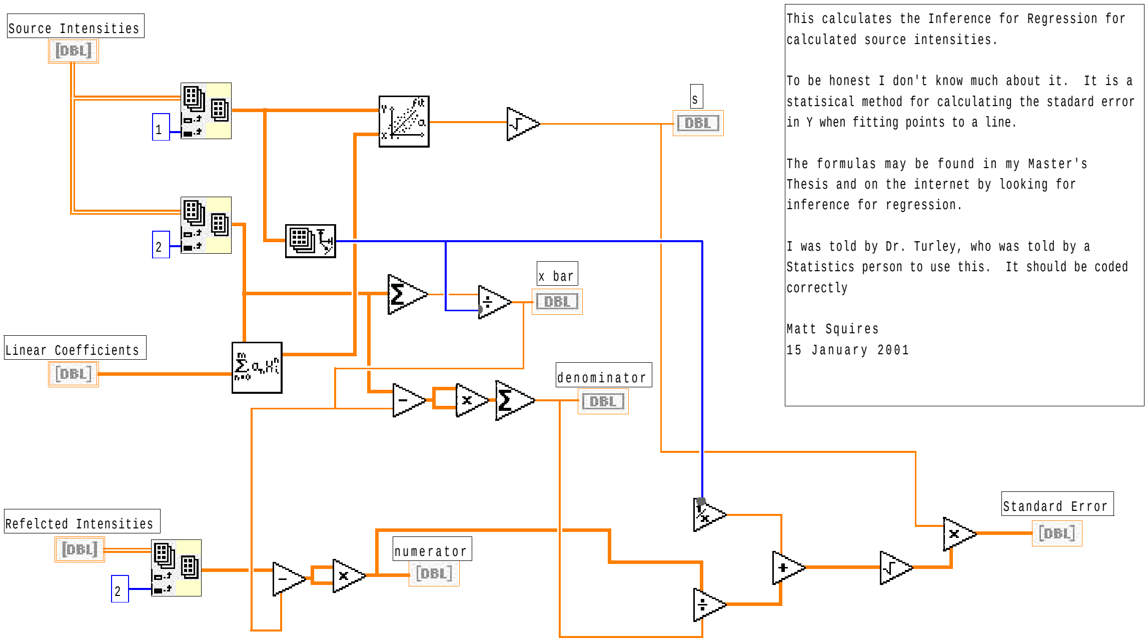

This calculates the Inference for Regression for calculated source intensities.

To be honest I don't know much about it. It is a statisical method for calculating the stadard error in Y when fitting points to a line.

The formulas may be found in my Master's Thesis and on the internet by looking for inference for regression.

I was told by Dr. Turley, who was told by a Statistics person to use this. It should be coded correctly

Matt Squires
15 January 2001

Figure C.18: Documentation on InferenceForRegression VI page 1.

C.2 Parts List

Part	Company	Part Number or Description	Aprox. Price
rotational stepper motors	EAD motors (Eastern Air Devices Inc.)	LH17	85 + 15(vacuum prep)
linear stepper motors	Haydon Switch and Instrument	26000 non-captive shaft	60 + 12(vacuum prep)
Stepper Drivers	Haydon Switch and Instrument	Spectrum Drive PN 42103	100
linear motion carriage	Techno-Isel Linear Motion components	linear bearing system	?
linear motion rail	Techno-Isel Linear Motion components	linear bearing sys series 1 double rail	?
Detector	Amptek	MD-501 AMPTEKTRON	1200

C.3 CAD Drawings

These parts were drawn by Wes Lifferth.

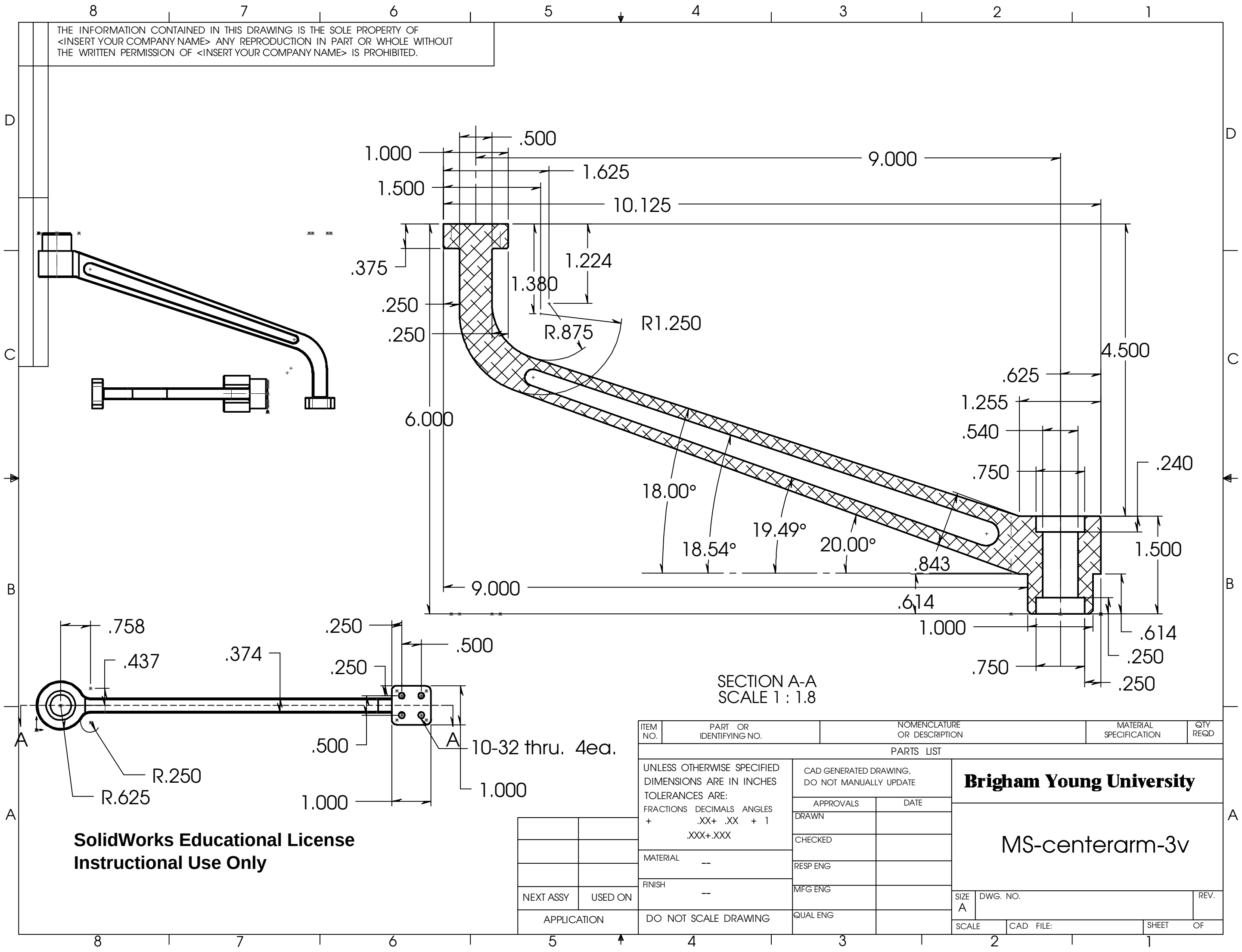

Figure C.19: Assembly drawing of detector arm.

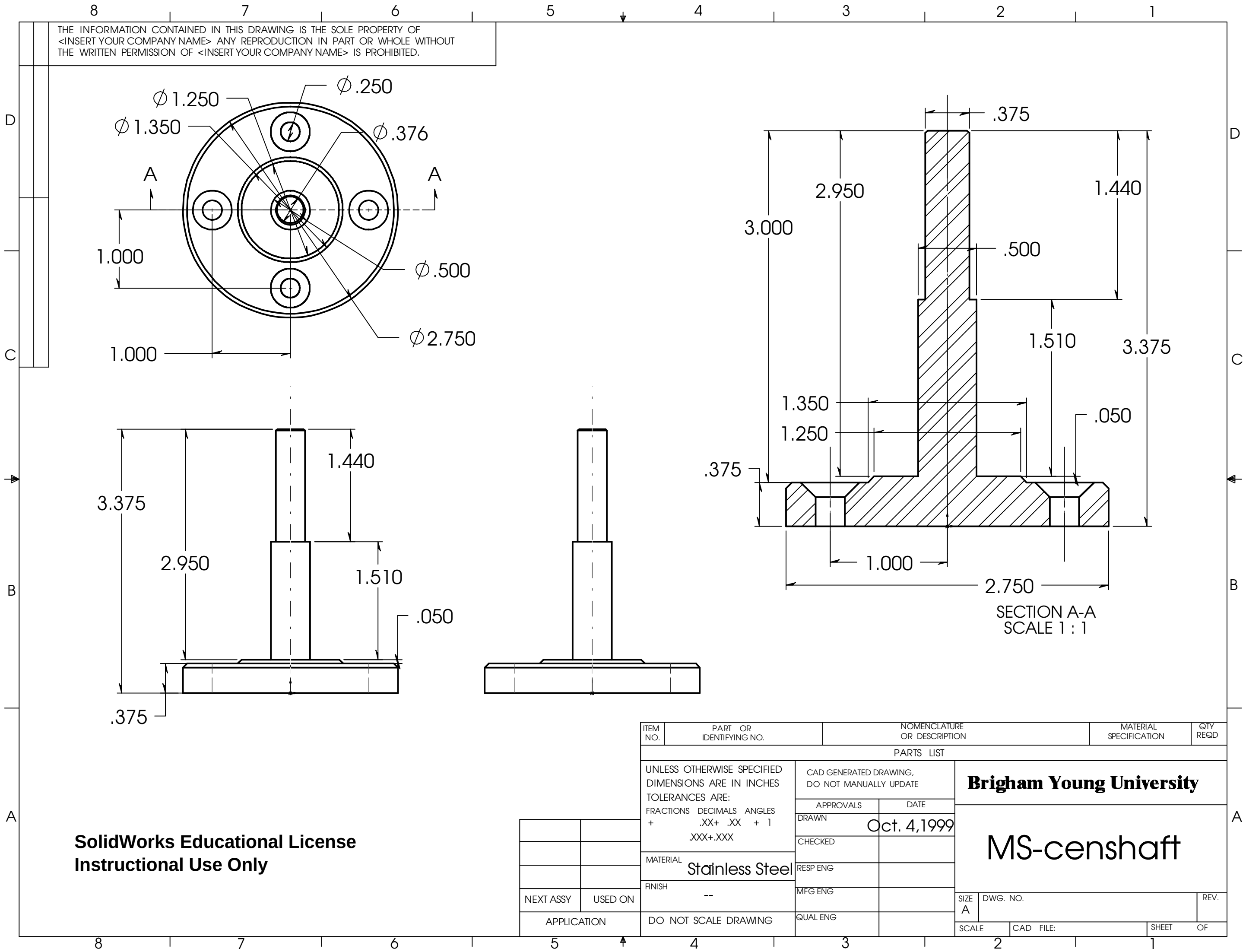

Figure C.20: Assembly drawing of center shaft.

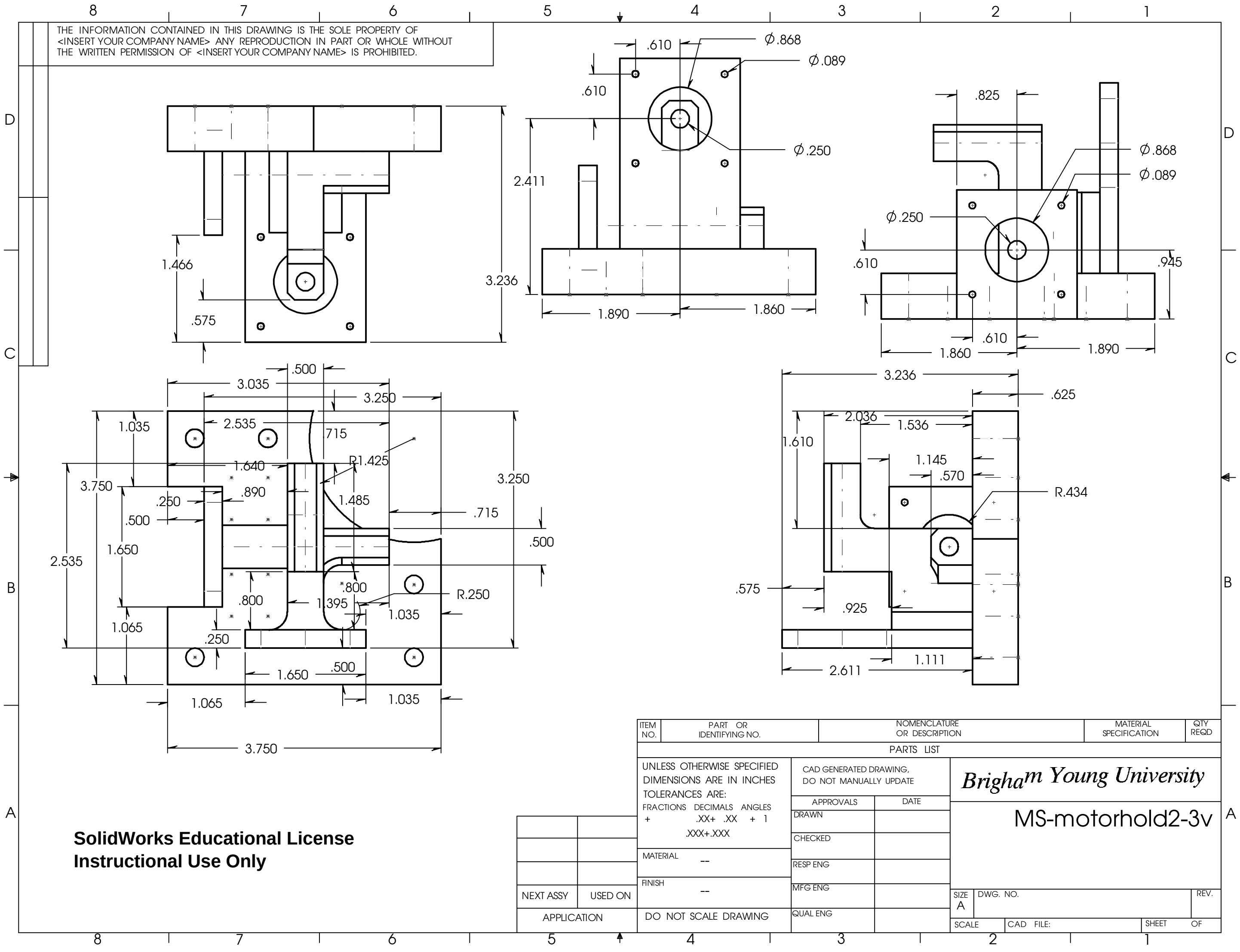

Figure C.21: Assembly drawing of motor holder.

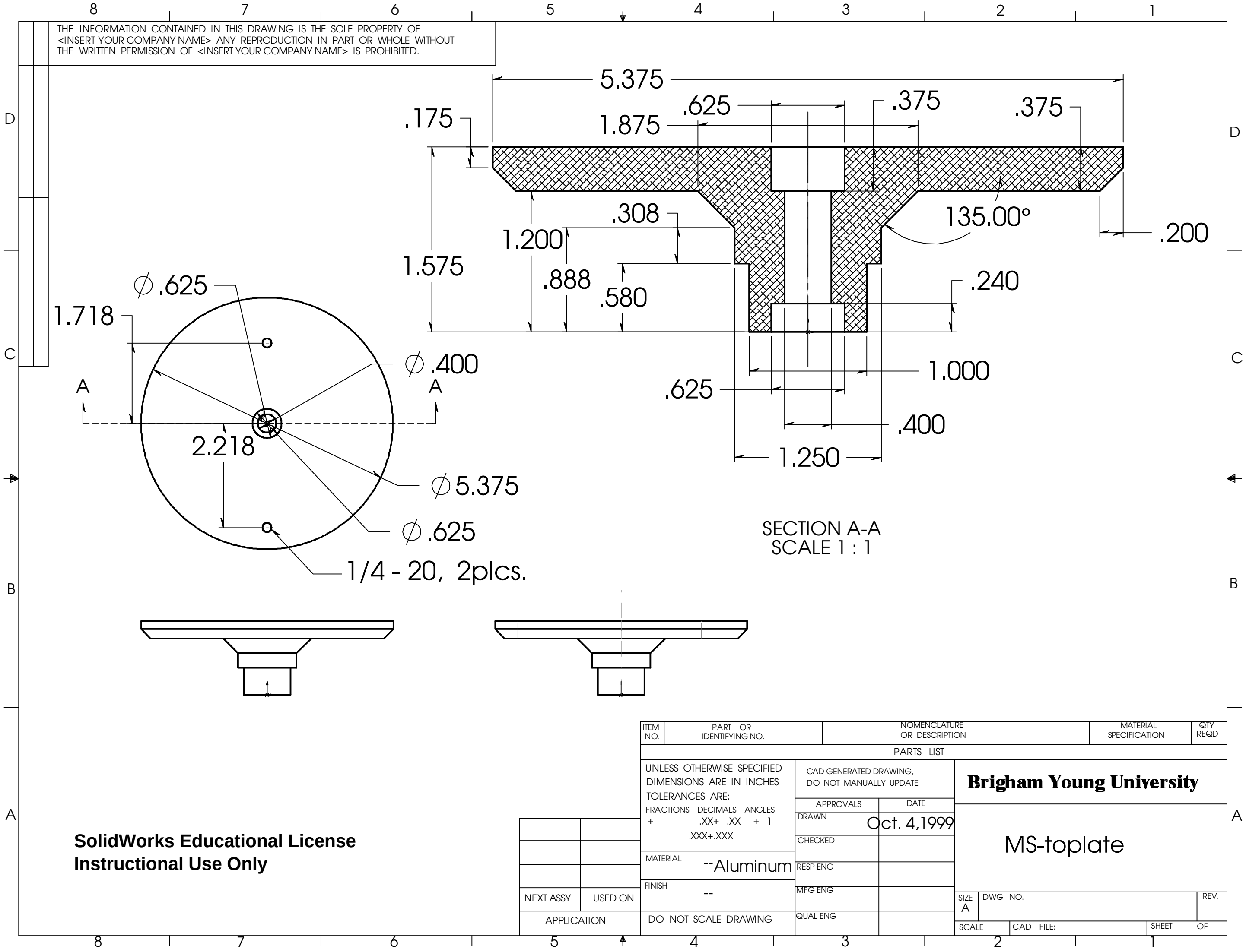

Figure C.22: Assembly drawing of theta stage.

Channel Name	Device Channel (DIO line)	Description	Device Type	Device Name
Direction	0	Tells the X, Y, Z, Theta, and Detector drivers which way the motor should move	DAQ Virtual DIO Channel	PCI-MIO-16E-4
Step Detector	5	Sends a clock pulse to the detector driver to move the detector arm		
Step Theta	4	Sends a clock pulse to the theta driver to move the theta arm		
Step X	1	Sends a clock pulse to the X driver to move the X stage		
Step Y	2	Sends a clock pulse to the Y driver to move the Y stage		
Step Z	3	Sends a clock pulse to the Z driver to move the Z stage		

Table C.1: Digital IO channel configuration information.

C.4 DIO Configuration

The following figures show where the configuration panel can be found.

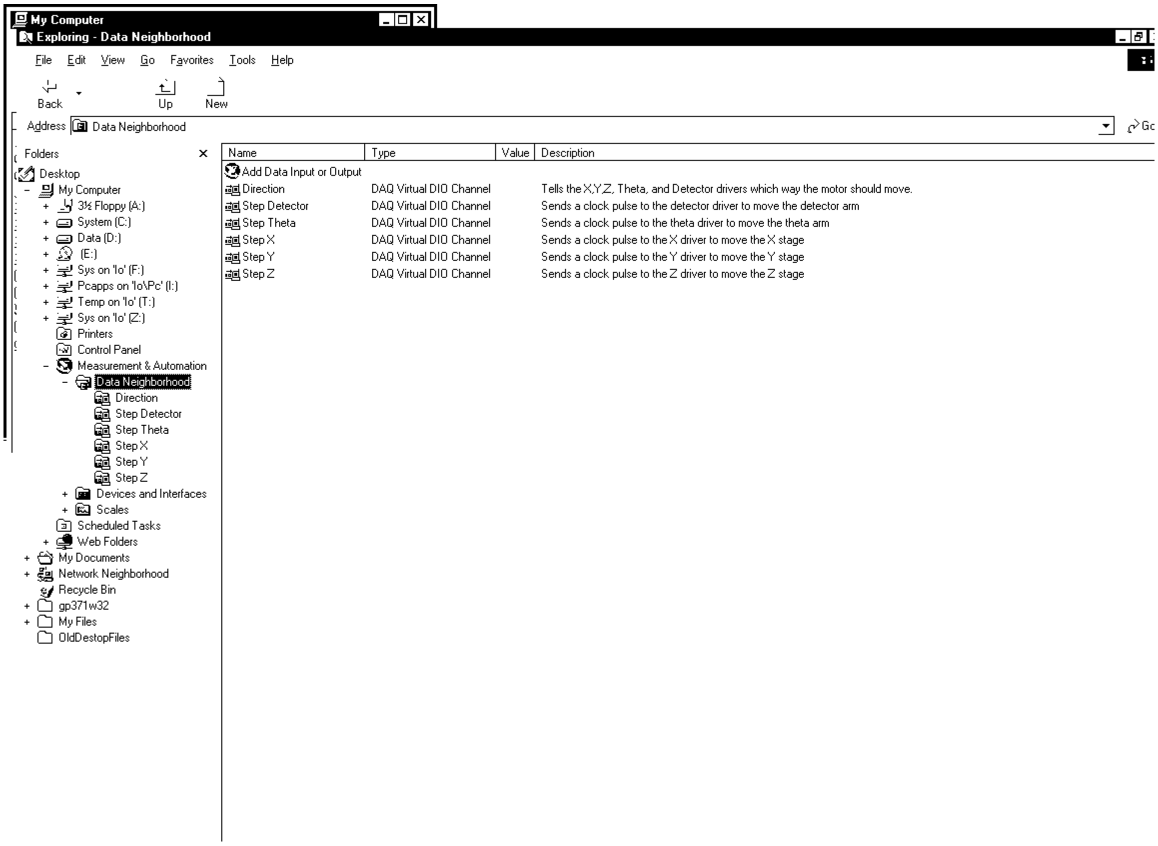

Name	Type	Value	Description
Add Data Input or Output			
Direction	DAQ Virtual DIO Channel		Tells the X,Y,Z, Theta, and Detector drivers which way the motor should move.
Step Detector	DAQ Virtual DIO Channel		Sends a clock pulse to the detector driver to move the detector arm
Step Theta	DAQ Virtual DIO Channel		Sends a clock pulse to the theta driver to move the theta arm
Step X	DAQ Virtual DIO Channel		Sends a clock pulse to the X driver to move the X stage
Step Y	DAQ Virtual DIO Channel		Sends a clock pulse to the Y driver to move the Y stage
Step Z	DAQ Virtual DIO Channel		Sends a clock pulse to the Z driver to move the Z stage

Figure C.23: Picture where to find National Instruments Measurements and Automation files using Window Explorer. If the software has been reinstalled click on Add Data Input or Output.

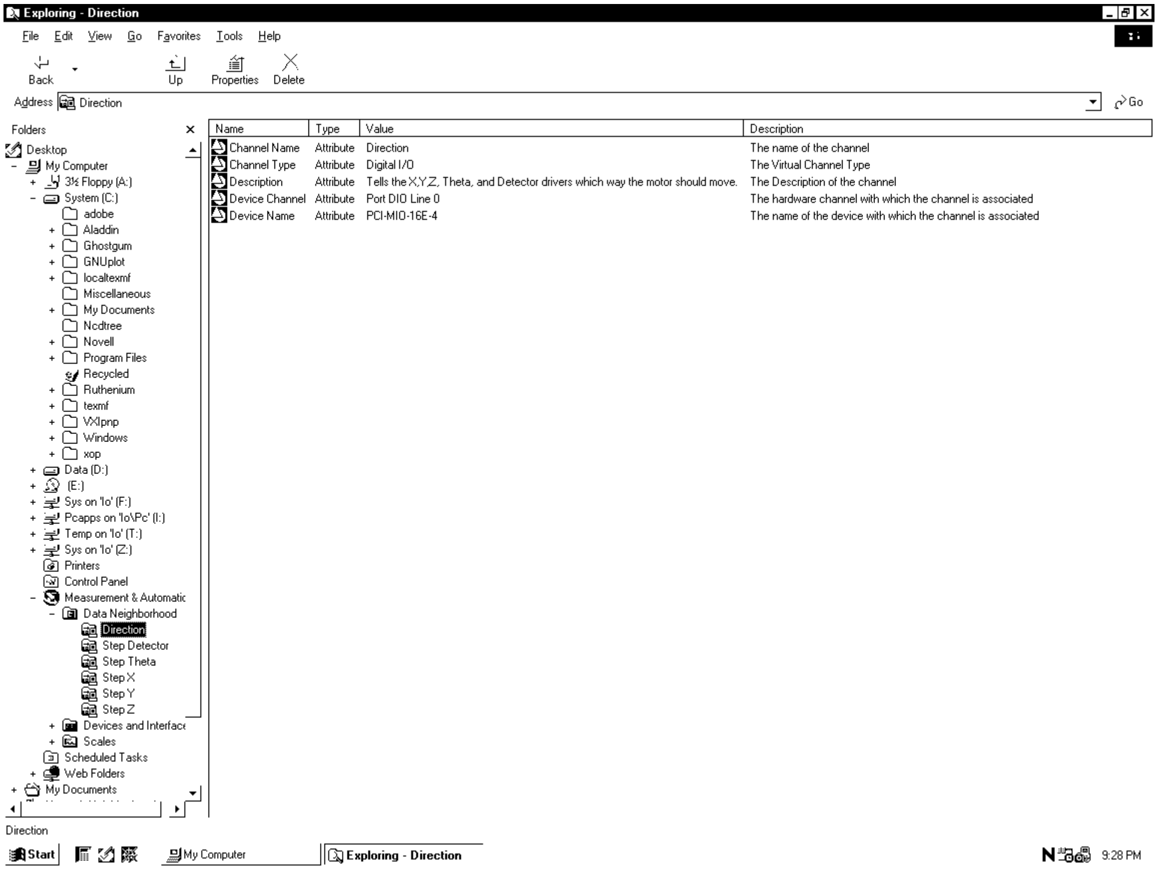

Name	Type	Value	Description
Channel Name	Attribute	Direction	The name of the channel
Channel Type	Attribute	Digital I/O	The Virtual Channel Type
Description	Attribute	Tells the X,Y,Z, Theta, and Detector drivers which way the motor should move.	The Description of the channel
Device Channel	Attribute	Port DIO Line 0	The hardware channel with which the channel is associated
Device Name	Attribute	PCI-MIO-16E-4	The name of the device with which the channel is associated

Figure C.24: Picture of icons involved in configuring DIO channels. This is where the information from Table C.1 is entered.

Appendix D

VAR Data and Analysis

D.1 HOPG

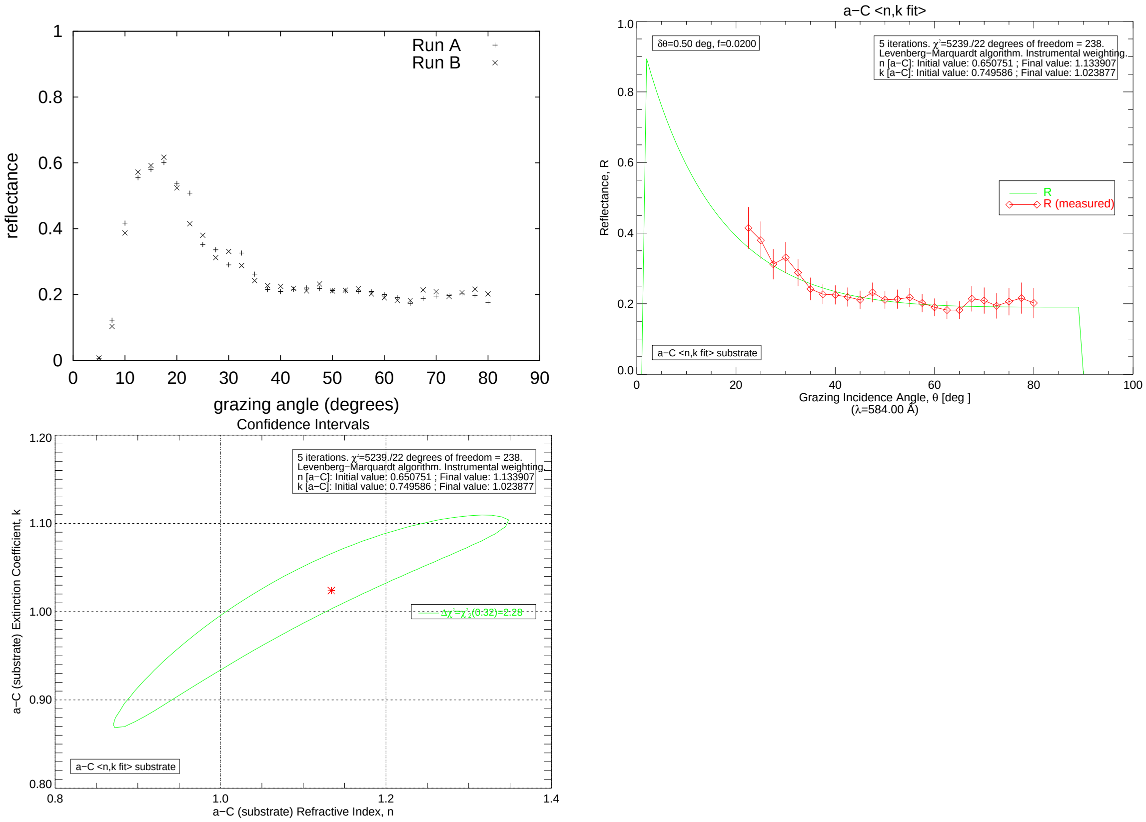

Figure D.1: Variable angle reflectance data and confidence intervals for graphite at 584 Å.

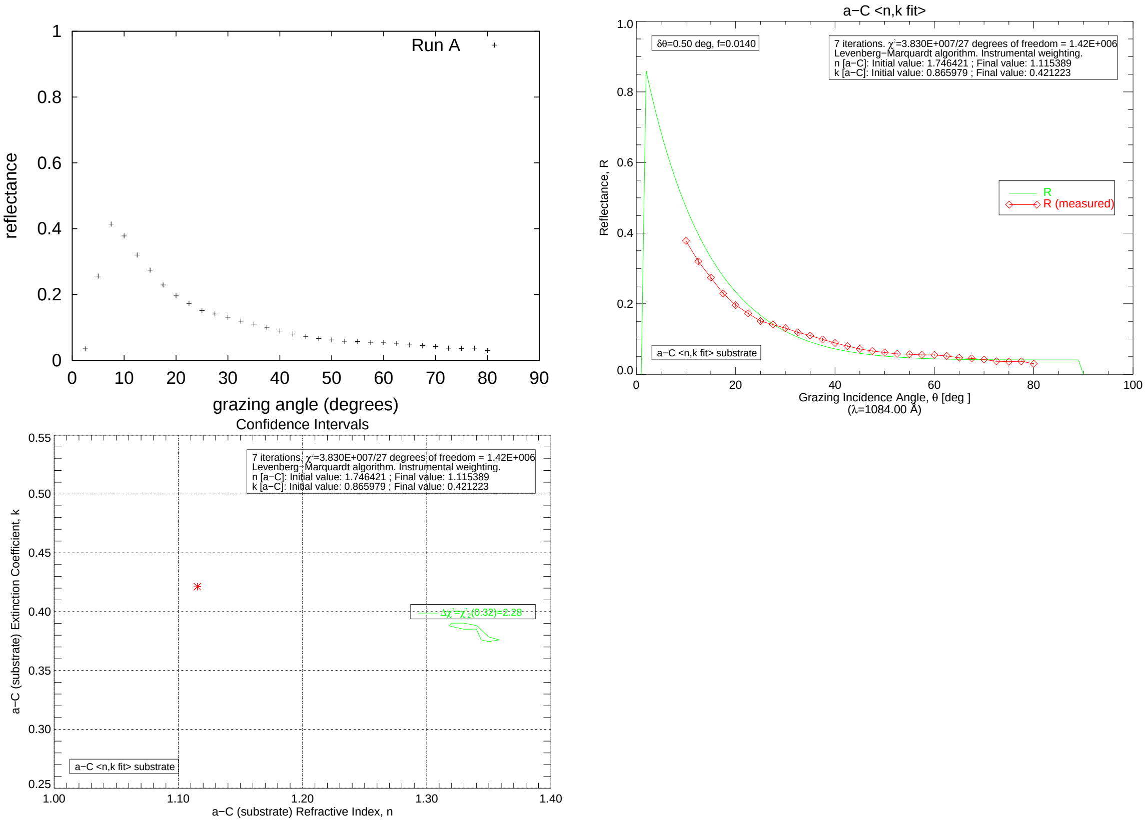

Figure D.2: Variable angle reflectance data and confidence intervals for graphite at 1084 Å.

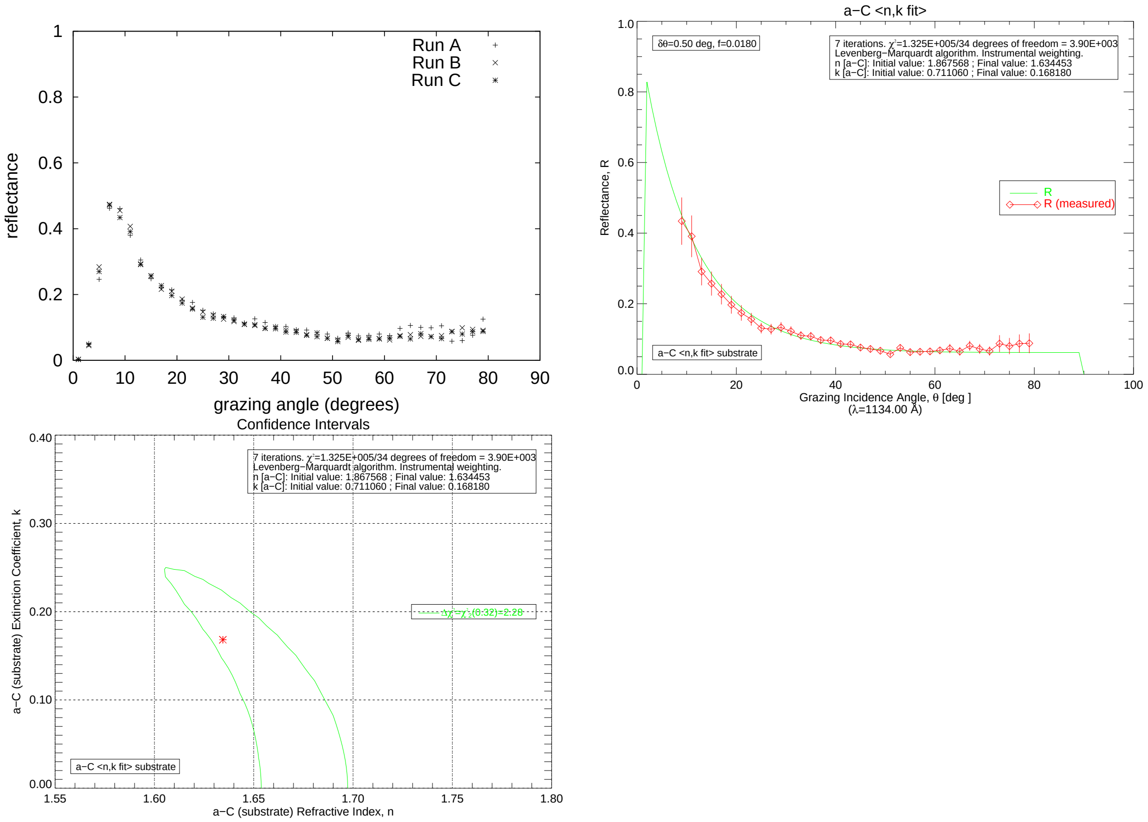

Figure D.3: Variable angle reflectance data and confidence intervals for graphite at 1134 Å.

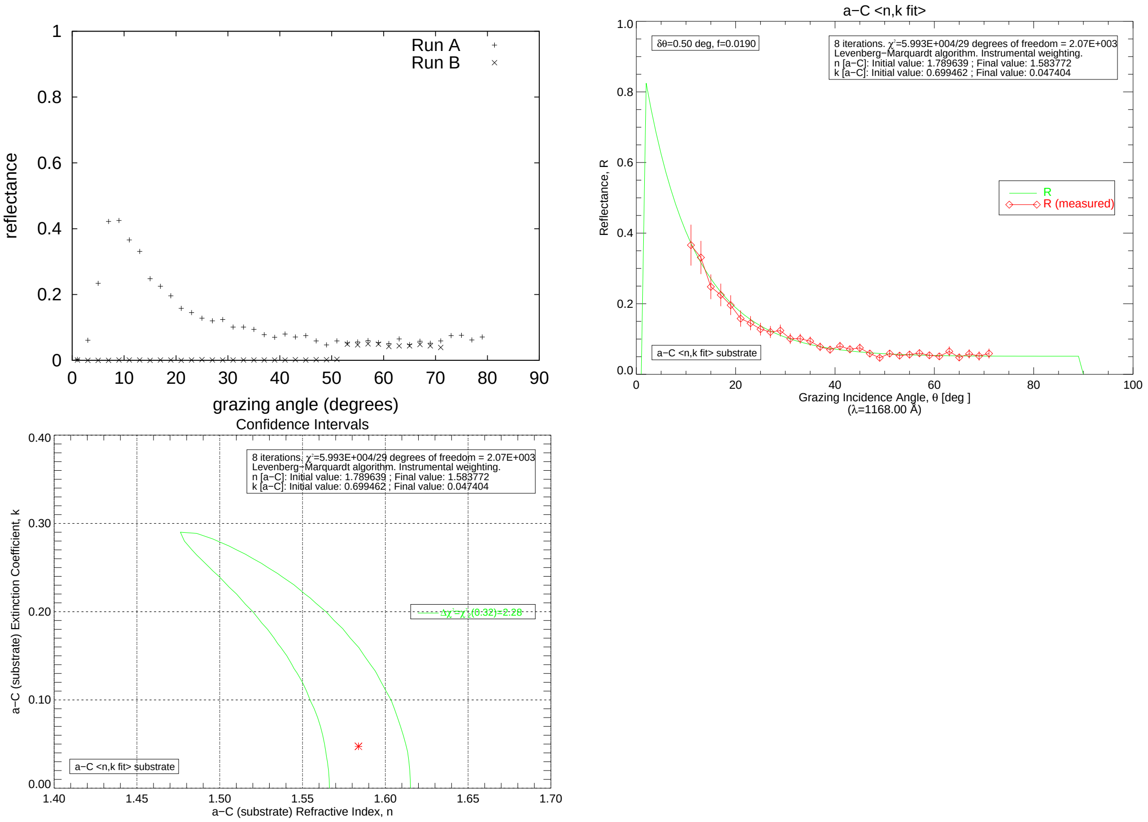

Figure D.4: Variable angle reflectance data and confidence intervals for graphite at 1164 Å.

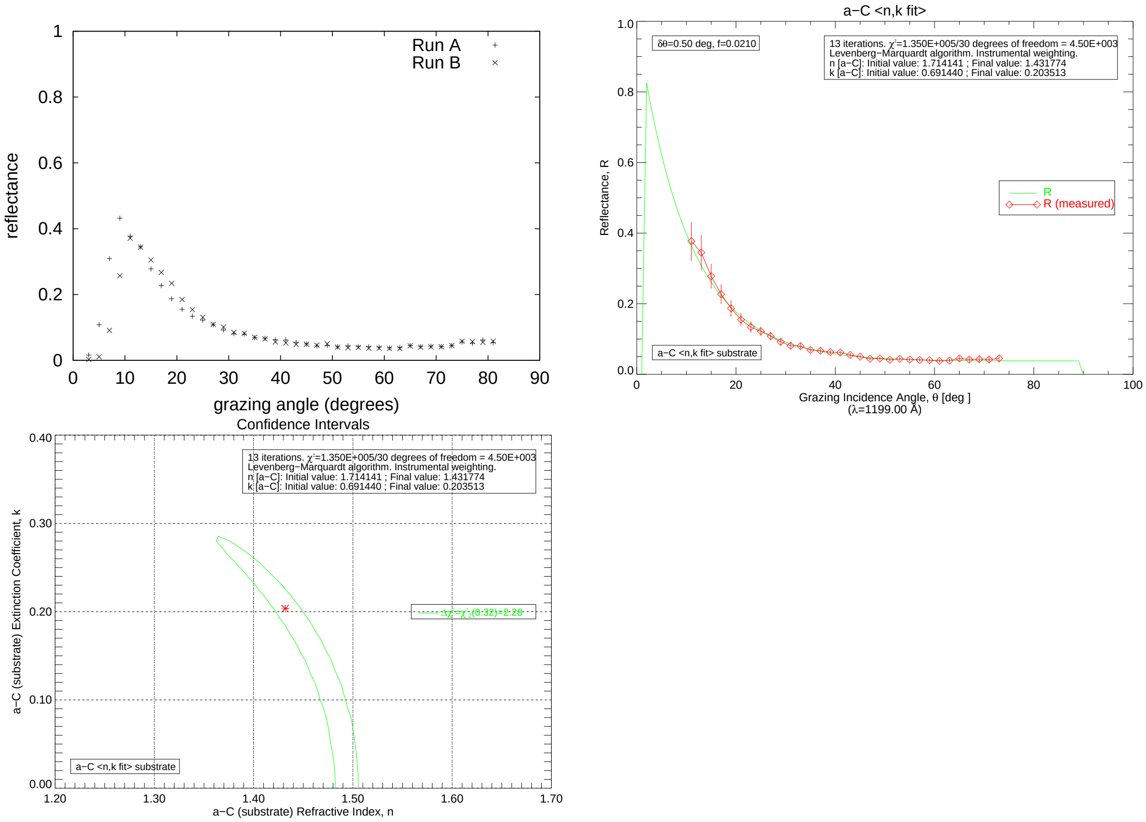

Figure D.5: Variable angle reflectance data and confidence intervals for graphite at 1199 Å.

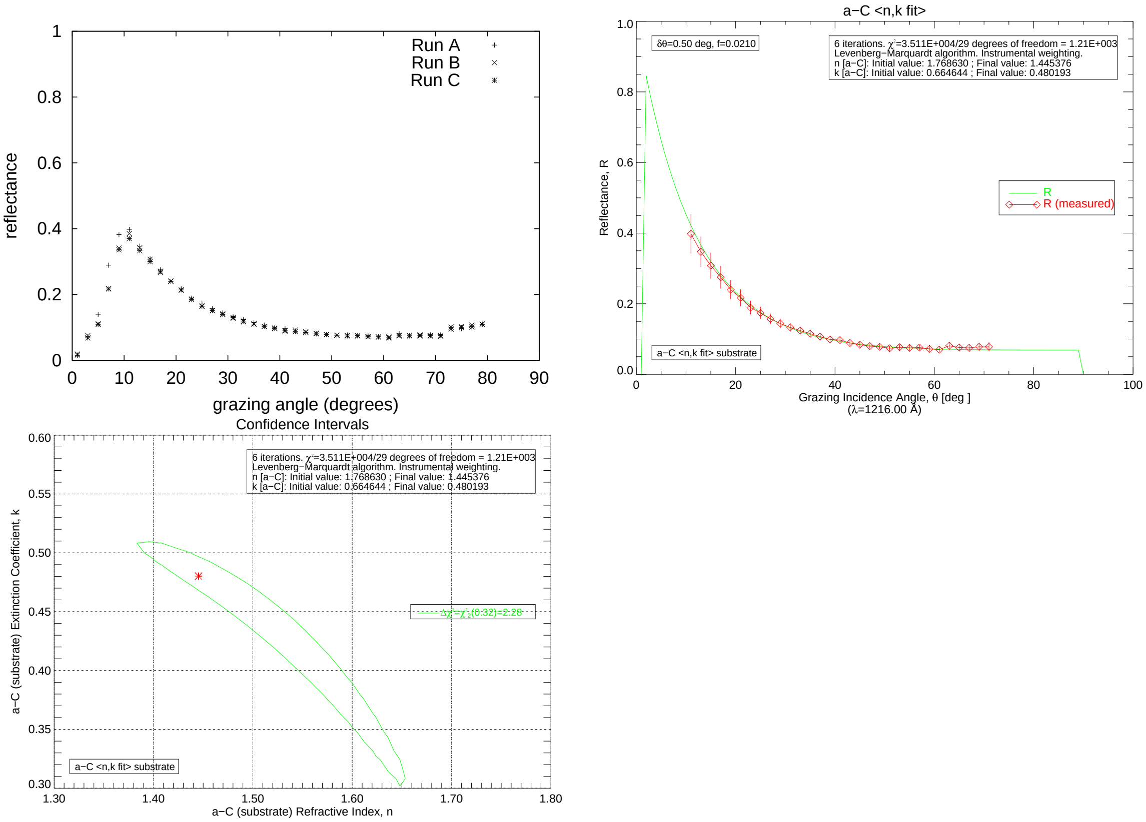

Figure D.6: Variable angle reflectance data and confidence intervals for graphite at 1216 Å.

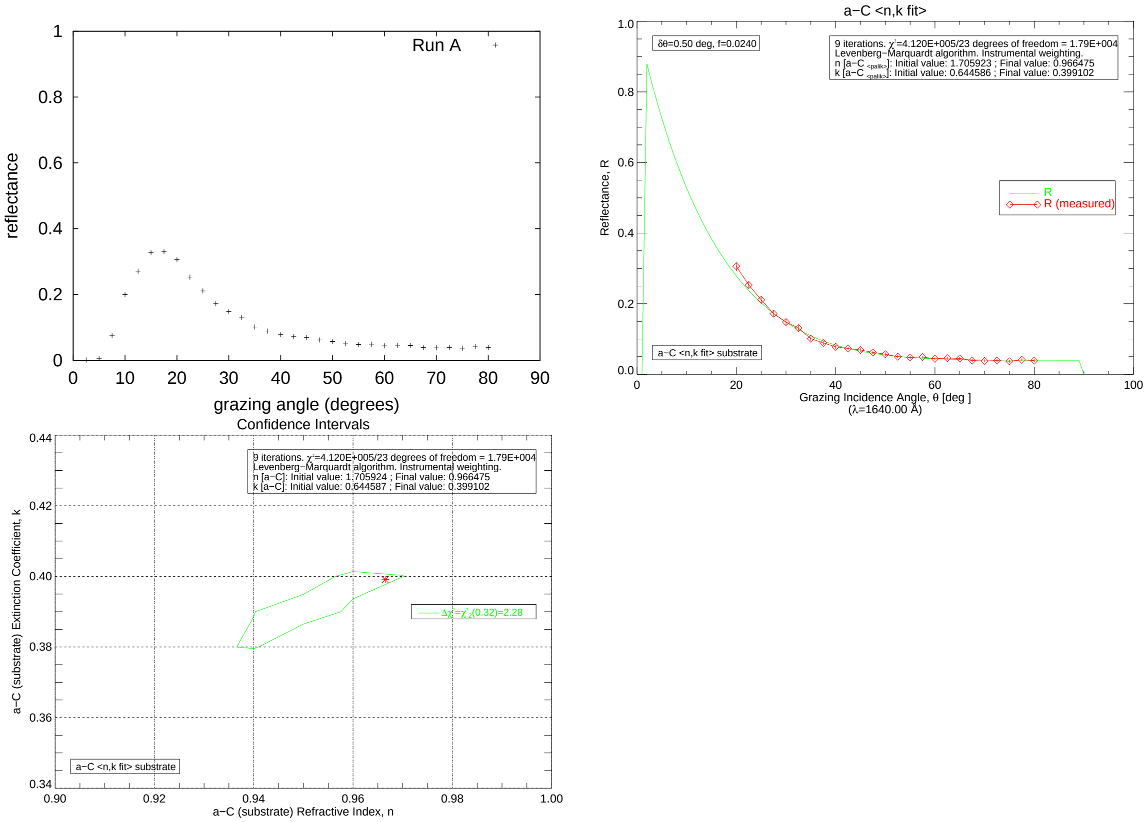

Figure D.7: Variable angle reflectance data and confidence intervals for graphite at 1640 Å.

D.2 Industrial Diamond

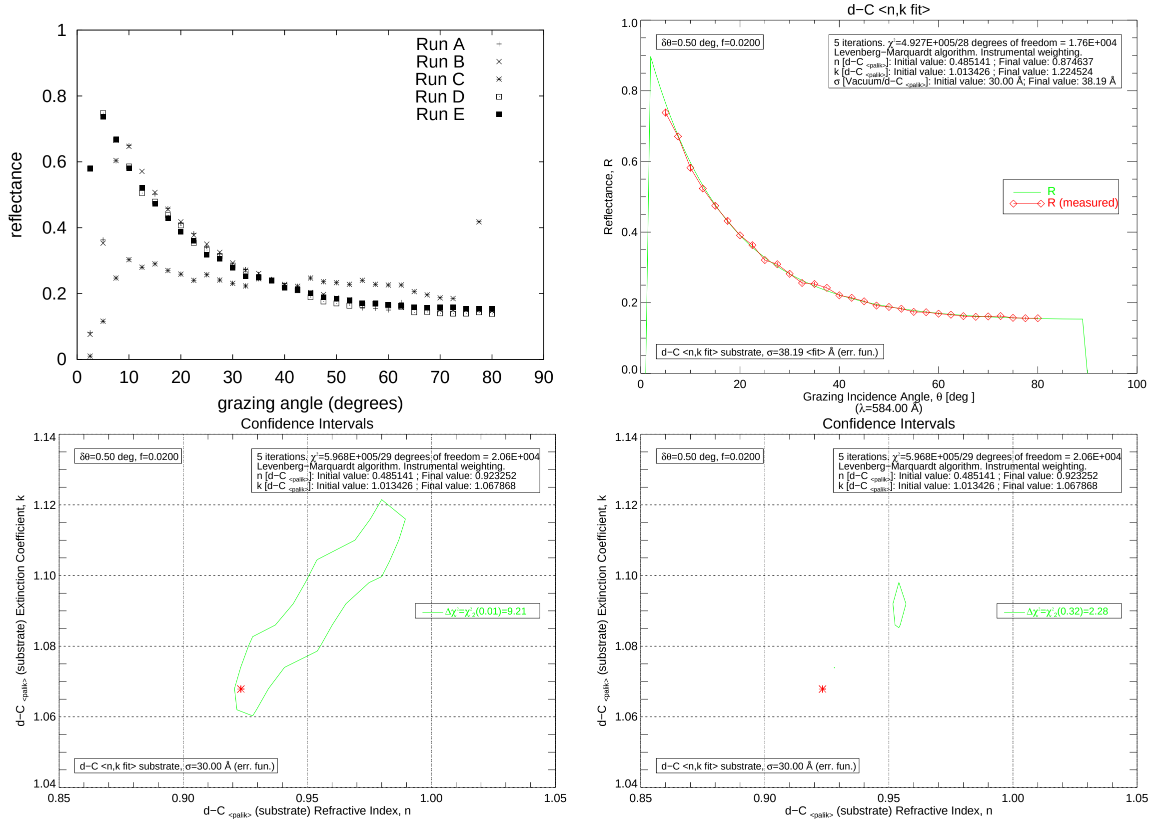

Figure D.8: Variable angle reflectance data and confidence intervals for diamond at 584 Å.

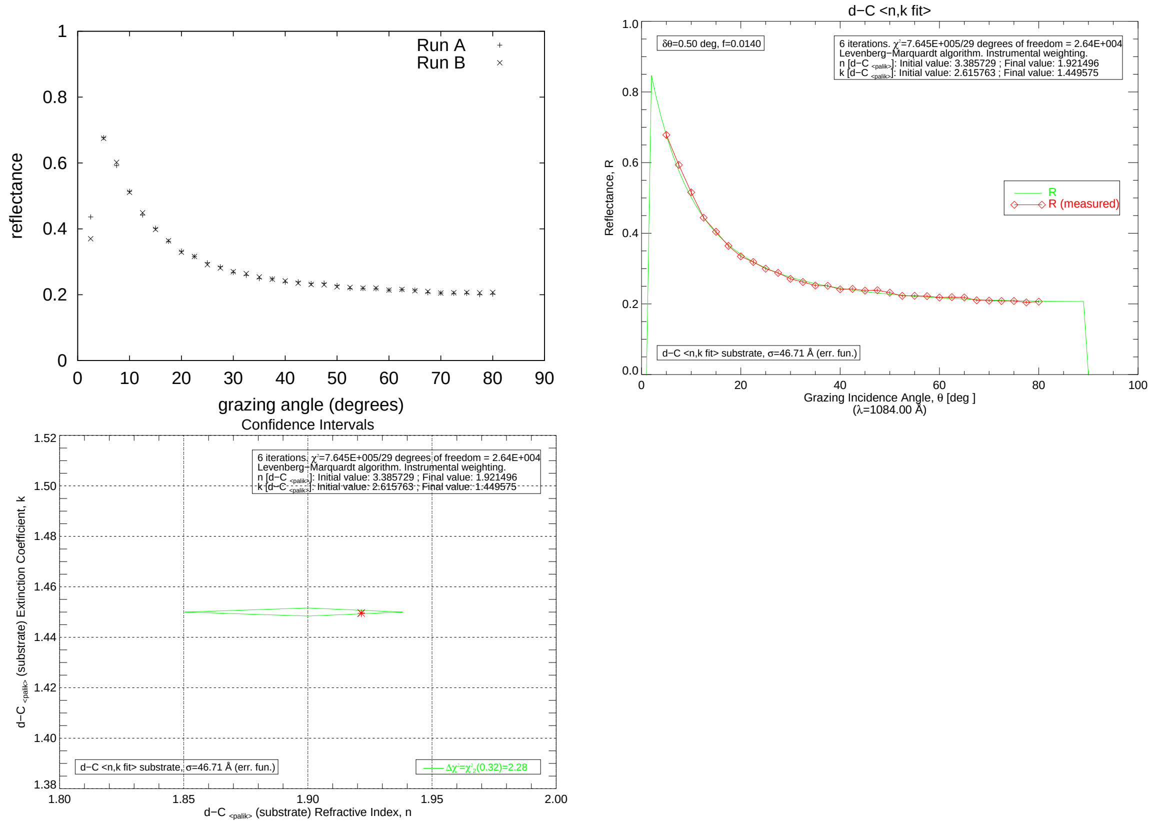

Figure D.9: Variable angle reflectance data and confidence intervals for diamond at 1084 Å.

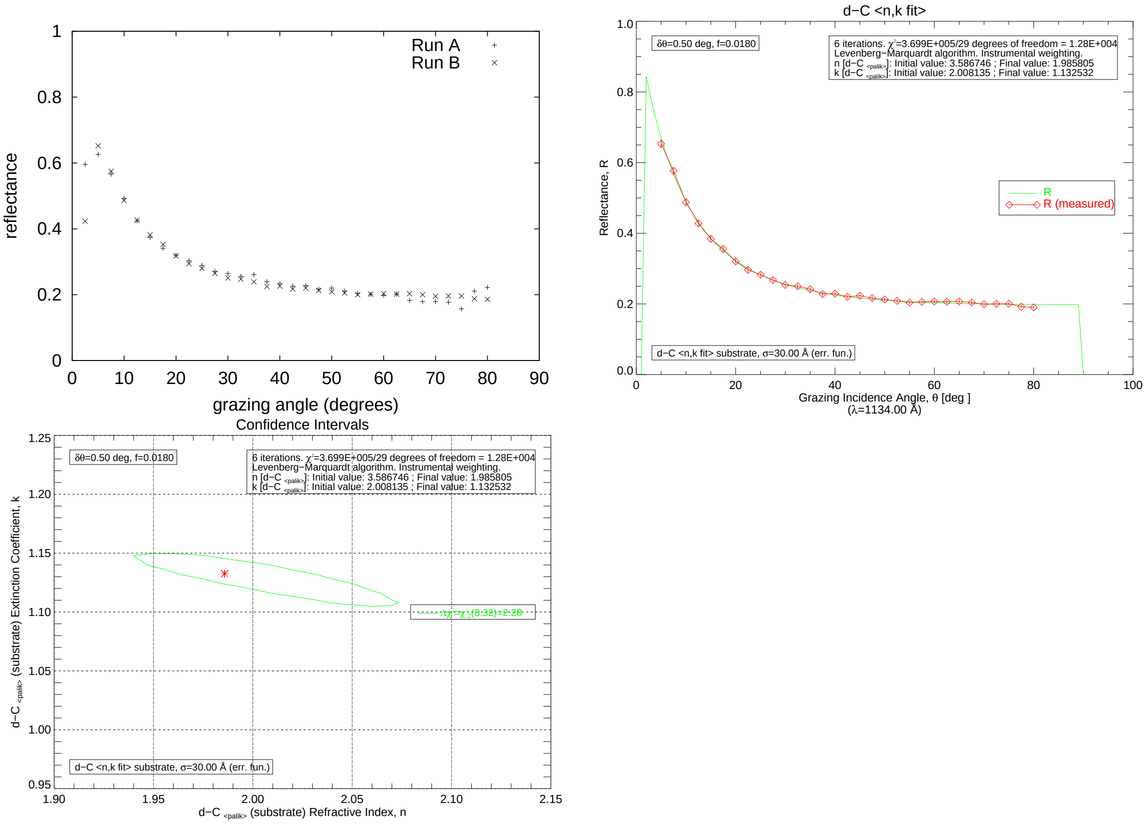

Figure D.10: Variable angle reflectance data and confidence intervals for diamond at 1134 Å.

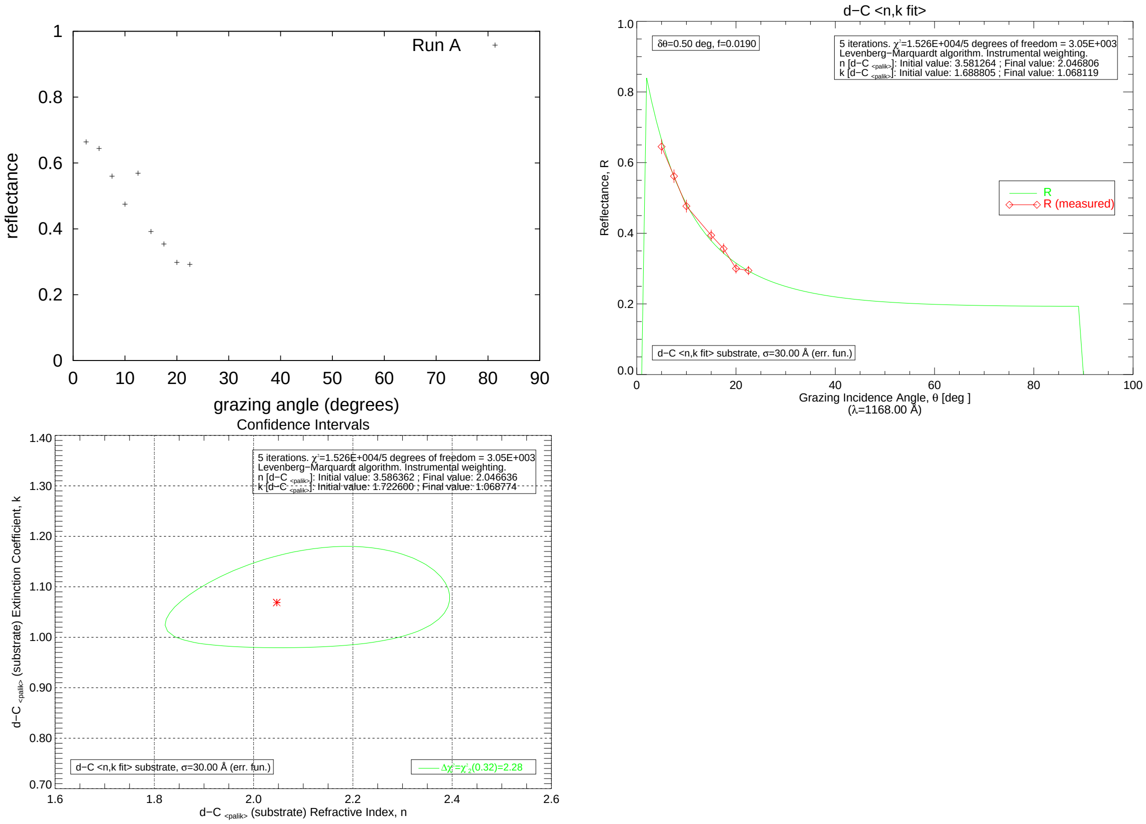

Figure D.11: Variable angle reflectance data and confidence intervals for diamond at 1164 Å.

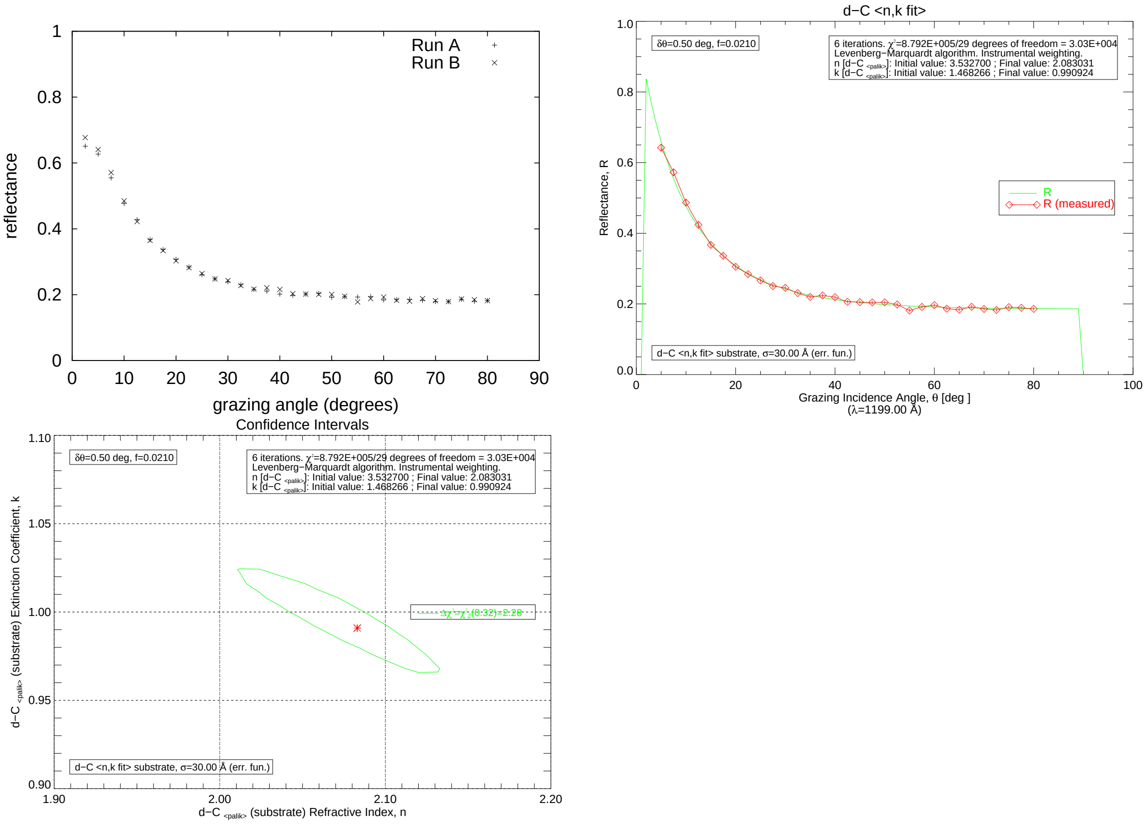

Figure D.12: Variable angle reflectance data and confidence intervals for diamond at 1199 Å.

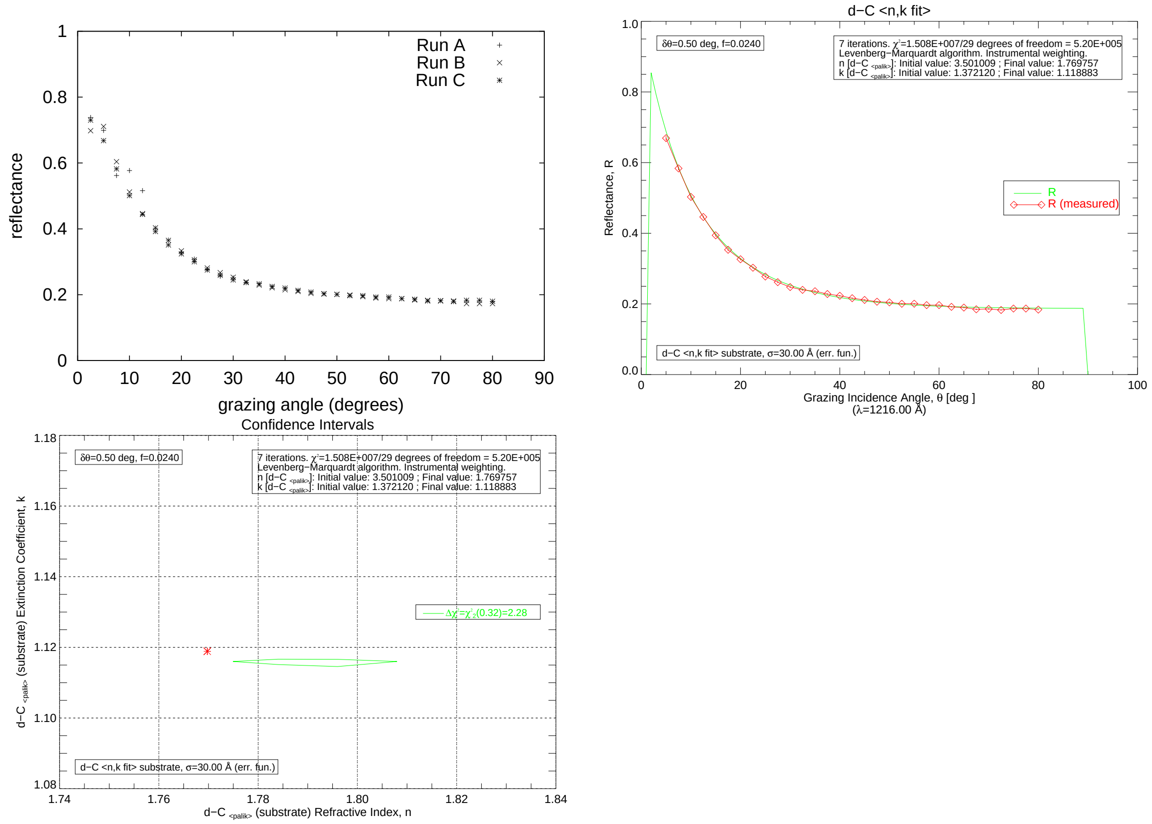

Figure D.13: Variable angle reflectance data and confidence intervals for diamond at 1216 Å.

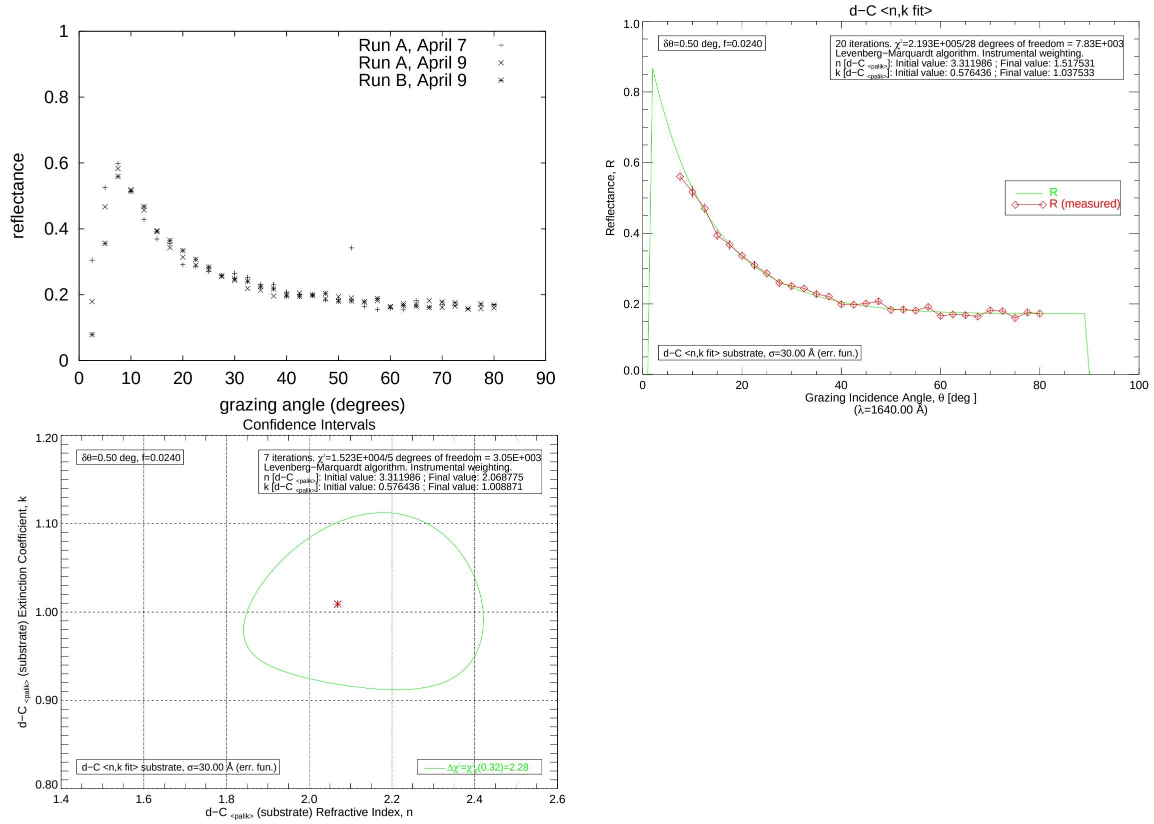

Figure D.14: Variable angle reflectance data and confidence intervals for diamond at 1640 Å.

D.3 MATLAB Program

CountDarkSpots.m calculates the fraction of black spots from a tiff file.

```
% This will read a graphics file and count the number of black pixels
% It will also calculate the fraction that are black
% Matt Squires April 2001



% Open file, convert to numbers, & add 1
A = double(imread('PieceOfDiamond.tif'))+1;

% Create dummy arrays
A2 = A(1:135,1:248);

frac(1:256) =0;



% Determine the frequency of each shade of grey
for x = 1:135,
    for y = 1:248,
        for t =1:256,
        if (A2(x,y)<=1*t & A2(x,y)>1*(t -1))
            frac(t) = frac(t) +1;
        end
        end
    end
end

frac

% Index 1 is black pixels, compare to total number of pixels
frac(1)/(135*248)
```

Appendix E

Standard Operating Procedures

List of SOP's in this Appendix.

1. How to align the interior hardware in the O-chamber
2. How to align the O-chamber with the monochromator
3. How to replace the glass to metal seal in hollow cathode

E.1 SOP for aligning the Interior Hardware

1. Align laser with crosshairs on back of chamber
    (a) Bolt laser and mount to the back of the O-chamber table if not already mounted
    (b) Make sure the mirror is out of the way so there is no reflection from any mirror in the chamber. All reflections should be off of the surface of the plexiglass
    (c) Get retroreflection off to the side of the crosshairs
        i. Rotate laser until it retroreflects above, below, or right on the pinhole in front of the laser
        ii. If needed, turn adjustment screw below laser until the laser reflects off the plexiglass and into pinhole in front of the laser
    (d) Center laser on crosshairs
        i. Use adjustment screws on optical base to align laser with crosshairs
2. Level base with laser
    (a) Turn mirror so it reflects light back into pinhole
    (b) Adjust level of base from front to back
        i. Turn screws in front and back of base until laser is centered on the crosshairs OR until the edge of a crosshair splits the reflected laser beam
        ii. Make sure both front and back screws are touching the floor of the O-chamber by trying to rock the base front to back
        iii. If the front and back screws are both touching the floor of the O-chamber the base should not wobble and the reflected laser beam should not move after touching the floor
    (c) Rotate mirror 90^o clockwise
    (d) Move laser to the side of the chamber
        i. This is only needed when leveling the base withe the laser, and does not need to be done during a regular run, unless the level of the base is suspect
    (e) Repeat steps 4.20 and 4.20
3. Center plum bob with laser
    (a) Borrow a plum bob from Wes Lifferth (Make sure to take it back)
    (b) Move laser to the back of the chamber and align using step 4.20
    (c) Hang the plum bob from a meter stick so the laser is centered on the string
        i. Hold a piece of paper in the laser after it passes through the string
        ii. If the string is centered the intensity will be equal on both sides of the shadow

4. Center base
    (a) Slightly loosen interior alignment block screws at the front and back using an allen wrench or ball driver
    (b) Move the center post so it is aligned under the plum bob
        i. Loosen and tighten opposite screws in the right and left interior alignment blocks to move the center post under the plum bob
        ii. The only alignment that really matters is the lateral alignment (The front to back alignment of the center post does not matter)
        iii. Fix the base into place by carefully tighten the screws in all the interior alignment blocks until the they are tight against the O-chamber walls
5. Double check alignment and adjust detector height
    (a) Move the detector so the laser is shining directly into the detector
        i. This may require removing the bolts that hold the motors in place and moving them out of the way
    (b) Note the relative position of the laser and the opening of the detector
    (c) Move the mirror into the laser so it is reflecting inside the chamber
    (d) Swing the detector so the laser is shining into the detector
    (e) The relative position of the laser and opening of the detector should be the same as step 4.20
    (f) If the positions are not the same the base needs to be realigned
    (g) Adjust the laser so it is centered on the opening of the detector
        i. Loosen the four screws that hold the detector in place
        ii. Adjust the height of the detector by turning the screw at the bottom of the detector
        iii. If the detector's height cannot be adjusted any more the leveling screws in the base are extended too much and need to be retracted and then realigned
        iv. Tighten the four screws to hold the detector in place

E.2 SOP for aligning the O-Chamber with the monochromator

1. Position O-chamber on table
    - (a) Move the chamber so it is centered in the lateral alignment blocks, and parallel to the angular alignment blocks.
2. Move table out of the way
    - (a) Lift the entire table using a pallet jack
    - (b) This may require using 4x4 beams to get the right height
    - (c) Make sure the table is balanced on the pallet jack
3. Align laser with monochromator
    - (a) Move the monochromator wavelength to zero
    - (b) Mount the laser with translation stage on a table
        - i. The table should not interfere with the position of the table
        - ii. The laser should go in the exit slit, because the gate value will block the entrance slit in later steps
    - (c) Align the laser with the exit slits
        - i. The laser should be centered horizontally and vertically
    - (d) Align the laser with the center of the grating
        - i. *Don't touch, wipe, or breath on the grating*
        - ii. Rotate and translate the laser until the laser is centered on the exit slits and hits the center of the grating
    - (e) Align laser with exit slit
        - i. The laser should emerge from the entrance slit centered horizontally and vertically
        - ii. If it is not refer to the McPhereson grating instructions on how to change the alignment of the grating
    - (f) Make sure the entrance and exit slits are as small as possible to confine the beam to one path
4. Move table into beam
    - (a) *USE the PALLET JACK for the alignment*
    - (b) The plexiglass with crosshairs should be in place on the rear port of the O-chamber
    - (c) Position the table where the nipple will not have to move much to be attached to the monochromator

   (d) Carefully rotate and translate the pallet jack (This will also move the table and O-chamber) until the laser retro reflects off the plexiglass back onto the laser
   (e) Adjust the lateral position of the table so the laser is retroreflecting and is directly below the center of the cross hairs
   (f) GENTLY lower the table using the pallet jack
   (g) The lateral and rotational alignment should still be good
   (h) If the vertical alignment can be changed by turning the pads below each leg
   (i) The vertical alignment is also easily performed while the table is lifted by the pallet jack

5. Fine tune the alignment
   (a) Using the external lateral and rotational alignment blocks move the O-chamber on the table until the laser is exactly centered on the crosshairs and retroreflects on itself
6. Attach the nipple to the monochromator
   (a) Remove the screws that support the loose flange. Though the bellows will support the weight of the smaller flange it is best support the loose end with your hand or something else.
   (b) Place the aluminum spacer between the monochromator and the flange with the O-ring on the spacer facing the O-chamber.
   (c) Position the bolt holes of the spacer so they match the bolt holes on the monochromator. There are only five holes on the spacer and the monochromator where there could be six.
   (d) Using a hex screw that is about 1.25 inches long stretch the bellows out a little bit until the screw is able to fit into the flange and spacer. It may be easier to put all the screws in place before screwing any into the monochromator.
   (e) Tighten the screws down in a star pattern to make sure the flanges seat evenly. Don't tighten any screw all the way in one pass. Tighten each screw gradually to prevent the flange from pressing evenly against the O-rings. This is same principle behind putting on a car tire.
7. Bolt the laser mount to the back of the table and align the laser with the cross hair on the back of the O-chamber

E.3 SOP for Replacing Glass to Metal Seal

1. Vent hollow cathode
    (a) Close entrance slit flap valve
    (b) Using dry argon as a backfill open valve on the side of the entrance slit
2. Remove vacuum fittings from metal half of glass to metal seal
    (a) Loosen compression fitting
    (b) Hold the metal tube to support any tension
    (c) Gently pull compression fitting off metal tube
3. Free up cooling tubes
    (a) Loosen and remove the two external fittings that route the cooling water
    (b) One hose is connected to the in coming water
    (c) One hose goes from the hollow cathode back to the hollow cathode
    (d) Don't worry about the internal fittings, but the tubes must be free to move around
4. Hold Tubes out straight
5. Slide Plexiglass guard down tubes
    (a) Be careful not to bend the interior connections to the hose. This will create water leaks
6. Loosen internal compression fitting
    (a) Old glass to metal seal may be removed by gently pulling
7. Install glass to metal seal
    (a) Gently push the glass part of the glass to metal seal into the compression fitting
    (b) The O-ring does not need grease
    (c) Don't force the tube
8. Reverse steps to reinstall Plexiglass guard

Bibliography

[1] Matthew B. Squires, David D. Allred, and R. Steven Turley. Optical Constants of Sputtered U and a-Si at 30.4 and 58.4 nm. *Proceedings of SPIE*, 3736, 1999.

[2] David D. Allred, Matthew B. Squires, and R. Steven Turley. Dual-function EUV Multilayer Mirrors for the IMAGE Mission. *Proceedings of SPIE*, 3736, 1999.

[3] Matthew B. Squires. On Determining the Optical Constants of Sputtered U and a-Si at 304 and 584 å. Honors Thesis, 1999.

[4] R. Soufli. *Optical Constants of Materials in the EUV/Soft X-Ray Region for Mulitlayer Mirror Applications.* PhD thesis, University of California at Berkeley, 1997.

[5] Edward D. Palik ed. *Handbook of Optical Constants of Solids.* Academic Press, Orlando, 1985.

[6] Edward D. Palik ed. *Handbook of Optical Constants of Solids II.* Academic Press, Orlando, 1988.

[7] F. Paresce, S. Kumar, and C.S. Bowyer. Continuous Discharge Line Source for the Extreme Ultraviolet. *Applied Optics*, 10:1904–1908, 1971.

[8] Wolf Born and Emil Wolf. *Principles of Optics.* Pergamon Press, 1959.

[9] W. R. Hunter. Measurement of Optical Properties of Material in the Vacuum Ultraviolet Spectral Region. *Applied Optics*, 21:2103, 1982.

[10] Cynthia E. Mills. Multi-Angle Reflectance Measurements in the EUV. Honors Thesis, 2001.

[11] www.amptek.com. html document, 2001. Picture copied from web site.

[12] David L. Windt. *The Optical Properties of 21 Thim Film Materials in the 10 eV to 500 eV Photon Energy Range.* PhD thesis, University of Colorado, 1988.

[13] Shannon Lunt. The Use of Genetic Algorithms in Multilayer Mirror Optimization. Honors Thesis, 1999.

[14] E. Spiller. *Soft X-Ray Optics.* SPIE Optical Engineering Press, 1994.

[15] N.C. Barford. *Experimental Meassurements: Precision, Error, and Truth.* John Wiley & Sons, 1985.

[16] P. R. Bevington. *Data Reduction and Error Analysis for the Physical Sciences.* McGraw-Hill, 1969.

[17] John R. Taylor. *An Introduction to Error Analysis.* University Science Books, 1982.

[18] David T. Attwood. *Soft X-Rays and Extreme Ultraviolet Radiation.* Chambridge University Press, 2000.

[19] J.J. Thomson. *Conduction of Electriciy Through Gases.* Cambridge University Press, 1906.

[20] G.B. Arfken and H.J. Weber. *Mathmatical Methods for Physicists.* Academic Press, fourth edition, 1968.

[21] David J. Griffiths. *Introduction to Electrodynamics.* Prentice Hall, 1989.

[22] R.W James. *The Optical Principles of Diffraction of X-Rays.* Bell, 1962.

[23] R.L. Liboff. *Introductory Quantum Mechanics.* Addison-Wesley, 1998.

[24] J.C. Slater. *The Quantum Theory of Matter.* McGraw Hill, 1995.

[25] David L. Windt. IMD- Software for modeling the optical properties of multilayer films. *Computers In Physics*, 1998.

[26] B.L. Henke, E.M. Gullikson, and J.C. Davis. X-ray interactions: photoabsorption, scattering, transmission, and reflection at E=50-30000 eV, Z=1-92. *Atomic Data and Nuclear Data Tables*, 54:181–342, 1993.

[27] Center for X-Ray Optics, Materials Sciences Division, LBNL. html document, 2001. www-cxro.lbl.gov.

[28] R. Soufli and E. M. Gullikson. Absolute photoabsorption measurements of molybdenum in the range 60 to 930 eV for optical constant determination. *Applied Optics*, 1997.

[29] R. Soufli and E. M. Gullikson. Reflectance measurements on clean surfaces for the determination of optical constants of materials in the EUV/soft x-ray region. *Applied Optics*, 1995.

[30] C. S. Nelson, T. H. Markert, Y. S. Song, H. L. Marshall, M. L. Schattenburg, D. E. Graessle, K. A. Flanagan, R. L. Blake, J. Bauer, and E. M. Gullikson. Efficiency measurements and modeling of the Advanced X-ray Astrophysics Facility (AXAF) high-energy transmission gratings. *Proceedings of the SPIE*, 2280:191–203, 1994.

[31] E. M. Gullikson, P. Denham, S. Mrowka, and J. H. Underwood. Absolute photoabsorption measurements of Mg, Al, and Si in the soft-X-ray region below the L2,3 edges. *Physical Review B*, 49:16283–8, 1994.

[32] C. T. Chantler. Theoretical Form Factor, Attenuation, and Scattering Tabulation for Z = 1 - 92 from E = 1 - 10 eV to E = 0.4 - 1.0 mev. *J. Phys. Chem. Ref. Data*, 24:71, 1995.

[33] J. H. Weaver, C. Krafka, D. W. Lynch, and E. E. Koch. *Physik Daten,Physics Data: Optical Properties of Metals.* Fach-Information Zentrum, 1981.

[34] D. L. Windt, Webster C. Cash Jr, M. Scott, P. Arendt, B. Newnam, R. F. Fisher, A. B. Swartzlander, P. Z. Takacs, and J. M. Pinneo. Optical Constants for thin films of C, diamond, Al, Si, and CVD SiC from 24 to 1216 a. *App. Opt.*, 1988.

[35] D. L. Windt, Webster C. Cash Jr, M. Scott, P. Arendt, B. Newnam, R. F. Fisher, and A. B. Swartzlander. Optical Constants for thin films of Ti, Zr, Nb, Mo, Ru, Rh, Pd, Ag, Hf, Ta, W, Re, Ir, Os, Pt, and Au from 24 to 1216 A. *App. Opt.*, 1991.

[36] Ashcroft, N. W., and N. D. Mermin. *Solid State Physics*. Holt, Rinehart, and Winston, New York, 1976.

[37] Gerald Burns. *Solid State Physics*. Academic Press, Orlando, 1985.

[38] Rosenberg. *Solid State Physics*. Academic Press, Orlando, 1985.

[39] Robert C. Weast. *Handbook of Chemistry and Physics*. CRC Press, 1988.